

# Charge Generation, Transport and Recombination in Organic Solar Cells



Max Planck Graduate Center   
mit der Johannes Gutenberg-Universität Mainz

## Ralf Mauer

### Dissertation

zur Erlangung des Grades eines  
„Doktor rerum naturalium (Dr. rer. nat.)“  
der Fachbereiche:

- 08 - Physik, Mathematik und Informatik
- 09 - Chemie, Pharmazie und Geowissenschaften,
  - 10 - Biologie,
  - Universitätsmedizin

der Johannes Gutenberg-Universität Mainz

Datum der Prüfung: 19. April 2012

---

---

I hereby declare that I wrote this dissertation submitted without any unauthorized external assistance and used only sources acknowledged in the work. All textual passages which are appropriated verbatim or paraphrased from published and unpublished texts as well as all information obtained from oral sources are duly indicated and listed in accordance with bibliographical rules. In carrying out this research, I complied with the rules of standard scientific practice as formulated in the statutes of the Johannes Gutenberg-University Mainz to insure standard scientific practice.

Ralf Mauer

---

---

# Summary

This thesis presents a study of the charge generation, transport, and recombination processes in organic solar cells performed with time-resolved experimental techniques. Organic solar cells based on polymers can be solution-processed on large areas and thus promise to become an inexpensive source of renewable energy. Despite significant improvements of the power conversion efficiency over the last decade, the fundamental working principles of organic solar cells are still not fully understood. It is the aim of this thesis to clarify the role of different performance limiting processes in organic solar cells and to correlate them with the molecular structure of the studied materials, i.e. poly(3-hexylthiophene) (P3HT) and [6,6]-phenyl C61 butyric acid methyl ester (PCBM).

By combining time-of-flight charge transport measurements, transient absorption spectroscopy, a newly developed experimental technique called time delayed double pulse experiment and drift-diffusion simulations a comprehensive analysis of the working principles of P3HT:PCBM solar cells could be performed. It was found that the molecular structure of P3HT (i.e. the regioregularity) has a pronounced influence on the morphology of thin films of pristine P3HT and of blends of P3HT with PCBM. This morphology in turn affected the charge transport properties as well as the charge generation and recombination kinetics. Well-ordered regioregular P3HT was found to be characterized by a high charge carrier mobility, efficient charge generation and low but field-dependent (non-geminate) recombination. Importantly, the charge generation yield was found to be independent of temperature and applied electric field as opposed to the expectations of the Onsager-Braun model that is commonly applied to describe the temperature and field dependence of charge generation in organic solar cells. These properties resulted in a reasonably good power conversion efficiency. In contrast to this, amorphous regiorandom P3HT was found to show poor charge generation, transport and recombination properties that combine to a much lower power conversion efficiency.

---

---

# Zusammenfassung

Diese Dissertation beinhaltet ein mittels zeitaufgelöster experimenteller Methoden angefertigte Studie der Ladungserzeugungs-, Transport- und Rekombinationsprozesse in organischen Solarzellen. Organische Solarzellen können auf großen Flächen aus Lösungen prozessiert werden und gelten deshalb als vielversprechende kostengünstige Quelle erneuerbarer Energie. Trotz einer deutlichen Verbesserung der Effizienz organischer Solarzellen in den vergangenen zehn Jahren ist die fundamentale Funktionsweise organischer Solarzellen noch immer nicht vollständig verstanden. Ziel dieser Dissertation ist es, zur Aufklärung der Rolle der verschiedenen wirkungsgradbegrenzenden Mechanismen in organischen Solarzellen beizutragen. Ferner wird die Korrelation dieser Mechanismen mit der molekularen Struktur der untersuchten Materialien (P3HT und PCBM) erörtert.

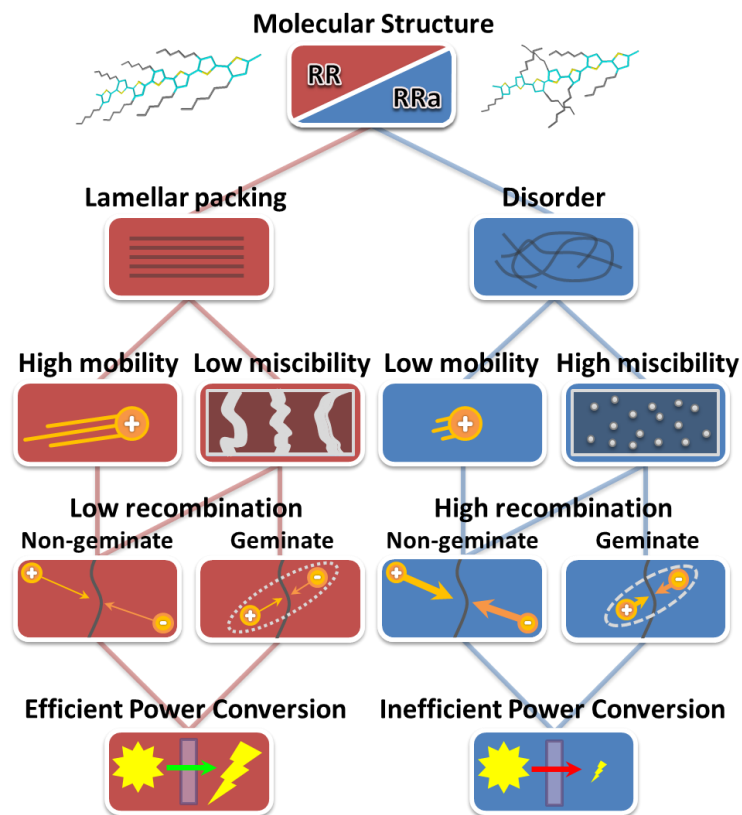
Durch die Kombination von Time-of-Flight Ladungstransportmessungen, transientser Absorptionsspektroskopie, einer neu entwickelten Methode namens zeitverzögertes Doppelpuls Experiment sowie Drift-Diffusions-Simulationen wurde eine umfassende Analyse der Funktionsweise organischer Solarzellen durchgeführt. Dabei wurde deutlich, dass die molekulare Struktur von P3HT, das heißt dessen Regioregularität, einen starken Einfluss auf die Morphologie dünner Schichten aus P3HT und PCBM hat. Diese Morphologie wiederum beeinflusste sowohl den Ladungstransport als auch die Ladungsgeneration und -rekombination. Das geordnete regioregulare (RR) P3HT zeichnete sich durch eine hohe Ladungsträgermobilität, effiziente Ladungserzeugung und niedrige nicht geminale Rekombination aus. Besonders bemerkenswert war die Beobachtung, dass die Ladungserzeugung weder von Temperatur noch elektrischem Feld abhing. Dies steht im Widerspruch zu dem üblicherweise verwendeten Onsager-Braun-Modell für Ladungserzeugung. Die Kombination dieser Eigenschaften erklärte die relativ gute Effizienz der RR-P3HT:PCBM-Solarzellen. Das amorphe, regioirregulare P3HT hingegen zeigte schlechte Ladungserzeugungs-, Transport- und Rekombinationseigenschaften, die in Summe eine sehr schlechte Effizienz der Solarzellen bedingten.

---



---

# Graphical Summary



Graphical summary of the relation between the main experimental results of this thesis.

Regioregular (RR) P3HT packs in a lamellar structure, which leads to a high hole-mobility and a low miscibility with PCBM. The low miscibility in turn leads to low geminate and non-geminate recombination losses. The high charge carrier mobility results in a fast charge carrier extraction and thus further reduces non-geminate recombination in solar cells. It does not however influence the amount of geminate recombination. Altogether, this combines to give efficient power conversion in solar cell devices. The regiorandom (RRa) P3HT does not show signs of ordering and forms amorphous films. The lack of order leads to a low hole-mobility and a high miscibility with PCBM. The latter gives rise to high geminate and non-geminate recombination losses. The low hole-mobility adds to these losses, as charge extraction is not sufficiently fast. In combination, this results in a poor power conversion efficiency.

---

---

---

# Danksagung

The acknowledgements are only contained in the printed original.

---

# Contents

<b>1</b>	<b>Introduction</b>	<b>1</b>
<b>2</b>	<b>Theoretical Framework</b>	<b>7</b>
2.1	Organic Semiconductors	7
2.2	Absorption of light: Exciton Formation	12
2.3	Charge Separation: Dissociation of Charge-transfer excitons	15
2.3.1	Formation of Charge-transfer excitons	15
2.3.2	Theory of field and temperature dependence of charge separation	19
2.3.3	The role of charge-transfer excitons for charge separation	22
2.4	Charge Transport	36
2.4.1	The Gaussian Disorder Model	36
2.4.2	Experimental methods for determining charge carrier mobilities	41
2.5	Non-geminate Charge Recombination	50
2.6	Organic Solar Cells	54
<b>3</b>	<b>Experimental Techniques</b>	<b>59</b>
3.1	Solar Cell Performance	60
3.1.1	Current-voltage characteristics	60
3.1.2	External quantum efficiency	63
3.1.3	Device preparation	64
3.2	The Time-Of-Flight Technique	66
3.3	Transient Absorption Spectroscopy	70
3.4	Time Delayed Double Pulse Experiment	73
3.5	Device Simulations	77
3.6	Materials – P3HT:PCBM	79
<b>4</b>	<b>Results and Discussion</b>	<b>83</b>
4.1	Charge Transport	84
4.2	Charge Generation and Recombination	93
4.3	Field and Temperature Dependence of Charge Generation and Recombination	105
4.4	Charge Extraction	112

---

<b>5 General Discussion.....</b>	<b>121</b>
5.1 Charge Generation .....	123
5.2 Charge Recombination .....	126
5.3 Charge Extraction .....	129
5.4 Charge Injection.....	134
<b>6 Conclusions and Outlook.....</b>	<b>137</b>
6.1 Conclusions .....	137
6.2 Outlook .....	142
6.2.1 New donor materials .....	142
6.2.2 New acceptor materials.....	142
6.2.3 Charge Generation.....	143
6.2.4 Charge Transport .....	143
<b>References .....</b>	<b>145</b>
<b>List of Abbreviations.....</b>	<b>153</b>
<b>List of Scientific Contributions.....</b>	<b>157</b>

---

# 1

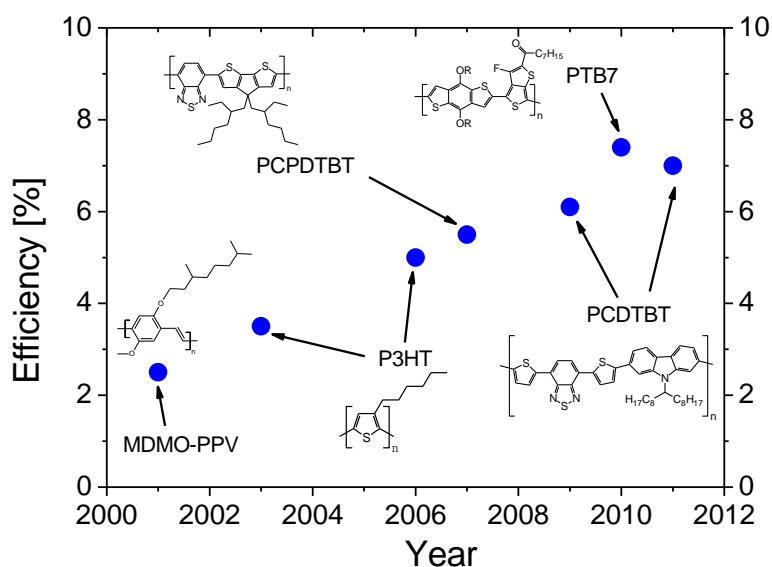
## Introduction

In the last decades the developments in the field of organic electronics have been strongly driven by both academic and industrial research. Properties like flexibility, low weight, high abundance and facile processability open up possible applications for organic materials either as a replacement for products based on more expensive inorganic materials, or as completely new products that cannot be realized by conventional means. Several types of electronic devices based on organic semiconductors have been proposed. Among these are organic field effect transistors (OFET), organic light emitting diodes (OLED), organic laser diodes and organic solar cells (OSC/OPV). The stages of development differ very much between these device types. OLEDs based on small molecule organic semiconductors have entered mass production and can be found mainly in display applications for consumer electronic devices like mobile phones, digital cameras or television sets. On the other end of the scale, organic laser diodes have not even been realized as proof-of-principle laboratory prototype devices [1]. Concerning organic solar

cells, the first low-performance products are currently entering in niche markets like solar mobile phone battery chargers. In order to be able to fully compete with inorganic solar cells, both the power conversion efficiency and the lifetime of devices need further improvement.

Despite significant advancement concerning the power conversion efficiency of organic solar cells over the past decade (see **Figure 1**) there is still an ongoing debate over the physical processes limiting the device performance. At the beginning of the work for this thesis the efficiency of organic solar cells was essentially limited to below 5%, which was reached by empirical variations of the processing conditions of the first readily available material system poly(3-hexylthiophene) :phenyl C61 butyric acid methyl ester (P3HT:PCBM) [2,3]. Subsequent progress was almost exclusively based on tuning the energy levels of the absorbing polymer semiconductor to improve the overlap of its absorption spectrum with the solar emission spectrum and to decrease energy losses due to relaxation during the charge generation process [4,5]. Considerations of the exact mechanisms of charge generation, recombination and extraction and more importantly their correlation with the molecular structures of the materials have, if at all, only played a minor role in the development of new materials. However, such an understanding might contribute to a more target-oriented synthesis of new materials and a faster achievement of power conversion efficiencies relevant for mass production of organic solar cells. Among the various physical mechanisms contributing to the device performance of organic solar cells, especially the role of interfacial charge-transfer excitons (CTE) as an intermediate state between singlet exciton dissociation and free charge carrier generation is heavily disputed. Theoretical models describing the working principles of organic solar cells based on Onsager-Braun theory for the description of charge generation through CTE dissociation rely on dissociation and recombination rate constants [6,7] that largely exceed experimentally observed values [8].





**Figure 1.** Development of the best organic solar cell efficiencies over the past decade [4,9-14].

The aim of this thesis is to clarify the influence of the different physical mechanisms on the device performance of organic solar cells. For this purpose, a series of poly(3-hexylthiophenes) with varying regioregularity is investigated in order to develop a deeper understanding of the impact of the molecular structure on the physical mechanisms influencing device performance. The experimental methods used in this thesis range from time-of-flight charge transport measurements over time resolved spectroscopy to a newly developed technique for studying charge extraction kinetics in organic solar cells. Further, macroscopic drift-diffusion simulations are employed to correlate the results with solar cell device performance. All of these studies have the charge carrier mobility as a shared motif, as it can potentially influence all processes from exciton dissociation to charge extraction. Transient absorption spectroscopy is applied to gain insight into the charge generation process on a picosecond to nanosecond time scale and also into the non-geminate charge carrier recombination mechanism on a nanosecond to microsecond time scale. The newly developed time delayed double pump technique offers the possibility to observe charge extraction kinetics on a nanosecond to hundreds of microseconds time scale and to estimate charge

recombination losses during charge extraction at applied voltages directly relevant to solar cell device operation. All experiments are performed on the material system poly(3-hexylthiophene): phenyl C61 butyric acid methyl ester (P3HT:PCBM). This material system is the fruit fly [15,16] among organic semiconductors suitable for use in organic solar cells with more than 2000 publications that contain the topic P3HT listed in ISI Web of Knowledge [17] in the years 2009 to 2011 alone. It owes its popularity mainly to its good device performance (~3-4% power conversion efficiency) and commercial availability on a multi-gram scale. Slight variations in the molecular structure of the P3HT chains, i.e. variations in the regioregularity, make it possible to determine the relationship between the molecular structure and solar cell device performance. The regioregularity is expected to have a pronounced influence on the morphology of P3HT in the solid state and thus also on the photophysics and device performance.

This thesis consists of six chapters. The first chapter (1 Introduction) contains a brief introduction to organic electronics and contains the motivation and aim of the presented work.

Chapter two (2 Basic Concepts) sets the theoretical framework needed for the discussion of the experimental results. It starts with a basic description of organic semiconductors and their primary photoexcited states. Subsequently, the theoretical description of the generation, recombination and dissociation of charge-transfer excitons is discussed and placed into the context of recent experimental observations. The part on charge transport focuses on an outline of the Gaussian disorder model and a comparison of a selection of experimental methods for determining the charge carrier mobility in organic semiconductors. Finally, a kinetic model for non-geminate recombination of charge carriers based on Langevin recombination is developed and a short overview of the working principles of organic solar cells is presented.

Chapter three (3 Experimental Techniques) contains an outline of the employed experimental techniques, starting with the methods used for

characterizing the performance of solar cell devices. It further contains a description of the time-of-flight technique for studying charge carrier mobilities, a brief introduction to transient absorption spectroscopy, the newly developed time delayed double pulse method and information on macroscopic drift-diffusion simulations of device performance. These sections contain both details about the experimental setups as well as some basic instructions on the type of data acquired and their analysis. At the end of chapter 3 the materials studied in this thesis are presented along with some of their physical properties, like molecular weight and regioregularity.

In chapter four (4 Results and Discussion) all experimental results are presented and discussed in detail. As the results and discussions within the framework of this thesis were all published in peer reviewed journals, this chapter is simply a collection of all relevant published articles.<sup>1</sup> A complete overview of all scientific contributions in the framework of this thesis can be found in the list of scientific contributions on page 157.

In chapter five (5 General Discussion) the results are summarized in a comprehensive discussion with a special emphasis on correlating molecular structures, reaction kinetics and device performance of organic solar cells.

The thesis ends with a final conclusion of all results and an outlook towards promising new research projects in chapter six (6 Conclusions and Outlook).

---

<sup>1</sup> In accordance with the MPG examination regulations §11.1.



# 2

## Theoretical Framework


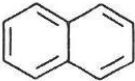
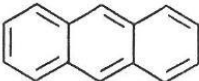
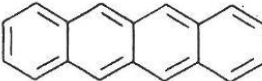
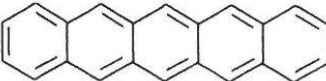
### 2.1 Organic Semiconductors

All properties of the material class of organic, i.e. carbon based, semiconductors directly derive from the chemical properties of the carbon atom. Carbon has the electronic configuration  $1s^2 2s^2 2p^2$  with four electrons in the outer shell that take part in bonding interactions. The s- and p-orbitals of this outer shell can hybridize to form various new hybrid orbitals. One of these configurations consists of 3 planar  $sp^2$ -orbitals with a fourth  $p_z$ -orbital perpendicular to the plane of the  $sp^2$ -orbitals. When the  $sp^2$ -orbitals of two carbon atoms overlap, they form covalent bonds called  $\sigma$ -bonds that are localized. The energetic difference between bonding and anti-bonding  $\sigma$ -bonds is relatively large so that they do not contribute to the absorption of visible light. Contrary to that,  $\pi$ -bonds formed from overlapping  $p_z$ -orbitals are strongly delocalized in the plane of the  $\sigma$ -bonds. The energy difference between the bonding and anti-bonding  $\pi$ -bonds in organic molecules thus

depends on the size of the molecule over which the  $\pi$ -bonds are delocalized. Similar to the picture of a quantum well, the energy gap decreases with increasing size of the molecule. This is shown in **Figure 2** for molecules of the polyacene family. It means that sufficiently large delocalized  $\pi$ -electron systems can strongly absorb light in the visible range ( $\sim 400\text{-}700$  nm). Furthermore, due to the delocalized nature of the electron system, such molecules can possess a high (intramolecular) electrical conductivity. As each carbon atom in a molecule contributes one  $p_z$  electron to a  $\pi$ -bond, the resulting sequence of bond distributions in organic molecules with  $\pi$ -bonds can, in a simplified picture, be considered as an alternation of single bonds (i.e. only  $\sigma$ -bonds) and double bonds (i.e.  $\sigma$ - and  $\pi$ -bonds). Such an arrangement of bonds is called a  $\pi$ -conjugated system.

As all electrons of the constituting carbon atoms of such molecules are participating in the intramolecular covalent bonds, the interactions between different molecules are typically limited to van der Waals attractions. This has drastic consequences for the physical properties of molecular solids. As van der Waals interactions are very weak compared to covalent bonding, molecular solids are much softer than solids based on covalent bonds and also have much lower melting temperatures.

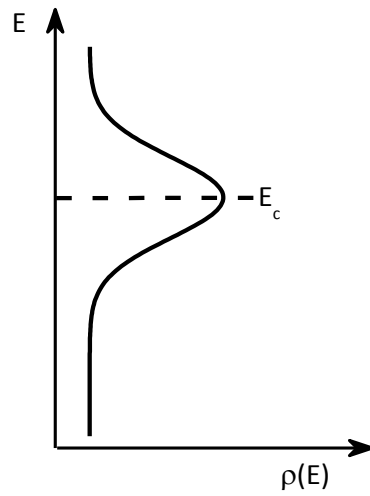
The same is true for materials consisting of larger macromolecules, i.e. polymers. When carbon atoms are arranged in a linear array, as for example in polyacetylenes, the  $\pi$ -bonds can delocalize along this array leading to the formation of an essentially one dimensional wire. As each carbon atom within such a wire contributes one electron to the  $\pi$ -band, the  $\pi$ -band is only half populated, corresponding to a metallic state [19]. However, as was first shown theoretically by Peierls in the 1930s such one dimensional periodic structures are instable with respect to redistributions of the bond lengths leading to the formation of a band gap and so to semiconductor like behavior [20]. Typically, polymers are not perfect one dimensional wires, because they bend and twist, leading to interruptions in the  $\pi$ -conjugated system and essentially rendering

Molecule	Delocalized system	Absorption region
Benzene		2550 Å
Naphthalene		3150 Å
Anthracene		3800 Å
Naphthacene		4800 Å
Pentacene		5800 Å

**Figure 2.** The molecular structure of the first few polyacenes, together with the wavelength of the main absorption peak [18]. These wavelengths correspond to transition energies of 4.86 eV (benzene), 3.94 eV (naphthalene), 3.26 eV (anthracene), 2.58 eV (naphthacene) and 2.14 eV (pentacene).

polymers to be covalently bound chains of smaller oligomer units. For this reason the properties of conjugated small molecules and polymers are generally very similar. In both of these classes of materials the wave functions of electrons are limited by the size of the  $\pi$ -conjugated system (in small molecules due to the size of the molecule and in polymers due to the length of the conjugated chain-segments). Consequently, quantum confinement effects rather than bulk effects govern the photophysical properties of such materials. In other words, a  $\pi$ -conjugated system rather corresponds to the picture of a charge carrier in a quantum well than to a “classical” semiconductor crystal with translational symmetry in a periodic potential.

Because in a polymer the  $\pi$ -conjugated system is segmented into localized sites by randomly occurring defects like kinks, twists and chemical defects, the exact energetic value varies between sites, depending on the exact implementation of the defect. This variation is intensified by the fact that every site has a slightly different energetic environment that can also influence the energy of a site, e.g. through variations in the surrounding molecules. All this leads to a



**Figure 3.** Schematic of a Gaussian density of states centered around the energy  $E_c$ .

statistical distribution of the ensemble of states in a polymer that is best described by a Gaussian distribution of the density of states (DOS)  $\rho(E)$ :

$$\rho(E) = \frac{1}{\sqrt{2\pi\sigma^2}} \exp\left[-\frac{(E-E_c)^2}{2\sigma^2}\right]. \quad (2.1)$$

The width  $\sigma$  of this distribution corresponds to the energetic disorder in the polymer and is typically on the order of 100 meV, the energy  $E$  is given relative to  $E_c$ , the center of the DOS. In small molecules the size of the  $\pi$ -conjugated system is much more uniform than in polymers, thus basically reducing the origin of the energetic disorder to fluctuations in the environment of a molecule. Consequently, the energetic disorder in small molecules tends to be lower than in polymers. The lower limit for energetic disorder to play a relevant role in physical processes naturally is the thermal energy  $kT$ , which is 25 meV at room temperature. Experimentally energetic disorder can be observed for example by an inhomogeneous broadening of optical transition spectra.

As in every semiconductor (or virtually every conducting solid state material), charge carriers in organic semiconductors polarize their environment, which leads to a deformation of the molecular structure due to the displacement of the surrounding atomic nuclei. A charge carrier together with its associated



deformation is called a polaron. Because of the rather localized character of charge carriers in organic semiconductors the coupling between charge carriers and molecules (i.e. electron-phonon coupling) is particularly pronounced and is not always negligible. In the remainder of this thesis, whenever the terms charge carrier, electron or hole are used, polaronic states are assumed if not stated otherwise explicitly.

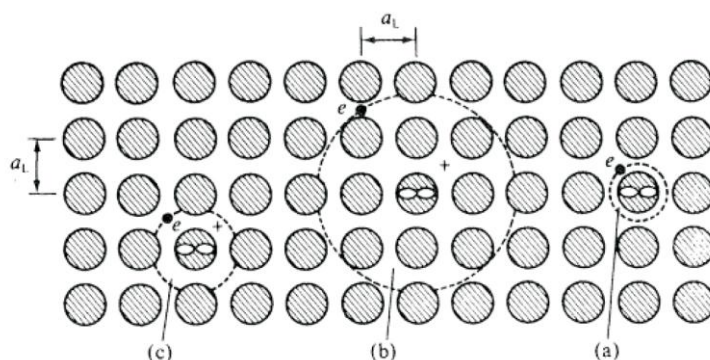
## 2.2 Absorption of light: Exciton Formation

In inorganic semiconductors the dielectric constant is rather high ( $\epsilon > 10$ ) compared to organic semiconductors ( $\epsilon \cong 3 - 4$ ). This has a direct consequence for the primary photoexcitation in these materials. In inorganic semiconductors the absorption of a photon leads to the promotion of an electron from the valence band to the conduction band, resulting in a free electron in the conduction band and a free hole in the valence band. These two charge carriers usually do not feel their mutual electrostatic attraction, because it is effectively screened by the surrounding material. Only at very low temperatures is the kinetic energy of the charge carriers lower than their Coulomb attraction and they form a bound state termed an exciton. In organic semiconductors the electrostatic attraction between the charge carriers is not screened as efficiently because of the lower dielectric constant. This leads to a much stronger attraction between the charge carriers and ultimately to binding energies of more than 0.5 eV that far exceed the thermal energy at room temperature [18]. It was hotly debated in the 1990s whether free charge carriers or bound excitons comprise the primary photoexcitations in conjugated polymers. Meanwhile, there has been consensus that excitons indeed are the primary photoexcitation, mainly because photoexcitation near the bandgap does not directly lead to photoconduction as would have been expected for the generation of free charge carriers [21]. One consequence of this is that optical excitation does not lead to a transition of an electron from the highest occupied molecular orbital (HOMO) to the lowest unoccupied molecular orbital (LUMO), but to a transition to an exciton state that is lower in energy than the LUMO by the binding energy of the exciton.<sup>2</sup>

Generally, three different types of excitons are differentiated: Wannier-Mott, Frenkel and charge transfer excitons. The main difference between these three

---

<sup>2</sup> In this context the LUMO is defined as the state an electron would occupy, if it were added to the molecule while the molecule is in its ground state. The lowest excited state of an organic molecule is not identical to this state because of the electrostatic interaction of the electron in the excited state with the hole in the HOMO.



**Figure 4.** The diameter of a) a Frenkel exciton is comparable to the inter-site distance or lattice constant  $a_L$ , b) Wannier-Mott excitons is much larger than  $a_L$  and c) charge-transfer excitons is in between large Wannier-Mott and small Frenkel excitons [18].

is their size. Wannier-Mott excitons are mostly found in inorganic semiconductors and are delocalized over several lattice constants. Frenkel excitons are localized on single sites such as small molecules or single conjugated segments of a polymer chain. Charge-transfer excitons are comparable to Frenkel excitons apart from that the two charge carriers are not located on the same site but rather on two adjacent sites. These sites can be within the same polymer chain, on two identical neighboring molecules or even on different adjoining molecules. Furthermore, depending on the orientation of the spins of the involved charge carriers, excitons are termed singlets if the spins are anti-parallel (total spin 0) and triplets if they are parallel (total spin 1). Due to the nature of carbon bonds (*vide supra*) the ground state of organic molecules always is a singlet state. A dipole transition between a ground and an excited state requires a change in the symmetry of the (space) wave function that can only be achieved by a change in the angular momentum quantum number ( $\Delta l = \pm 1$ ). A photon involved in such a transition can compensate this change with its spin ( $s = 1$ ), it cannot however counteract an additional change in the spin. For this reason optical transitions between the singlet ground state and the triplet excited state are spin-forbidden and optical excitation of organic molecules leads to the formation of singlet excitons. However, under certain circumstances transitions between singlet and triplet states are possible. Such

transitions require that the difference in spin is compensated by the molecule, for example by spin-orbit coupling in the presence of heavier atoms like sulfur or by spin-lattice relaxation. This process is called intersystem crossing and typically occurs on a time scale of  $10^{-10}$  to  $10^{-8}$  s [22].

## 2.3 Charge Separation: Dissociation of Charge-transfer excitons

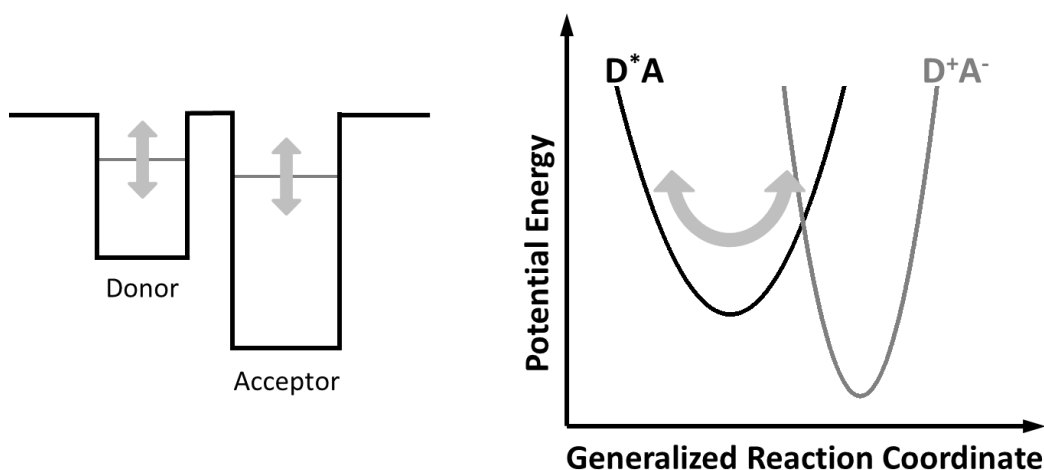
In the preceding section it was established that in organic semiconductors the absorption of a photon primarily leads to the formation of a strongly bound singlet exciton. In order to obtain free charge carriers, the exciton has to be dissociated. This can be achieved by blending two organic semiconductors with different energy levels, so that it is favorable for an electron to undergo a charge-transfer process from the bound singlet exciton state to a less tightly bound charge-transfer exciton. This section will start with an introduction of the mechanism leading to the formation of charge-transfer excitons, i.e. the charge-transfer process, and will later on discuss the subsequent dissociation or recombination of charge-transfer excitons.

### 2.3.1 Formation of Charge-transfer excitons

At the heart of the dissociation of a singlet exciton and the formation of a charge-transfer exciton at an interface is the charge-transfer process itself. A theoretical description of charge-transfer reactions was first described in a rather intuitive classical approach by Marcus [23] and later extended to a full many-particle quantum mechanical analysis by Jortner [24]. Second only to the formation of an exciton after the absorption of a photon, the charge-transfer process at an interface between two organic semiconductors is the fastest process reported in this thesis. It happens on a sub-100 fs time scale and thus cannot be resolved with the experimental methods presented here. Consequently, even though it is an interesting field of research with some yet unanswered questions, only a short introduction to the theoretical basics of charge transfer will be given. A detailed introduction to charge-transfer theory can be found elsewhere [25].

In a simplified quasi one particle picture, the transfer of an electron from an excited donor site  $D^*$  to an acceptor site  $A$  in the form  $D^*A \rightarrow D^+A^-$  involves the movement of an electron in the potential energy landscape created by the atomic nuclei of the donor and the acceptor sites. This potential energy landscape essentially creates donor and acceptor quantum wells with width and depth depending on the momentary configuration of the atomic nuclei. A

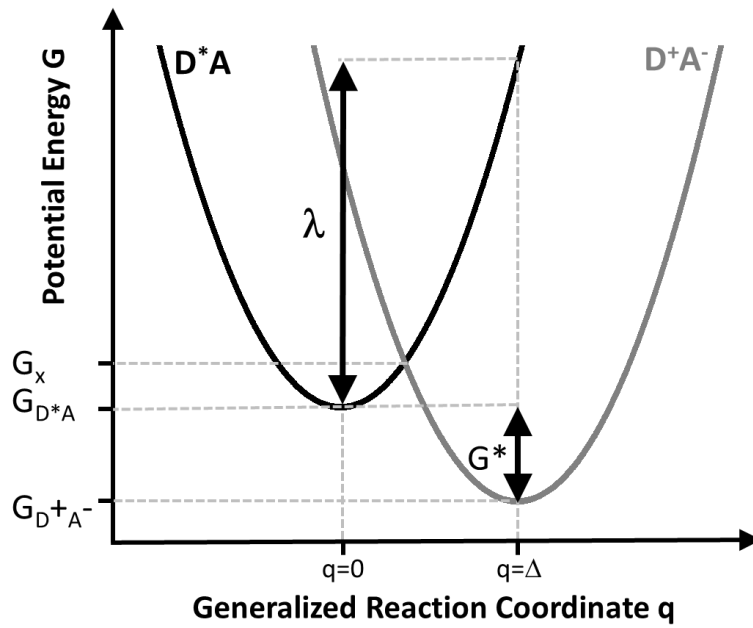
sketch of such quantum wells along with the corresponding electronic energy levels are shown on the left side of **Figure 5**. Assuming no exchange of energy between the electron and its environment, the electronic energy levels of the donor and the acceptor have to be equal in order to satisfy the conservation of energy during the transfer. Consequently, all nuclei involved in the transfer process have to reorganize by statistical fluctuations about their equilibrium positions in such a way, that the energy levels in the donor and the acceptor quantum well match. This can also be illustrated with the help of so called potential energy surfaces. On the right side of **Figure 5** these potential energy surfaces before (labeled  $D^*A$ ) and after charge transfer (labeled  $D^+A^-$ ) are represented by parabolas plotted against a generalized reaction coordinate accounting for all degrees of freedom of the nuclear configurations. Vibrations, rotations and similar fluctuations of the nuclei cause the system to oscillate along the potential energy surface  $D^*A$ , as indicated by arrows in **Figure 5**. When the system reaches the point where the energy of the states before and after charge separation are identical (intersection of the parabolas), charge transfer can occur.



**Figure 5.** Quantum well and potential energy surfaces relevant for charge transfer. Arrows indicate fluctuations about the generalized reaction coordinate leading to changes in the energy levels of the quantum wells which corresponds to oscillations along the potential energy surface.

In classical Marcus theory the molecular fluctuations along a potential energy surface are described by harmonic oscillations about an equilibrium position (minimum of a parabola). The parameters used for describing the problem are defined in **Figure 6**. Both potential surfaces are assumed to be parabolas with identical curvature  $c$ . The equilibrium configurations of the initial ( $D^*A(q) = cq^2 + G_{D^*A}$ ) and of the charge transferred ( $D^+A^-(q) = c(q - \Delta)^2 + G_{D^+A^-}$ ) states are denoted with  $q = 0$  and  $q = \Delta$  and they are energetically displaced by the value of  $G^* = G_{D^*A} - G_{D^+A^-}$ .  $G_B^*$  is the energy barrier the system needs to overcome before charge transfer can occur and  $G_X$  is the intersection of the parabolas. The reorganization energy  $\lambda = D^*A(\Delta) - D^*A(0) = c\Delta^2$  is defined as the amount of energy that would be needed to change the molecular configuration of the initial state to that of the equilibrium position  $\Delta$  of the charge transferred state. It can be divided into a so called inner sphere and outer sphere contribution. In this context inner sphere describes the contribution of the molecule(s) directly involved in the transfer process, while outer sphere refers to all molecules in the closer vicinity of the directly involved molecule(s). In other words, through the formalism of reorganization Marcus' theory explicitly takes the polaronic nature of charge carriers into account by considering the energy it takes for a charge carrier to move its associated lattice distortion along during the transfer process. All energies mentioned here are Gibbs free energies to account for entropic effects.

From geometrical considerations, it follows that the energy barrier is given by  $G_B = \frac{(\lambda + G^*)^2}{4\lambda}$ . While the reorganization of the system directly constitutes a barrier for charge transfer, the influence of the energetic displacement  $G^*$  of the equilibrium configurations is a bit more complicated. In the regime  $0 > G^* \geq -\lambda$  it acts as a driving force for charge transfer by decreasing the energy barrier. However, if the absolute value of  $G^*$  exceeds  $\lambda$ ,  $G^* < -\lambda$ , then it has the opposite effect and increases the barrier. The prediction of this so called Marcus inverted region is one of the main achievements of Marcus theory.



**Figure 6.** Potential energy surfaces of the initial ( $D^*A$ ) and the charge transferred ( $D^+A^-$ ) state approximated by parabolas.

In thermodynamic equilibrium the charge-transfer rate of the system can be determined by Boltzmann statistics as

$$k_{CT} = A \exp\left[-\frac{G_B}{k_B T}\right] = A \exp\left[-\frac{(G^* - \lambda)^2}{4\lambda k_B T}\right], \quad (2.2)$$

with Boltzmann's constant  $k$ , at Temperature  $T$ , and with the coupling constant  $A$  that depends on the specific type of transfer reaction (e.g. intra- or intermolecular transfer).

In some cases not every site in a material is suitable for charge transfer so that an additional transport step precedes the transfer process. If this transport step is slow compared to the actual transfer time then the overall rate of the transfer process is reduced. For a transport mechanism of three dimensional isotropic diffusion an estimation of the reduced transfer rate can be obtained. Assuming an excitation on average has to travel a distance  $x$  between the site where it was created and a site suitable for charge transfer, the average rate  $k_D$  for the excitation to reach a transfer site is given by

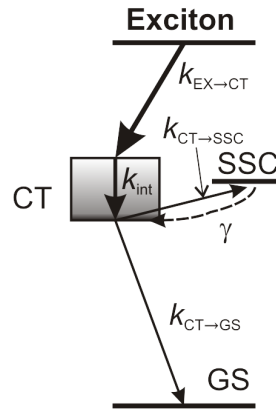
$$k_D = \frac{D}{x^2}, \quad (2.3)$$



with diffusion constant  $D$ . In the limit of very fast transfer and very slow diffusion the total charge-transfer rate  $k_{CT}$  can be approximated by the diffusion rate  $k_{CT} \approx k_D$ . Diffusion limited charge transfer can be found in blends of organic semiconductors if the phases segregate to form large, pure domains so that the diffusion time of excitons to the interface between the phases is larger than the duration of the charge-transfer process itself. For a diffusion constant of  $D = 10^{-3} \text{ cm}^2/\text{s}$  and assuming that the charge-transfer time is lower than 100 fs, an average diffusion distance of as little as 0.1 nm will lead to a diffusion limited charge-transfer rate [26]. As domain sizes in blends for efficient organic solar cells usually exceed 1 nm, it seems likely that diffusion indeed limits the charge-transfer rates in such systems. Cowan et al. recently argued that in donor-polymers for organic solar cells, excitons are initially highly delocalized and relax into more localized excitons on a timescale comparable to charge transfer [27]. Such an initial delocalization could increase the critical domain size at which diffusion effects start to become important.

### 2.3.2 Theory of field and temperature dependence of charge separation

Charge-transfer excitons (CTE), also called geminate pairs, are less tightly bound than singlet excitons in pure polymers, because the distance between electron and hole is increased after the transfer. The decreased binding energy potentially makes it susceptible to dissociation under the influence of moderate external electric fields or thermal activation. A commonly used theory for such electric field and temperature assisted dissociation of charge-transfer excitons was first developed by Onsager [28] in the 1930s and later refined by Braun [29] and Tachiya [30]. The pathways for generation, dissociation and recombination of CTEs (geminate recombination) according to this model are sketched in **Figure 7**.



**Figure 7.** Schematic representation of the Onsager-Braun model including generation of a charge-transfer (CT) exciton from an exciton followed by vibrational relaxation, dissociation to and reformation from spatially separated charges (SSC) and recombination to the ground state (GS) [31]. Reprinted with permission from Howard et al. Journal of the American Chemical Society 2010, 132, 14866. Copyright 2010 American Chemical Society.

A relaxed charge-transfer exciton is assumed to be metastable with a field ( $F$ ) and temperature ( $T$ ) dependent lifetime  $\tau(F, T)$  that is given by the inverse of the sum of the rate of dissociation to spatially separated charges (SSC),  $k_{CT \rightarrow SSC}(F, T)$ , and the recombination rate to the ground state (GS),  $k_{CT \rightarrow GS}$ . The probability for a charge-transfer exciton to dissociate into spatially separated charges  $P(F, T)$  then follows from the product of the dissociation rate and its lifetime:

$$P(F, T) = \frac{k_{CT \rightarrow SSC}(F, T)}{k_{CT \rightarrow SSC}(F, T) + k_{CT \rightarrow GS}}, \quad (2.4)$$

where the dissociation rate is given by

$$k_{CT \rightarrow SSC}(F, T) = \nu \exp[-\Delta E/kT] \left(1 + b + \frac{b^2}{3} + \frac{b^3}{18} + \dots\right), \quad (2.5)$$

with the separation attempt frequency

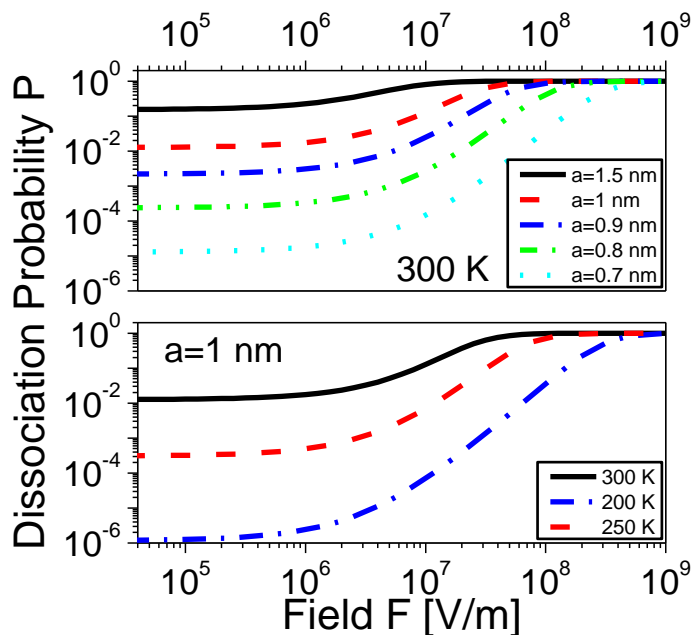
$$\nu = \frac{3 \langle \mu \rangle e}{4 \pi \langle \epsilon \rangle \epsilon_0 a^3}, \quad (2.6)$$

and the effective field parameter

$$b = \frac{e^3 F}{8 \pi \langle \epsilon \rangle \epsilon_0 (kT)^2}. \quad (2.7)$$

In this context the dissociation barrier  $\Delta E$  is given only by the Coulomb binding energy at the separation distance  $a$  between charge carriers and does not consider that the energetic environment of the electron in the fullerene is much different from that in the polymer. The value of this dissociation barrier is typically found to be 0.1 to 0.5 eV, corresponding to a separation of the charge carriers in the charge-transfer exciton of roughly 1 to 4 nm [32-37]. Also the explicit morphological structure of the interface is not taken into account by Onsager-Braun theory and the interface is assumed to be perpendicular to the applied electric field, which is generally not the case in randomly distributed polymer:fullerene composites. In fact, the only way to consider any difference in the materials is to use appropriate values for the spatially averaged sum of electron and hole mobilities  $\langle\mu\rangle$  and the dielectric constant  $\langle\varepsilon\rangle$ . Following along this line an increase in the dielectric constant should cause a decrease in the charge-transfer exciton binding energy. However, in a compositional study Vandewal et al. [38] found that if increasing the average dielectric constant by increasing the amount of PCBM in a polymer:PCBM blend, the charge-transfer exciton is stabilized by a higher binding energy. This implies that other factors have to be taken into account in order to explain all aspects of charge-transfer binding energies.

Even though Onsager-Braun theory is a limited effective medium approximation, it can still give some useful qualitative insight into the separation mechanism, and especially into its dependence on electric field, charge-transfer distance and temperature. **Figure 8** shows the field dependence of the dissociation probability at various charge separation distances and temperatures for a representative set of parameters. For fields below  $10^8$  V/m (corresponding to an applied voltage of 10 V at a sample thickness of 100 nm) both the charge separation distance after the charge-transfer step (upper panel) and the temperature (lower panel) have a strong influence on the dissociation probability. According to this model, charge separation distances of more than 1 nm, high charge carrier mobilities and



**Figure 8.** Dissociation probability  $P$  as a function of electric field  $F$  at various charge separation distances  $a$  at room temperature (upper panel) and at various temperatures  $T$  and fixed charge separation distance of  $a = 1$  nm (lower panel). The parameters used for the calculation are:  $\langle\mu\rangle = 10^{-4}$  m<sup>2</sup>/Vs,  $\langle\varepsilon\rangle = 3$ ,  $k_{CT\rightarrow GS} = 10^8$  s<sup>-1</sup>.

high temperatures are prerequisites for the efficient dissociation of charge-transfer excitons at moderate electric fields.

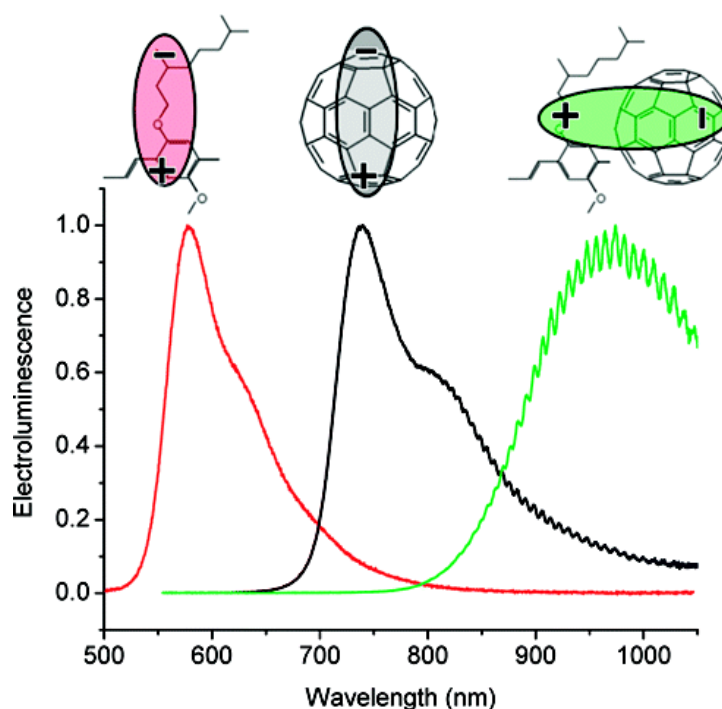
### 2.3.3 The role of charge-transfer excitons for charge separation

In this section the experimental evidence for the role of charge-transfer excitons during the formation of spatially separated charge carriers will be discussed. Much of the material presented herein has also been reviewed excellently by Clarke [39] and Deibel [40].

The charge-transfer process in polymer:fullerene composites, i.e. the separation of an exciton at an interface, has been found to be ultra-fast, happening on a sub 100 fs time scale, and very efficient with only a few percent of fullerene needed for almost quantitative exciton dissociation [41-46]. In material systems with a high degree of separation between the phases of polymer and fullerene the rate of the transfer process is usually limited by the diffusion of excitons to the interface within less than 100 ps after their

formation [31,47,48]. However, as already indicated above, charge transfer does not necessarily lead to the creation of spatially separated charges but can also result in bound interfacial charge-transfer excitons.

Such charge-transfer excitons can be uniquely identified by their photophysical properties. When two organic semiconductors are blended together and charge-transfer excitons at the interface are formed, sometimes additional features in both absorption and emission spectra are observed that cannot be assigned to any of the individual components. As charge-transfer excitons are generally lower in energy than singlet excitons, these features show a bathochromic shift relative to the transitions of the unblended materials. Electroluminescence measurements are particularly well suited for analyzing the emission from charge-transfer excitons, because here charge-transfer excitons are formed directly by the recombination of injected free charge carriers so that there is no emission from higher lying singlet excitons superimposed on the charge-transfer emission [49,50].



**Figure 9.** Electroluminescence spectra of MDMO-PPV (red line), PCBM (black line) and of a blend of these two materials [49]. Reprinted with permission from Tvingstedt et al. *Journal of the American Chemical Society* 2009, 131, 11819. Copyright 2009 American Chemical Society.

An example for this is shown in **Figure 9** by the means of electroluminescence spectroscopy of MDMO-PPV (red line), PCBM (black line) and a blend of these two materials (green line). In this case it is very obvious that the emission spectrum of the blend is not a superposition of the emission of the pristine materials, but rather originates from a charge-transfer exciton lower in energy. Similar studies have provided evidence for the existence of charge-transfer excitons in numerous polymers blended with PCBM, as well as in polymer:polymer composites. In some material systems the emission of charge-transfer excitons can be quenched by the recombination of CTEs to triplets in the donor. This requires that the energy level of the donor triplet is below the CTE level, which can be the case in polymers with very low highest molecular orbitals [39].

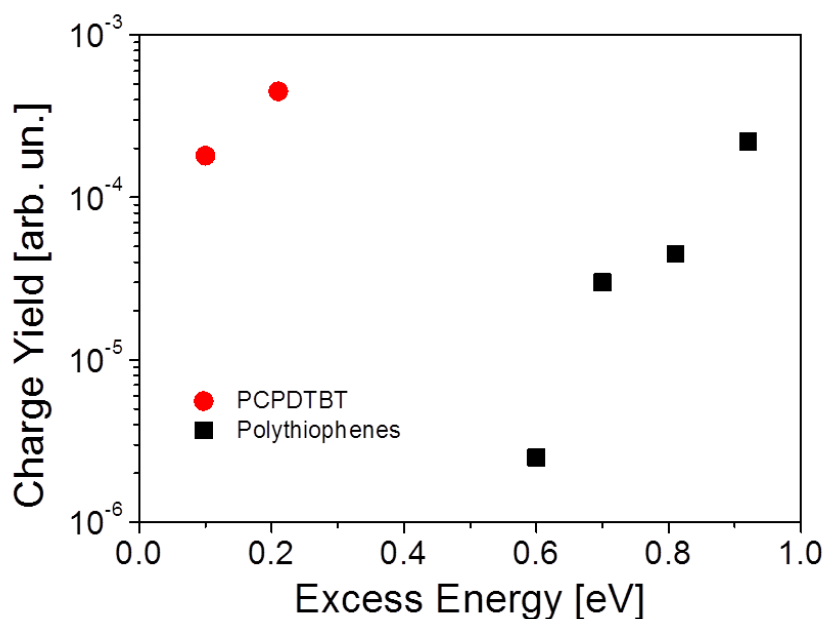
A study of the photoluminescence quenching of a series of polythiophenes blended with PCBM performed by Ohkita et al. [41] indicated that even though the charge-transfer process itself was equally efficient for all polythiophenes of the series blended with PCBM the yield of spatially separated charges differed by two orders of magnitude, depending on the ionization potentials of the polymers. This suggests that the formation of charge-transfer excitons is an intermediate step involved in charge separation. Further evidence for this assumption came from observations of the correlation between the reduction of the photoluminescence intensity of charge-transfer excitons upon the application of an electric field and a simultaneous increase of the yield of spatially separated charge carriers by Offermans et al. [33].

There are several factors that influence the ratio of recombination through charge-transfer excitons and spatial separation of charge carriers. In the following sections of this chapter the role of excess energy, morphology, charge carrier mobility, electric field and temperature on the suppression of geminate recombination and gain in the yield of spatially separated charge carriers will be discussed.

### 2.3.3.1 Excess Energy

In many cases the energy difference between the relaxed singlet exciton, i.e. the initial state of the charge-transfer process, and the relaxed charge-transfer exciton is much larger (typically  $0.1 \text{ eV} < G^* < 1 \text{ eV}$ ) [41] than the reorganization energy of the transfer process. In this situation the rate of the charge transfer between these two relaxed states is reduced, because this direct transition occurs in the Marcus inverted regime (vide supra). However, because of the strong electron-phonon coupling in organic semiconductors the charge-transfer exciton features a quasi-continuum of vibronically excited states. The transition rate from the singlet exciton to each of these levels is governed by the ratio of the respective energetic offset and the reorganization energy, with the highest transition rate to the level for which this ratio approaches unity. Consequently, the charge transfer will mainly occur between the relaxed exciton and a 'hot' vibronically excited charge-transfer exciton. These hot states have a larger electron hole distance than the relaxed state and are thus more likely to split into free charge carriers. In fact, Morteani et al. [51] found that the electron-hole distance in relaxed charge-transfer excitons is so small that they virtually do not decompose into free spatially separated charges, but only recombine geminately to the ground state. The generation of spatially separated charges was consequently assigned to the dissociation of hot charge-transfer excitons in kinetic competition with its vibrational relaxation.

Ohkita et al. [41] studied the influence of this excess energy with respect to the relaxed charge-transfer exciton on the yield of spatially separated charge carriers with a series of polythiophenes with differing singlet exciton energy levels. They found that increasing the excess energy from 0.6 to 1 eV resulted in an increase of the yield of spatially separated charge carriers by two orders of magnitude, strongly indicating that excess energy is beneficial for the separation of charge-transfer excitons. However, in a similar study Clarke et al. [52] reported a very high yield of free charge carriers for a low bandgap polymer:fullerene composite with an excess energy of less than 0.2 eV,



**Figure 10.** Yield of spatially separated charge carriers as a function of excess energy (data taken from [52]).

demonstrating that high excess energies are not a necessary prerequisite for efficient charge separation (see **Figure 10**). They speculated that the origin of the high yield of free charge carriers despite the low excess energy might be related to the donor-acceptor nature of the monomer of the studied polymer (PCPDTBT).

#### 2.3.3.2 Morphology

The morphology can potentially have a huge influence on the separation of charge-transfer excitons in various ways and consequently on a broad range of length scales, ranging from the orientation of molecules at the interface to the formation of interpenetrating phase segregated networks of blended materials. Unfortunately, collecting unambiguous and reliable structural information on the very short length scales involved is not a straightforward task. This is why most of the studies dealing with the influence of morphology on charge separation concentrate on the larger end of this scale, i.e. the influence of the extent and purity of phase segregation along with the size of phase segregated domains. To this end, a variety of methods for controlling the morphology have been exploited experimentally. Among these are variations of the sample



preparation conditions, e.g. use of different solvents [45] or annealing conditions [43,53], smaller modifications in the molecular structure such as a replacement of side-chains [31,47] or alterations of the composition of two blended materials [8]. All of these approaches have in common that they involve rather subtle changes within a series of samples under study in order to keep secondary effects that could influence charge separation, like excess energy, as minimal as possible. Following the majority of publications on this topic the following discussion will mainly concentrate on the nanoscale phase segregation within the blend films and will only give a brief outlook towards smaller length scales.

The optimal size for nanoscale phase segregation in terms of charge separation is determined by two processes. On the one hand there is an upper limit given by the exciton diffusion length (vide supra). Once the phase domains are larger than this diffusion length, not all excitons will reach the interface to undergo charge transfer but will instead recombine. On the other hand the charge carriers have to be able to move far enough from the interface to be considered spatially separated. In this context the Coulomb capture radius is often quoted as an estimation of the distance at which the Coulombic attraction of electron and hole is on the order of the thermal energy  $kT$ , and thus negligible:

$$r_c = \frac{e^2}{4\pi(\epsilon)\epsilon_0} \frac{1}{kT}. \quad (2.8)$$

For an organic semiconductor blend with an average dielectric constant of 3, this Coulomb capture radius is 19 nm at room temperature which is somewhat larger than the typical exciton diffusion length of 10 nm. Of course for this estimation it should be considered that an ideal nanomorphology does probably not exclusively consist of spherical domains, but rather of elongated structures that satisfy efficient exciton quenching along the smaller axis and at the same time allow for a sufficient separation of the charge carriers along the longer axis.

The effect of the composition of a fluorene copolymer:PCBM blend on the formation, dissociation and recombination of charge-transfer excitons was studied by Veldman et al. [8]. They used atomic force microscopy (AFM) and transmission electron microscopy (TEM) on blend films of a broad range of mixing ratios and found that while at low concentrations the PCBM is finely dispersed in the polymer, at very high concentrations the PCBM tends to aggregate and forms crystalline domains that are up to 100 nm large. Simultaneously, they performed time-resolved photoluminescence measurements and found that the emission from the charge-transfer exciton, which decayed within a few nanoseconds in the near infrared wavelength region, strongly depended on this variation in morphology. First of all the initial amplitude of the emission was reduced by the coarsening of the phase segregation. This can have three possible explanations. The simplest would be that the optical density of the films was reduced due to the larger amount of PCBM in the blend, which unfortunately was not quoted in their experimental details. Assuming the absorption was not strongly influenced by the composition, this means that either excitons were quenched less efficiently by the higher amount of PCBM or that excitons were quenched as efficiently but the relaxed (emissive) charge-transfer exciton was not populated as efficiently, meaning that at higher PCBM concentrations it might be more favorable for hot charge-transfer excitons to dissociate than to relax compared to at lower PCBM concentrations. Thus, the initial amplitude of the emission does not give an unambiguous conclusion as all of these effects can occur simultaneously. However, the lifetime of the emission is reduced at higher PCBM concentrations, which means that the charge-transfer excitons are depopulated much faster. Assuming that the recombination to the ground state is not accelerated by the addition of PCBM, this observation strongly suggests that the charge-transfer excitons are separated into free charge carriers more efficiently if the phase segregation between the polymer and the PCBM phases is increased. They also employed photo-induced absorption (PIA) experiments and measured a higher yield of long lived spatially separated charge carriers at higher PCBM concentrations, supporting these

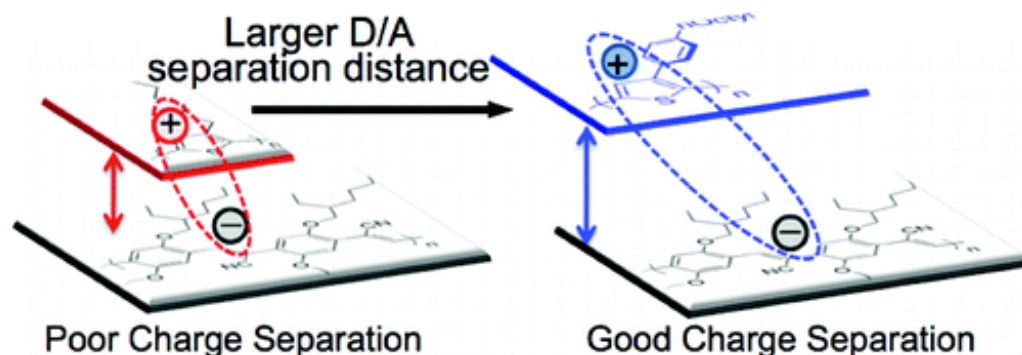
findings. Quist et al. [54] performed time-dependent microwave photoconductivity experiments and TEM on blends of MDMO-PPV and PCBM for a range of compositions prepared from both chlorobenzene and toluene solutions. They observed the same trend in phase segregation and formation of nanocrystallites with higher PCBM content. Additionally, the amount of the segregation was found to be different for the two solvents used, with a stronger segregation for the toluene cast films. Again, they found that the yield of spatially separated charges strongly correlates with the domain size.

Guo [47] and Howard [31] investigated the kinetics of singlet exciton quenching and the formation of charge-transfer excitons and spatially separated charges in blends of poly(3-hexylthiophene) (P3HT) and PCBM with transient absorption spectroscopy. They observed that for P3HT with a random distribution of head-to-tail and head-to-head couplings within the polymer chains (i.e. regiorandom P3HT) excitons were quenched ultrafast within 100 fs and that the yield of spatially separated charges from the resulting charge-transfer excitons was very low. From this they concluded that regiorandom P3HT and PCBM do not phase segregate even at modestly high PCBM concentrations (of 50%). The results for P3HT with an almost exclusively head-to-tail coupled chain (i.e. regioregular P3HT) blended with PCBM were quite different. Quenching of excitons was much slower, occurring on a 10 ps time scale, and led to a significantly higher separation probability of charge-transfer excitons. This was attributed to a much more pronounced phase segregation (also see chapter 4). In pure P3HT domains, excitons have to diffuse to the interface before charge transfer can occur, essentially reducing the charge-transfer rate to the diffusion limited case (*vide supra*). As in the studies by Veldman and Quist the larger phase segregation was found to be beneficial for the dissociation of charge-transfer excitons. Annealing in P3HT:PCBM was found to have a similar effect [43,53] and the simultaneous recovery of the photoluminescence [31,47], indicating an incomplete exciton quenching, further supported the conclusion that larger pure phase domains lead to a more facile dissociation of charge-transfer excitons.

Monte Carlo simulations by Groves et al. [55] suggested that in a polymer:polymer bilayer, charges can be considered effectively free when they are separated from each other by about 4 nm, which is clearly shorter than would be expected from the Coulomb capture radius. Nonetheless, in a blend a further increase of the phase segregation to domain sizes of up to 16 nm still increased the yield of spatially separated charges. This strongly supports the experimental findings reviewed above.

Holcombe et al. [56] directly controlled the separation distance between electrons and holes at the interface in a series of polythiophene:acceptor blends and correlated this distance with the binding energy of the charge-transfer exciton and its dissociation probability (see **Figure 11**). Not surprisingly, a larger distance between the donor and acceptor molecules resulted in a reduced charge-transfer exciton binding energy and a higher dissociation probability, showing that the precise interfacial structure strongly influences the formation of spatially separated charges. In a similar manner, Müller et al. [48] assigned an ultrafast (<0.5 ps) depolarization of the hole in a MDMO-PPV:PCBM blend to an intermolecular delocalization in the well-ordered MDMO-PPV phase and showed that by increasing the distance between electron and hole at the interface, the charge-transfer excitons were destabilized, leading to a more efficient generation of spatially separated charges. Deibel took this idea one step further and utilized Monte Carlo simulations to show that not only the order in one of the phases of the blend but also the order within single polymer chains at the interface, i.e. their conjugation length, can considerably enhance the charge separation yield [57].

In a very recent study Liu et al. performed molecular dynamics simulations on the basis of Marcus-Jortner charge transfer, explicitly accounting for structural variability at the interface of P3HT:PCBM [58]. They concluded that depending on the exact interface geometry either charge separated states or charge bridging states that can be assigned to charge-transfer excitons can be formed after the dissociation of a singlet exciton at the interface.



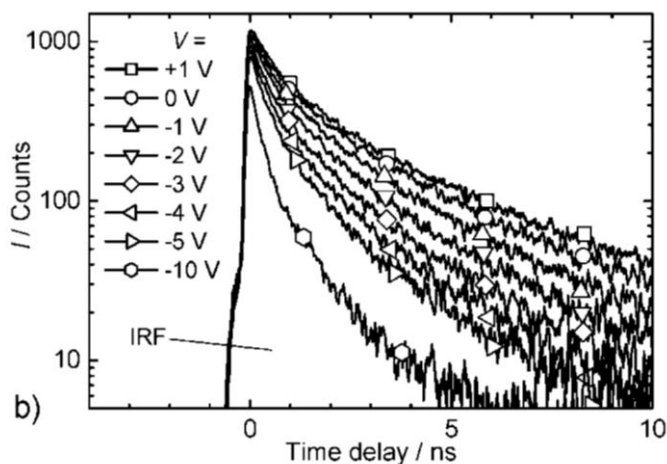
**Figure 11.** Schematic of the influence of the distance between donor and acceptor on the charge separation yield [56]. Reprinted with permission from Holcombe et al. *Journal of the American Chemical Society* 2011, 133, 12106. Copyright 2011 American Chemical Society.

Further theoretical calculations and experiments suggest that certain molecular arrangements can lead to the formation of dipoles at the interface that can reduce the Coulombic attraction between an electron and a hole in a charge-transfer exciton thus increasing the dissociation probability [59-61].

#### 2.3.3.3 Electric Field

From calculating the influence of the electric field on the dissociation of charge-transfer excitons with the Onsager-Braun model (*vide supra*), it can be expected that electric fields exceeding  $10^6$  V/m have a pronounced influence on the formation of spatially separated charge carriers. Fortunately, in many organic semiconductor composites this can be directly examined by field-dependent time-resolved photoluminescence spectroscopy of the emission from charge-transfer excitons [8,33,51]. As typical film thicknesses of such composites are on the order of 100 nm voltages of up to 100 V are more than sufficient to generate the required electric field strengths for these experiments.

Veldman et al. [8] investigated the electric field induced quenching of the emission from charge-transfer excitons in a fluorene copolymer (PF10TBT) PCBM blend as depicted in **Figure 12**. There are three especially remarkable aspects of the results of these measurements. First of all, the lifetime of the unquenched charge-transfer exciton is roughly 2.5 ns, which corresponds to a depopulation rate of the charge-transfer excitons of about  $4 \times 10^8$  s<sup>-1</sup>.



**Figure 12.** Field dependent time-resolved photoluminescence measurement of a PF10TBT:PCBM blend film of 220 nm thickness. The voltages given in the legend of the figure correspond to electric field strengths of  $F = 0 - 4.5 \times 10^7 \text{ Vm}^{-1}$  [8]. Reprinted with permission from Veldman et al. *Journal of the American Chemical Society* 2008, 130, 7721. Copyright 2008 American Chemical Society.

Second, the depopulation is strongly accelerated by the application of an electric field, increasing the total rate to above  $1 \times 10^9 \text{ s}^{-1}$  at an electric field of  $F = 4.5 \times 10^7 \text{ V/m}$ , strongly suggesting that charge-transfer excitons can indeed be split by the application of an electric field. Furthermore, by fitting the photoluminescence transients to a biexponential decay, they found that the sum of the initial amplitudes is independent of the electric field. This indicates that the formation of the CTEs is not influenced by the electric field, which was supported by the observation that the emission from singlet excitons in the polymer was not quenched simultaneously. It should be noted, that the choice of a biexponential fit was merely based on empirical findings and not on a solid consideration of the rate equation for the depopulation of charge-transfer excitons. Thus, the true physical meaning of the parameters extracted from fitting is somewhat unclear. A biexponential decay does suggest that the charge-transfer excitons are depopulated through exactly two decay channels. Applying Onsager-Braun theory, these channels could be assigned to recombination to the ground state and dissociation to spatially separated charge carriers. However, Veldman et al. observed that both rate constants are increased by the application of an electric field, whereas Onsager-Braun theory

assumes that the recombination to the ground state is independent of the electric field. One possible explanation of this deviation could be that in a polymer:fullerene composite the orientation of the interface with respect to the electric field is distributed randomly throughout the entire film. Consequently, there are some orientations of the charge carriers in the charge-transfer exciton that have a component parallel to the external field and some that have an antiparallel component. While the former will be more likely to dissociate into spatially separated charge carriers, the latter could show an enhanced likelihood for recombination, so that both rate constants would be increased. Such an effect is not considered by Onsager-Braun theory that only takes a homogeneous medium into account.

Kern et al. [37] also used field induced photoluminescence quenching of the emission from charge-transfer excitons to determine their binding energy according to the Onsager-Braun model. They observed that in this particular material system, fields in excess of  $10^8$  V/m had to be applied in order to dissociate a significant fraction of the charge-transfer excitons. Estimations of the binding energy yielded a value of 0.2 eV which corresponds to an average separation distance between the charge carriers of 2 nm.

It is further worthy of note that results from transient absorption spectroscopy suggest that in certain material systems like P3HT:PCBM a very high yield of spatially separated charges can be found, even in the absence of an external electric field, so that the electric field can only have a minor influence on the overall charge separation yield (see also chapter 4) [31,47,62]. Marsh et al. recently claimed to have observed field-assisted charge-transfer exciton dissociation in P3HT:PCBM at applied voltages between open circuit voltage and -5V by transient absorption spectroscopy [63]. However, their evidence is rather circumstantial, as their observed changes in the charge carrier kinetics upon application of a reverse bias is also compatible with a reduced non-geminate recombination. As they perform their experiments at an excitation density that leads to a reduction of the external quantum efficiency at short circuit by 50% due to non-geminate recombination (i.e. charge carrier

densities much higher than found in a solar cell under AM1.5G illumination), their experimental results cannot unambiguously be interpreted as a field-assisted separation of charge-transfer excitons, rather than suppression of non-geminate recombination by the applied electric field.

### 2.3.3.4 Other factors

While excess energy, morphology and electric field are the most frequently studied parameters influencing the dissociation of charge-transfer excitons, there are still a number of other factors that have to be considered. Among these are the temperature and charge carrier mobilities as already mentioned in the introduction of Onsager-Braun theory. But also of importance are the details of the charge-transfer process, like electronic coupling or reorganization energies or effects of energetic disorder.

In P3HT:PCBM blends Mauer et al. [64] reported that the high yield of spatially separated charges was not influenced by reducing the temperature down to as low as 80 K (see chapter 4). While this seems surprising considering that from Onsager-Braun theory one would expect an exponential dependence on the temperature, it can be argued that the thermal activation by  $\sim 25$  meV is negligible compared to the excess energy of 1 eV that results from the charge-transfer process. Furthermore, the mobility of holes and electrons is reduced by about two orders of magnitude when decreasing the temperature to 80 K. This suggests that in this case the charge carrier mobilities also do not play a crucial role for the dissociation of charge-transfer excitons. This finding was supported by observations by Ohkita et al. who found no correlation between the hole mobility and dissociation yield when studying polymers with hole mobilities varying over four orders of magnitude [41].

McMahon et al. have recently demonstrated, with the help of a combination of classical and quantum simulation methods, that the electronic structure of P3HT in contact with PCBM is significantly altered compared to bulk P3HT [65]. It is characterized by an increase in energetic disorder at the interface that is accompanied by an increase of the bandgap of P3HT. This increase of



the bandgap could present a driving force for charge separation, pushing charge carriers away from the interface into the more ordered bulk-like regions of the pure P3HT domains.

Finally, density functional theory calculations of the localization of the involved molecular wave-functions predicted a bridging state across the interface of P3HT and fullerene molecules that promotes an adiabatic charge-transfer process [66]. Additionally, this bridging state was found to have a considerable overlap with LUMO states in the fullerene, thus increasing the separation probability of the charge-transfer excitons.

## 2.4 Charge Transport

Charge transport is an omnipresent motif repeating itself in the physical mechanisms that govern the device performance of organic solar cells. A detailed understanding of the underlying principles of charge transport is thus very important when trying to correlate molecular structures, charge transport properties and device performance. In this section an introduction to the Gaussian disorder model for the description of the temperature and electric field dependence of the charge carrier mobility in organic semiconductors, along with extensions that cover the charge carrier density dependence of the mobility, is presented. Further information on charge transport in disordered semiconductors can be found elsewhere [67].

### 2.4.1 The Gaussian Disorder Model

As described above, organic semiconductors lack translational symmetry, but instead rather consist of an ensemble of localized sites with slightly varying energetic levels and distances between them. For this reason the well-established concept of band-like transport is not applicable to charge carriers in organic semiconductors. Instead hopping of electrons (holes) between localized LUMO (HOMO) states has to be taken into account. Bässler was the first to suggest a model of charge transport based on hopping of charge carriers in a Gaussian density of states [68]. The hopping rate  $\nu$  is assumed to depend both on the energetic offset and on the spatial distance between the sites. It follows the Miller-Abrahams [69] rate for a jump from site  $k$  to site  $l$  with the energies  $E_k$  and  $E_l$  at a distance  $\Delta r_{k,l}$  and temperature  $T$ :

$$\nu_{k,l} = \nu_0 \exp[-\Gamma \Delta r_{k,l}] \begin{cases} \exp\left[-\frac{E_l - E_k}{kT}\right], & E_k < E_l \\ 1, & E_k \geq E_l \end{cases} \quad (2.9)$$

Here  $\nu_0$  is the attempt to jump frequency. The first exponential depends on the inverse localization radius  $\Gamma$  and the distance between sites. If the initial site of the hopping process  $k$  is lower in energy than the final site  $l$ , i.e.  $E_k < E_l$ , an additional Boltzmann-factor has to be taken into account. In this formalism the reorganization of the molecular structure due to the movement of the charge

carrier, i.e. its polaronic nature, is not included and electron-phonon coupling is limited to the thermal activation of the charge-transfer step during the hopping process. This description takes into account the fact that there is a penalty on the hopping rate for hopping to distant sites and to sites higher in energy. It should be noted, that while jumps to and from distant sites without energy difference have identical transition rates this is not the case for sites with an energetic offset. An important consequence of this observation is that sites that are very low in energy can act as traps for charge carriers, because they accept charge carriers very quickly but release them only slowly. Spatially isolated sites however cannot trap charges as efficiently because of the symmetry of the trapping and detrapping rates [70].

During macroscopic charge transport a large number of sites with different energetic and spatial distances are sampled by each charge carrier. This corresponds to a multiple trapping and detrapping mechanism of charge carriers, where the trapping time of every site is determined by the corresponding hopping distance and energetic offset to the next site. BäSSLER takes this into account in his model by assuming Gaussian distributions for the site energies  $E_i$  (as introduced above) and the jump distances  $\Delta r_{k,l}$  with widths  $\sigma$  and  $\Sigma$ , respectively. Using these assumptions in Monte Carlo simulations yields a formula describing the electric field (F) and temperature (T) dependence of the mobility of a charge carrier hopping in a disordered material

$$\mu(\sigma, \Sigma, T, F) = \mu_0 \exp \left[ - \left( \frac{2\sigma}{3kT} \right)^2 \right] \exp \left[ C \left\{ \left( \frac{\sigma}{kT} \right)^2 - \Sigma^2 \right\} \sqrt{F} \right], \quad (2.10)$$

with zero-field (and infinite temperature) mobility  $\mu_0$  and an empirical constant  $C = 2.9 \times 10^{-4} (\text{cm/V})^{1/2}$ .

This model is very successful at predicting a number of experimental observations. Among these are a  $1/T^2$  temperature dependence rather than an Arrhenius-type activation, a Poole-Frenkel like field dependence, i.e.  $\ln(\mu) = \beta\sqrt{F}$ , as well as an increase of the slope  $\beta$  with decreasing temperature

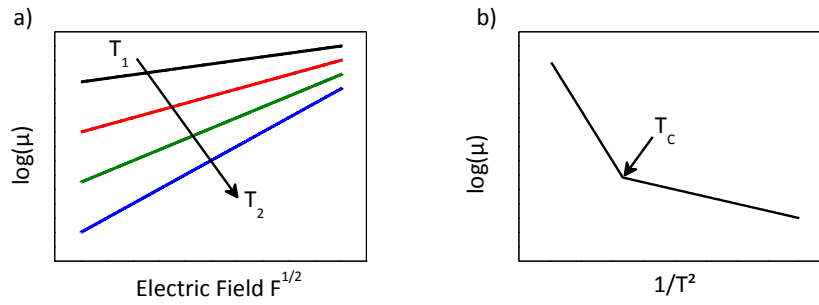
in a Poole-Frenkel plot (see **Figure 13a** ). It was also found that the equation above is only applicable to a temperature range between the glass transition temperature  $T_g$  and a critical temperature  $T_c$  of the polymer ( $T_g > T_c$ ) [71]. This critical temperature was empirically found to depend on the energetic disorder and the length of the charge transport distance  $L_0$ , i.e. the thickness of a sample, according to

$$\left(\frac{\sigma}{kT_c}\right)^2 = 44.8 + 6.7 \times \log(L_0). \quad (2.11)$$

Typical values of energetic disorder of  $\sigma = 100$  meV and thickness of  $L_0 = 5$   $\mu\text{m}$  yield a critical temperature of around 250 K [72]. At temperatures below  $T_c$  the slope of the temperature dependence (i.e. the prefactor in the exponent) of the mobility at zero field decreases (see **Figure 13b** ).

$$\mu(\sigma, T) = \begin{cases} \mu_0 \exp\left[-\left(\frac{2\sigma}{3kT}\right)^2\right], & T > T_c \\ \mu_0 \exp\left[-\left(\frac{\sigma}{2kT}\right)^2\right], & T < T_c \end{cases} \quad (2.12)$$

The origin of this phenomenon is closely related to the disordered nature of the energy landscape. At high temperatures the charge carriers created in a sample can equilibrate within the density of states much faster than their average transit time through the sample. Consequently, the average charge carrier mobility obtained from an experiment does correspond to the equilibrium charge carrier mobility and is independent of the sample thickness. At temperatures below  $T_c$  the time needed for equilibration is longer than the transit time of charge carriers through the sample, which means that the charge carrier mobility determined from an experiment would no longer be the equilibrium charge carrier mobility and the actual value would strongly depend on the sample thickness. These two regimes of charge transport are termed non-dispersive and dispersive charge transport, respectively.



**Figure 13.** Schematic a) of the electric field dependence of the charge carrier mobility  $\mu$  at various temperatures ( $T_1 > T_2$ ) and b) of the temperature.  $T_c$  indicates the critical temperature at which the transition from non-dispersive to dispersive transport occurs.

Another consequence of hopping transport in a Gaussian density of states that has not been taken into account by Bässler's model is the effect of the charge carrier density on the mobility. Qualitatively, for charge carriers occupying sites in the tail of the DOS the mobility is smaller, because the number of unoccupied sites that are accessible by a jump is smaller than for sites closer to the center of the density of states. As the DOS is filled by an increasing charge carrier density in a sample more charge carriers occupy sites closer to the center of the DOS, which means that a larger number of charge carriers, each with a higher mobility, are available for charge transport. Consequently, the mobility averaged over all charge carriers increases as the DOS is successively filled by the introduction of additional charge carriers. This effect has been described quantitatively by Pasveer et al. [73]. Using numerical simulations they were able to develop a parametrization scheme to quantitatively describe the density dependence of the mobility:

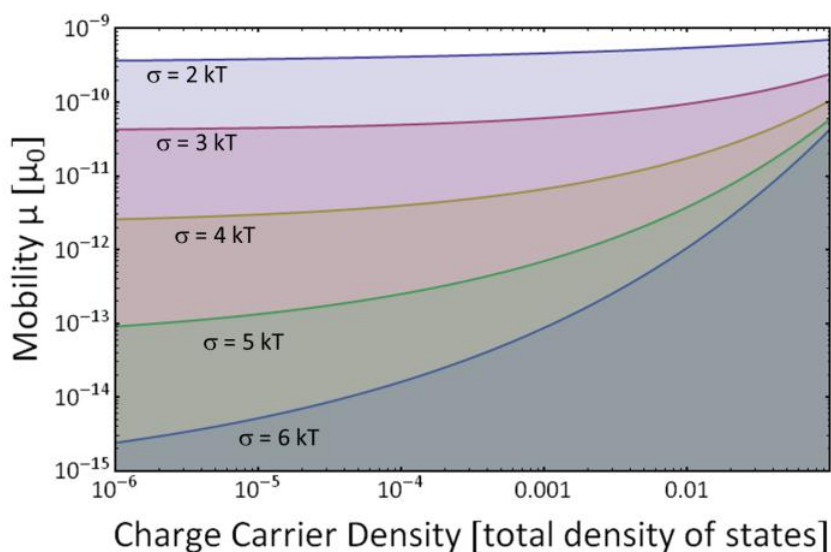
$$\mu(T, n) = 1.8 \times 10^{-9} \mu_0 \text{Exp} \left[ -0.42 \hat{\sigma} + \frac{1}{2} (\hat{\sigma}^2 - \hat{\sigma}) \left( 2 \frac{n}{n_{tot}} \right)^\delta \right], \quad (2.13)$$

with

$$\delta = 2 \frac{(\ln[\hat{\sigma}^2 - \hat{\sigma}] - \ln[\ln[4]])}{\hat{\sigma}} \quad (2.14)$$

and

$$\hat{\sigma} = \frac{\sigma}{kT}. \quad (2.15)$$



**Figure 14.** Dependence of the charge carrier mobility  $\mu$  (in units of the prefactor  $\mu_0$ ) on the charge carrier density (given in relative numbers with respect to the total Gaussian density of states with width  $\sigma$ ) at various ratios of energetic disorder  $\sigma$  to thermal energy  $kT$ .

This dependence is shown in **Figure 14** for ratios of the energetic disorder to the thermal energy between 2 and 6 (an energetic disorder of 100 meV at room temperature corresponds to a ratio of 4). The total density of states in organic semiconductor blends used for organic solar cells is on the order of  $10^{19} \text{ cm}^{-3}$  and the occupied density of states in an organic solar cell under solar illumination is  $10^{15} - 10^{17} \text{ cm}^{-3}$  [74]. Thus a ratio of  $n/n_{\text{tot}} = 10^{-4} - 10^{-2}$  is typical for organic solar cells under standard operating conditions. Clearly, the density dependence gains importance when the energetic disorder increases or the temperature decreases, in agreement with the qualitative discussion presented here. In both cases the charge carriers predominantly occupy states in the tail of the DOS which limits the number of sites that are accessible by a jump. At low charge carrier densities the temperature dependence predicted by Bässler's model is recovered.

Shuttle et al. [75] empirically observed that the relation between the charge carrier mobility and the charge carrier density in an organic solar cell can be approximated by a power-law at room temperature and if only low charge carrier concentrations are present in the device:

$$\mu(n) = \mu_0 n^\delta. \quad (2.16)$$

In a blend of P3HT and PCBM they found that  $\delta = 0.35$  for charge carrier densities between  $10^{-14}$  and  $10^{-16}$  cm<sup>-3</sup>. The energetic disorder in P3HT:PCBM blends is well below 100 meV [76] and consequently the ratio of energetic disorder to thermal energy is smaller than 4 at room temperature. In this regime the parameterization scheme by Pasveer can be approximated by a power-law so that it is qualitatively in agreement with Shuttle's findings.

Furthermore, in material systems with comparable energetic and static disorder the density dependence can be more important than the field dependence of the mobility. Experimentally it is not always straightforward to discriminate between the effects of temperature, field and charge density, as often the determined charge carrier density in a sample depends on the temperature or on the electric field (or on both) as for example is generally the case for mobility measurements in diode-like device structures.

#### **2.4.2 Experimental methods for determining charge carrier mobilities**

The charge carrier mobility in an organic semiconductor is not a well-defined property. It can range from very high mobilities during transport within a  $\pi$ -conjugated system to very low hopping mobilities that can depend both on the sample thickness and on the time scale considered. This complicates a meaningful experimental determination of "the" mobility. In the past a number of experimental techniques have been established that each cover a certain range of experimental boundary conditions, like electric field strengths, charge carrier densities or transport length scales. When studying charge transport in an organic semiconductor, one has to carefully choose the technique that best suits the requirements for a given problem. A short introduction to a selected few of these techniques will be given in this section along with some examples of resulting charge carrier mobilities.

#### 2.4.2.1 The Time-Of-Flight Technique

The time-of-flight technique (TOF) is an integral part of the experimental methods used for this dissertation and will be discussed further in the experimental section. It was first used in the 1960s [77,78]. In short, the material to be tested is sandwiched between two electrodes of which at least one is semi-transparent, to allow photogeneration of charges. A pulsed laser (typical pulse length  $<10$  ns) is used to photogenerate a package of charge carriers close to one of the electrodes. By applying an electric field the charge carrier package is driven through the sample and is extracted when it reaches the counter electrode. The movement of the charge carrier package causes a transient current flow in the external circuit that can be recorded with an oscilloscope. From this transient the transit time  $t_{tr}$  of the package through the sample can be determined and with knowledge of the thickness  $d$  of the sample and the applied electric field  $F$  the mobility can be calculated:

$$\mu_{TOF} = \frac{d}{t_{tr} \times F}. \quad (2.17)$$

This method allows analyzing the charge carrier mobility over a relatively wide range of electric fields and temperatures. One big advantage of TOF is that by choosing the direction of the electric field (or the electrode at which the charge carriers are generated) it is possible to measure electron as well as hole mobilities independently. The range of mobilities that can be determined with this technique strongly depends on the time-resolution of the setup and the thickness of the sample. Usually transit times have to be longer than  $1 \mu\text{s}$ , due to RC effects in the external circuit. The film thickness has to be much larger than the spatial extension of the charge carrier package, which roughly corresponds to the penetration depth of the laser into the sample. This practically means that the sample thickness should be at least on the order of  $1 \mu\text{m}$ . Also the transit time has to be long enough to guarantee complete relaxation of the charge carrier package during the transport to give meaningful results.



TOF is particularly useful for testing the Gaussian disorder model, because it studies the transport of a rather low concentration of charge carriers that are initially randomly distributed in the DOS, so that for example relaxation effects can be observed. Also the current transient itself contains information about the influence of disorder on the charge transport properties that can be correlated with the results of the field and temperature dependence of the mobility.

Charge carrier mobilities of conjugated polymers determined with TOF measurements range from as high as  $10^{-2}$  cm<sup>2</sup>/Vs [79] down to  $10^{-9}$  cm<sup>2</sup>/Vs [80].

#### 2.4.2.2 Space-Charge-Limited Currents

In contrast to most of the techniques described here the space-charge-limited current (SCLC) method is a steady-state technique. For SCLC a similar sample preparation as for TOF is required, i.e. a diode-like sample geometry. If the current injection into such an organic semiconductor diode is not limited by the contacts (i.e. the contacts are Ohmic) but by a build-up of space charge in the sample the current density  $J$  follows a certain voltage ( $V$ ) dependence that allows the extraction of a charge carrier mobility (Mott-Gurney law) [81]:

$$J(V) = \frac{9}{8} \epsilon_0 \epsilon_r \mu \frac{V^2}{d^3}. \quad (2.18)$$

The most important prerequisite for this technique is that the current is actually limited by space charge effects and not by charge injection. This can be tested by preparing multiple samples of varying thicknesses to confirm the  $1/d^3$  dependence. Unfortunately, as the number of electrode materials with suitable work-functions to create Ohmic contacts is limited, this technique can only be applied to organic semiconductors with specific positions of the energy levels. Electron and hole mobilities can be measured independently from each other if electrode materials for creating Ohmic contacts selectively for electrons or holes can be found. This requires different samples for electron and hole mobility measurements of course (i.e. electron-only and hole-only

devices) [6]. Generally, the mobilities determined by SCLC [6] are comparable to TOF mobilities [76].

For this method it is assumed that the charge carrier mobility is constant over the entire voltage range studied. This is problematic, because both the electric field and the charge carrier density change with the applied voltage so that this technique is not easily applicable to organic semiconductors. For materials with only shallow traps, i.e. non-dispersive transport with relatively low energetic disorder, it can be used to determine an average charge carrier mobility if the fraction of trapped to mobile charge carriers can be estimated [82].

#### 2.4.2.3 Dark Injection-SCLC

The dark injection space-charge-limited currents (DI-SCLC) technique is the time-resolved analog of SCLC. For DI-SCLC a voltage step is applied to the sample and the evolution of the resulting current is monitored over time. The voltage step has to be high enough to inject a sheet of space charge into the sample, so that the current transient reflects the movement of the front of the space charge sheet through the sample. Similar to TOF, the characteristic shape of the transient can then be used to determine a transit time of the charge carriers through the sample. Furthermore, this space-charge-limited transit time can be related to the space-charge-free (SCF) transit time by

$$t_{SCL} = 2 \left( 1 - \exp\left(-\frac{1}{2}\right) \right) t_{SCF} \approx 0.787 t_{SCF}, \quad (2.19)$$

which corresponds to the transit time in a TOF experiment. The prerequisites for this technique are similar to the steady-state SCLC measurements concerning e.g. the choice of electrodes. Traps in the material that hinder charge transport influence the shape of the transient and complicate the extraction of the transit time. Nonetheless, a determination of the mobility is still possible in many cases. Importantly, for the determination of mobilities it is not necessary to assume that they are independent of the electric field or the charge carrier density. Theoretically with this technique it is also possible to

determine charge carrier mobilities from samples much thinner than with TOF measurements. However, as the capacitance of a sample increases with decreasing thickness, the RC constant of the setup starts to influence the shape of the current transient and eventually makes the extraction of a meaningful transit time impossible. For example, for a sample thickness of 100 nm, a relative dielectric constant of 3.5, a sample area of 0.1 cm<sup>2</sup>, a mobility of 10<sup>-4</sup> cm<sup>2</sup>/Vs, an applied voltage of 5 V and a resistance of 100 Ω in the external circuit, a RC time-constant of 310 ns and a transit time of only 157 ns would be expected. Even though it may still be possible to subtract the RC response from the transient experimentally [83] or during data analysis this still presents a major source of uncertainty for the determination of the charge carrier mobility in thin samples. As for SCLC, DI-SCLC gives mobilities comparable to TOF mobilities [76].

#### 2.4.2.4 Photo-CELIV

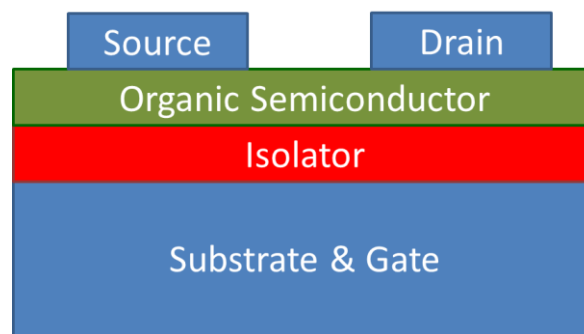
Photogenerated charge extraction by linearly increasing voltage (photo-CELIV) [84] is a technique comparable to TOF in that a certain number of charge carriers is created in the sample by a short laser pulse and then extracted by an electric field. There are two major points that differ between TOF and photo-CELIV. The first is that charge carriers do not have to be created as a small package near one of the electrodes but they can be generated homogeneously throughout the sample. This makes it possible to study thin samples (under the same constraints concerning the RC time constant of the setup as for all transient electronic techniques). The second difference is that for photo-CELIV, rather than using a steady-state electric field for the extraction, a linearly increasing voltage ramp that starts a defined time after the generation of the charge carriers is employed. By varying the delay time between charge generation and extraction both a change of the charge carrier mobility and the decay of the charge carrier density due to recombination can be studied as a function of time. However, it is important that the number of charge carriers is not changed by injection or extraction. It is not trivial to achieve this, because at room temperature the net current flowing in a solar cell is a superposition of

the extracted photocurrent and the injected dark current and there is not necessarily a voltage at which charges are neither extracted nor injected. At lower temperatures however, the injected dark current is strongly reduced, because injection from metals into organic semiconductors is a thermionic process (vide infra). If the injection of charge carriers is suppressed in such a way, the sample can be held at the voltage at which the photocurrent vanishes (i.e. close to the open circuit voltage) so that none of the photogenerated charge carriers are extracted [85]. As for the other techniques the mobility can be determined from the characteristic shape of the current transient. Mobilities determined by photo-CELIV [86] are comparable to TOF and SCLC measurements [76].

### 2.4.2.5 Organic Field-effect Transistors

All techniques mentioned so far use diode-like devices to determine the charge carrier mobility. This is very convenient, because except for thickness limitations this is the same configuration as is used for organic solar cells. So when studying the charge transport of materials for use in organic solar cells these techniques would be the obvious choice. It is however also possible to measure the charge carrier mobility in other device configurations, like in organic field-effect transistors. A field-effect transistor is an electronic switch with three electrodes, a source, a drain and a gate, as shown in **Figure 15**. The organic semiconductor connects the source and the drain electrodes and is separated from the gate electrode by an isolating layer, called the gate dielectric. A voltage applied across the organic semiconductor between gate and source ( $V_{GS}$ ) can be used to switch the current flowing between source and drain ( $I_{DS}$ ). If no gate source voltage is applied ( $V_{GS}=0$ ) the only current flowing in the organic semiconductor layer is caused by charge carriers injected from the source and drain electrodes. As the distance between drain and source is usually relatively large (several  $\mu\text{m}$ ) the electric field resulting from applying a voltage between drain and source ( $V_{DS}$ ) is rather weak so that only a small number of charge carriers can be injected, leading to a negligible source-drain current. If a gate-source voltage is applied, the electric field will induce charge

carriers at the semiconductor isolator interface. These additional charge carriers can be extracted at source and drain, resulting in a much higher source-drain current. In other words the gate-source voltage can be used to switch the resistance of the organic semiconductor layer and thus the current flow between source and drain by inducing additional charge carriers in the organic semiconductor. OFETs can be either n-type (corresponding to an electron only device), p-type (hole-only) or ambipolar depending on the position of the energy levels and the sign of the gate-source voltage.



**Figure 15.** Schematic of an organic field-effect transistor.

Similar to the SCLC method, the field-effect charge carrier mobility  $\mu$  can be determined from the (source-drain) current (gate-source) voltage characteristics:

$$I_{DS} = \frac{WC_i}{2L} \mu (V_{GS} - V_0)^2. \quad (2.20)$$

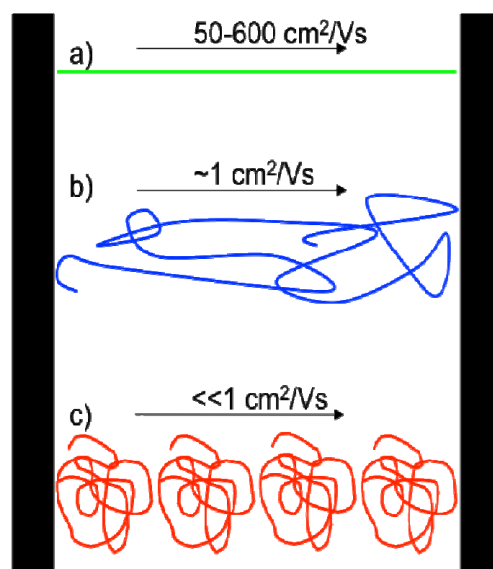
The channel length  $L$  corresponds to the distance between the source and drain electrodes, the channel width  $W$  to the size of the electrodes perpendicular to  $L$ .  $V_0$  is the threshold (gate-source) voltage needed to create a charge sheet at the interface between semiconductor and insulator. Finally,  $C_i$  is the capacitance per unit area of the insulating layer.

In an OFET the charge carrier density induced by the gate-source voltage is much higher than for all other techniques introduced in this section. Because of the charge carrier density dependence of the mobility in organic semiconductors, the mobility measured in OFETs is much higher than for the other methods. Brondijk et al. compared the hole-mobility in regioregular

P3HT measured by SCLC and in OFETS and found values of around  $10^{-4}$   $\text{cm}^2/\text{Vs}$  with SCLC (also comparable to TOF [76]) and up to  $3 \times 10^{-2}$   $\text{cm}^2/\text{Vs}$  in the OFETS [87]. They attributed the difference to the higher charge carrier density in the OFETS.

### 2.4.2.6 Pulsed-Radiolysis Time Resolved Microwave Conductivity

Pulsed-radiolysis time resolved microwave conductivity (PR-TRMC) experiments can be used to study the motion of charge carriers within  $\pi$ -conjugated systems. For PR-TRMC mobile charges are created in the sample through scattering ionization by a high energy ( $\sim 3$  MeV), pulsed ( $\sim 10$  ns) electron beam rather than by injection through electrodes or photogeneration [88]. These charges can oscillate in an applied microwave field ( $\sim 30$  GHz), thereby attenuating it. The amount of attenuation is proportional to the product of charge carrier mobility and density. As the charge carrier density can be calculated from the energy loss of the electron beam passing through the sample, this allows for the determination of the charge carrier mobility. By design this technique only samples very short length scales, that correspond to the distance a charge carrier moves during one oscillation cycle, i.e.  $\sim 30$  ps. The mobility obtained from PR-TRMC measurements is thus not governed by the inter-site hopping of charge carriers but rather by intra-site charge motion. Consequently, the results differ very much from techniques that study macroscopic hopping transport. Charge carrier mobilities as high as  $600$   $\text{cm}^2/\text{Vs}$  have been measured for isolated planar ladder-type poly(p-phenylene) chains in solution, which is close to charge carrier mobilities of crystalline inorganic semiconductors. Twists of the polymer backbone (**Figure 16b**), chemical interruption of the  $\pi$ -conjugation and interchain interactions (**Figure 16c**) were found to strongly reduce the mobility, demonstrating that disorder does not only influence macroscopic, but also microscopic intra-site transport [89].



**Figure 16.** Schematic representation of the influence of polymer chain configurations on the charge carrier mobility. In a) a single stretched, in b) a single coiled polymer chain and in c) multiple strongly coiled polymer chains connect the electrodes of a device [89]. Reprinted with permission from Grozema et al. *The Journal of Physical Chemistry Letters* 2011, 2 (23), 2951. Copyright 2011 American Chemical Society.

## 2.5 Non-geminate Charge Recombination

Non-geminate recombination is the recombination of spatially separated, i.e. “free”, charge carriers that do not necessarily originate from the same exciton, as opposed to the geminate recombination of charge carriers bound in an interfacial charge-transfer exciton. In this section, a fundamental description of the kinetics and charge carrier density dependence of non-geminate recombination will be given.

The most basic requirement for recombination of independently moving opposite charge carriers (i.e. electrons and holes) is that they approach each other close enough to enter their mutual capture radius. This is a random process that is basically dominated by the probability of two charge carriers meeting. This kind of recombination was first described by Langevin [18,90] for the recombination of ions in gases. An important requirement for Langevin recombination to be applicable is that the mean free path of a charge carrier (i.e. the typical length scale of the motion of a charge carrier) is much shorter than the capture radius of two opposite charges. The typical length scale of charge motion in an organic semiconductor can be considered to be limited either by the dimension of the  $\pi$ -conjugated system of the site or by the hopping distance between neighboring sites. In any case it is well below the Coulomb capture radius of more than 10 nm (vide supra), so that this prerequisite can be considered fulfilled in disordered organic semiconductors. The Langevin recombination rate  $R$  is proportional to the product of the electron ( $n$ ) and hole ( $p$ ) densities in the material:

$$R = \gamma np. \quad (2.21)$$

The proportionality factor  $\gamma$  depends on the sum of the mobilities of electrons ( $\mu_e$ ) and holes ( $\mu_h$ ) and the dielectric constant of the material  $\epsilon_r$ :

$$\gamma = \frac{e(\mu_e + \mu_h)}{\epsilon_0 \epsilon_r}. \quad (2.22)$$

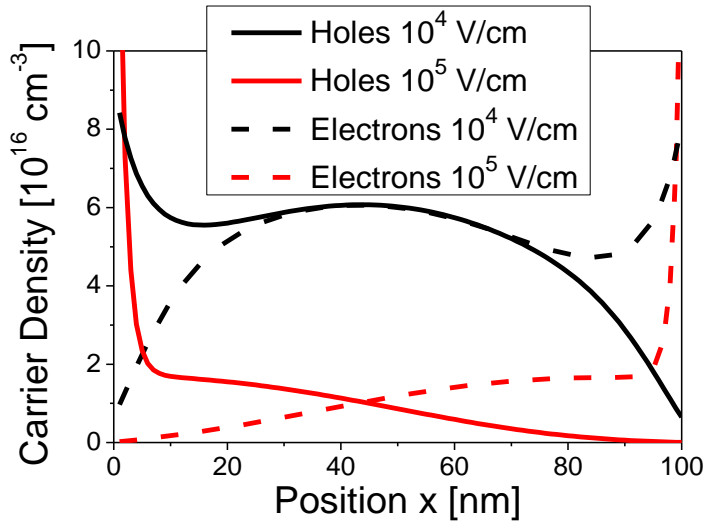
Here  $e$  is the elementary charge and  $\epsilon_0 = 8.854... \times 10^{-12} \text{ As/Vm}^2$ , the vacuum permittivity. Using values typically found in organic semiconductors of  $\mu =$



$\mu_e + \mu_h = 10^{-4} \text{ cm}^2/\text{Vs}$  and  $\epsilon_r = 3.5$  yields  $\gamma = 6 \times 10^{-11} \text{ cm}^3/\text{s}$ . Essentially, according to this formalism the recombination rate increases if there are more charge carriers and if the charge carriers move faster. In experiments that try to determine the recombination kinetics in organic semiconductors, deviations from the Langevin rate, concerning both the prefactor [84,85,91-93] and the density dependence [85,91,94], are frequently observed. This is not surprising, as organic semiconductors are not three dimensionally isotropic and homogeneous media as are the gases for which the theory was originally developed. In blends of organic semiconductors, as used for solar cell devices, electrons and holes are each confined to one of the material phases present in the blend, so that recombination can only occur at an interface. This strongly reduces the recombination rate and requires the insertion of an additional prefactor  $\xi$  into the Langevin recombination rate that accounts for the interfacial area and is typically about  $10^{-1}$  to  $10^{-3}$  [84,85,91-93]. Other effects, like a shift of the energy levels due to higher amounts of disorder close to the interface that rejects charge carriers, may also contribute to this prefactor. Concerning deviations from the intensity dependence, a number of explanations have been offered. One of these is that as introduced above, the charge carrier mobility itself can depend on the charge density, leading to an additional charge carrier density dependence of the recombination rate. Assuming equal charge carrier densities for electrons and holes  $n = p$  results in a recombination rate of

$$R = \xi \frac{e(\mu_e + \mu_h)}{\epsilon_0 \epsilon_r} n^2. \quad (2.23)$$

The assumption of equal charge carrier densities is valid for photogenerated charges due to the requirement of the conservation of charge. It is furthermore valid for every position  $x$  in a sample of thickness  $d$  in the absence of an electric field, i.e.  $n(x) = p(x)$  for  $0 < x < d$  (assuming similar diffusion coefficients of electrons and holes or vanishing concentration gradients). An electric field however drives the electrons towards the anode leading to an increase of electrons at the anode and to a depletion at the cathode (and oppo-



**Figure 17.** Example of the distribution of electron (dashed lines) and hole (solid lines) concentrations in a solar cell device (anode at  $x = 0$  nm and cathode at  $x = 100$  nm). At an electric field of up to approximately  $10^4$  V/cm (black) the relation  $n(x) = p(x)$  holds over roughly 60% of the layer thickness, at  $10^5$  V/cm (red) it is only valid for  $x \sim d/2$ . The average electron and hole densities are equal irrespective of the applied electric field. Note that for this example the injection barriers for holes and electrons are not exactly equal, resulting in a slight shift of the position where electron and hole densities are equal (i.e. 45 nm instead of 50 nm).

sitely for holes), so that generally  $n(x) \neq p(x)$  except for  $x \sim d/2$ . Still in this case the average electron and hole densities are equal irrespective of the applied electric field:  $n = \frac{1}{d} \int_0^d n(x) dx = \frac{1}{d} \int_0^d p(x) dx = p$ . This is shown in **Figure 17**. Different injection barriers for electrons and holes at the interfaces to the electrodes can lead to non-equal densities of electrons and holes injected into a sample, with electron-only or hole-only devices as the extreme cases.

As has been pointed out by Juska et al. [95], the reaction order of the recombination can also be limited by the dimensionality of the charge carrier motion. For two dimensional charge transport for example, the reaction order increases from 2 to 2.5 and the prefactor scales according to

$$\gamma_{2D} = \frac{3}{4} \sqrt{\pi l^3} \gamma_{3D}, \quad (2.24)$$

with  $l$  being the thickness of the limited dimension. Altogether, the modified Langevin recombination rate applicable to blends of organic semiconductors is best described by

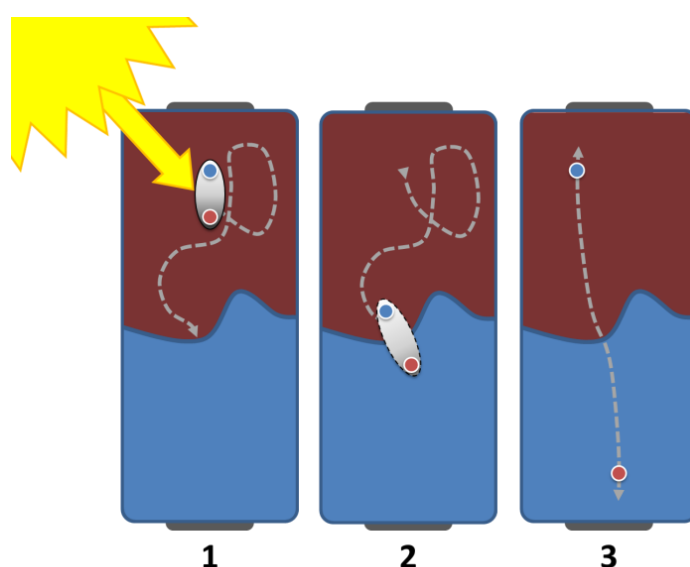
$$R = \xi \frac{e(\mu_e + \mu_h)}{\varepsilon_0 \varepsilon_r} n^{\lambda+1}. \quad (2.25)$$

It is not straightforward to predict the prefactor  $\xi$  and the reaction order  $\lambda+1$  as they both strongly depend on the exact morphology of a sample that can be influenced not only by material properties but also by sample preparation conditions. They therefore need to be determined empirically for any given sample.

## 2.6 Organic Solar Cells

Organic solar cells are devices that use organic semiconductors to convert the optical power of absorbed light into electrical power. The main figure of merit of any type of solar cell is the efficiency with which the power is converted, i.e. the power conversion efficiency (PCE). The PCE is a combination of how many charge carriers per incident photon can be collected at the electrodes and which fraction of the energy of each photon can be preserved by the charge carriers. In organic solar cells the ratio of incident photons to collected charge carriers, also called the external quantum efficiency, is the result of a cascade of processes. At the beginning of this cascade is the absorption of photons. For this, the absorption spectrum of any organic semiconductor that is to be used in an organic solar cell has to be tuned to absorb as many photons coming from the sun as possible. As was already pointed in the section on absorption of light, the absorption of a photon in an organic semiconductor does not directly lead to the generation of free charge carriers, but to the formation of bound singlet excitons. Consequently, the next step in the cascade after as many photons from the sun as possible have been converted into excitons is the dissociation of these excitons into free charge carriers. To achieve this in organic solar cells two organic semiconductors with different energy levels are blended together (a donor and an acceptor) to form a so called bulk heterojunction. If an exciton is created in one of these semiconductors it can diffuse to an interface between the two materials and be dissociated by a charge-transfer process. The advantage of a bulk heterojunction compared to a bilayer device architecture is that the area of the interface is much larger, thus allowing a much more efficient quenching of excitons. The result of the dissociation of singlet excitons can either be charge-transfer excitons or free charge carriers. In case charge-transfer excitons are created, care has to be taken to guarantee efficient dissociation of the charge-transfer excitons into free charge carriers, as has been discussed in the section on charge separation. A large number of parameters, like excess energy, morphology or the influence of the electric field, have to be considered to optimize the steps between exciton formation and free charge generation. Eventually, the free charge

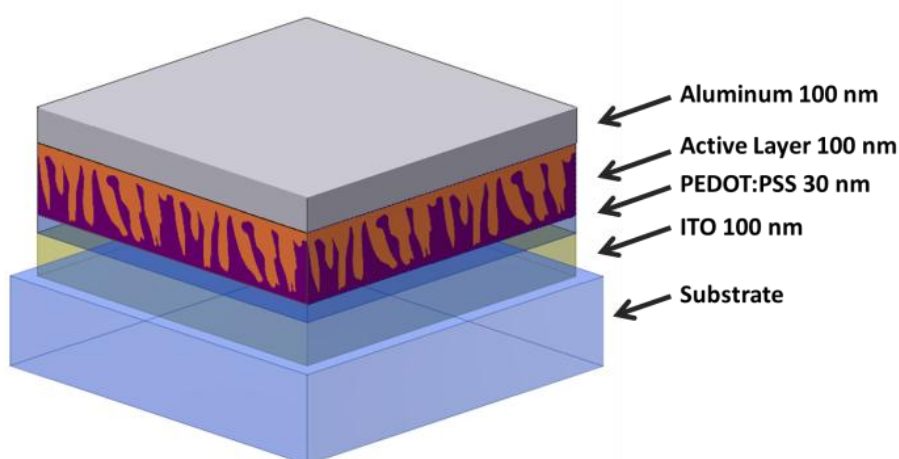
carriers have to be transported so they can be collected at the electrodes. The transport of the charges has to be fast enough to guarantee that the dwell time of the charge carriers in the active layer of the solar cell is much shorter than their non-geminate recombination life-time in order to minimize losses due to non-geminate recombination. This cascade of processes spanning from absorption of a photon to the collection of free charge carriers at the electrodes is schematically depicted in **Figure 18**.



**Figure 18.** Scheme of the cascade of processes leading from the absorption of light to the collection of charge carriers in an organic solar cell. First a photon is absorbed and a singlet exciton is created that has to diffuse to the interface between the donor (red) and acceptor (blue) materials. Second, at the interface the exciton is quenched by charge transfer from the donor to the acceptor. Third, the charges are spatially separated from each other and are transported towards the electrodes.

By the time the charge carriers are extracted from the active layer at the electrodes, the electrons (holes) have energetically relaxed to the LUMO (HOMO) of the acceptor (donor) material. The energy difference between electrons and holes, i.e. the difference between the HOMO of the donor and the LUMO of the acceptor, corresponds to the fraction of the photon energy that can be conserved during charge generation and transport to the electrodes. If the work functions of the electrode materials are not matched to the levels of

HOMO and LUMO additional energy may be lost when the charge carriers are extracted to the electrodes. This has direct consequences for the design and choice of the materials used for organic solar cells. On one hand it is desirable to decrease the optical band gap of the organic semiconductors in the active layer to achieve an optimum overlap between absorption and the solar emission spectrum, particularly in the low energy infrared region of the solar spectrum. On the other hand, this means that the HOMO-LUMO difference has to be decreased, which leads to an increased loss of energy of each photogenerated charge carrier. For single active layer devices (as opposed to e.g. tandem cells) the optimum energy difference between the donor HOMO and acceptor LUMO is 1.1 eV assuming the Shockley-Queisser limit and that no excess energy is needed for charge generation [96]. Furthermore, the choice of materials that can be used as electrodes with suitable work functions is very limited. Today, practically every organic solar cell uses indium tin oxide (ITO) modified by a hole transport layer (e.g. poly(3,4-ethylenedioxythiophene)-polystyrenesulfonic acid (PEDOT:PSS) or  $\text{MoO}_x$ ) as transparent front electrode and either calcium, aluminum, silver or a combination of these as reflective back electrode. A schematic device layout is shown in **Figure 19**.



**Figure 19.** Device layout of an organic solar cell consisting of an indium tin oxide (ITO) electrode, a PEDOT:PSS hole transport layer, the (bulk heterojunction) active layer and an aluminum top electrode, all on top of a substrate (glass or plastic foil).







# 3

## Experimental Techniques

In the following chapter the most important experimental methods that were used to acquire data for this thesis will be discussed. First, the experimental details for measuring current-voltage characteristics of organic solar cells for the determination of power conversion efficiencies and the figures of merit for device performance will be explained, followed by the time-of-flight technique for measuring charge carrier mobilities. Transient absorption spectroscopy is applied to study the temporal evolution of excited state populations like singlet, triplet and charge-transfer excitons or spatially separated charge carriers in organic semiconductors. The time delayed double pulse experiment gives insight into the field-dependence of the charge carrier extraction and recombination kinetics in organic solar cell devices and finally with the help of macroscopic drift-diffusion simulations all experimental results can be combined into a physical model of device operation. The sample preparation for all experimental techniques was kept as closely as possible to that of solar cell devices presented in section 3.1.3 in order to ensure comparability of results between the individual experimental methods. Further details for

sample preparation are given at the end of every section describing the respective method and also in the articles listed in chapter 4.

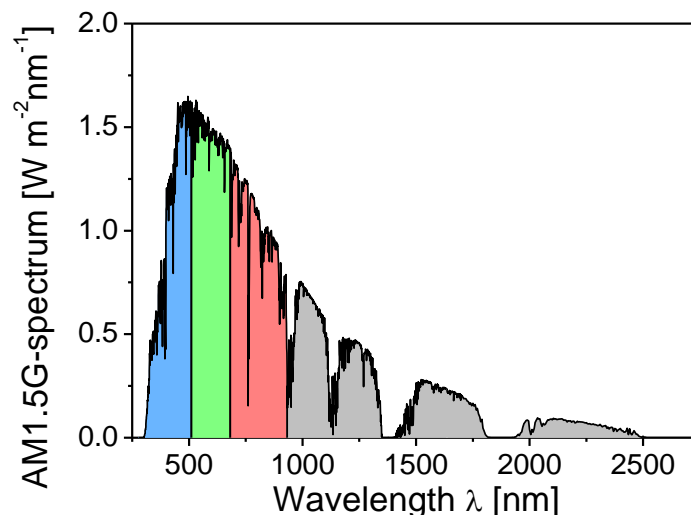
### 3.1 Solar Cell Performance

#### 3.1.1 Current-voltage characteristics

The power conversion efficiency (PCE) of a solar cell is defined as the ratio of the maximum extractable electrical power density  $P_{el}$  to the optical power density  $P_{opt}$  incident from illumination. The extractable electrical power density of a solar cell is not a constant quantity, but depends on the applied voltage  $V$ :

$$P_{el}(V) = V \times J(V). \quad (3.1)$$

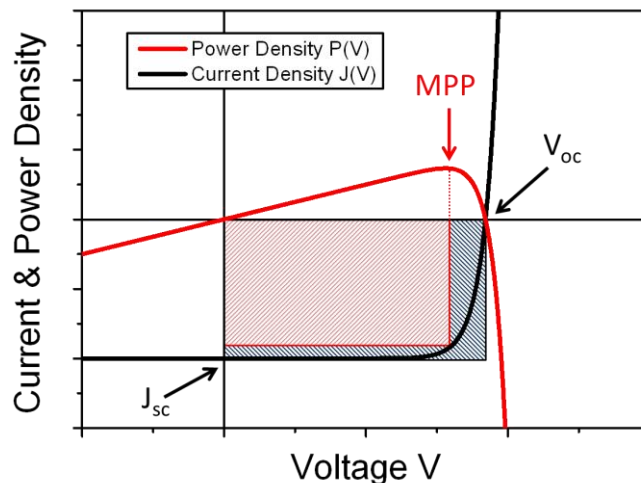
For the calculation of the PCE the dependence of the current density  $J$  on the applied voltage, also known as a current-voltage (JV) characteristic, has to be determined. In order to guarantee an as good as possible comparability of results measured in different laboratories, an internationally recognized set of standard conditions for measuring current-voltage characteristics has been established. The most important of these conditions refers to the illumination



**Figure 20.** The AM1.5G reference spectrum [97]. The colors each indicate a spectral region that contains 25 % of the total optical power (i.e. 25 mW/cm<sup>2</sup>). The corresponding wavelength ranges are 280-511 nm, 512-682 nm, 683-932 nm and 933 to 4000 nm.

spectrum and intensity. The spectrum defined to be closest to natural sunlight is called the AM1.5G spectrum (see **Figure 20**). It corresponds to black body radiation at a temperature of 5777 K that has travelled a path through the atmosphere that is a factor 1.5 longer than radiation that is incident normal to the surface of the Earth (AM stands for air mass). This corresponds to an angle of incidence of  $48^\circ$ , which happens to be the yearly average of the solar illumination in the USA. The appendix G indicates that not only direct illumination but also diffusive light scattered in the atmosphere or from the ground is taken into account. For ease of computation the integrated optical power density of the AM1.5G spectrum is exactly  $100 \text{ mW/cm}^2$  (or  $1000 \text{ W/m}^2$ ). The AM1.5G spectrum is often referred to as 1 sun illumination.

A current-voltage characteristic is recorded by illuminating the sample with a solar simulator, i.e. a lamp equipped with filters to resemble the AM1.5G spectrum as closely as possible, and measuring the current flowing through the sample while sweeping the applied voltage in a range from about  $-1 \text{ V}$  to  $+1 \text{ V}$ . An example current-voltage characteristic is depicted in **Figure 21**.



**Figure 21.** Schematic of a current-voltage (black) and power-voltage (red) characteristic of a solar cell under illumination. The maximum power point MPP, the open circuit voltage  $V_{oc}$  and the short circuit current  $J_{sc}$  are indicated by arrows. The fill factor FF corresponds to the ratio of the MPP and the product of  $V_{oc}$  and  $J_{sc}$ , i.e. the ratio of the red and black squares.

Besides the PCE there are other figures of merit frequently used to describe solar cell performance such as the short circuit current  $J_{sc}$ , the open circuit voltage  $V_{oc}$  and the fill factor FF. The short circuit current is defined as the current measured at 0 V applied to the cell and the open circuit voltage is the voltage at which no net current is flowing in the external circuit, as indicated in **Figure 21**. The definition of the fill factor is slightly more complicated. The maximum power that can be extracted from a cell is by definition given by the product of the voltage and the current at the maximum power point MPP, shown as a red square in **Figure 21**. The black square corresponds to the product of the open circuit voltage and the short circuit current, which is always bigger than the maximum extractable power. The ratio of these two squares is called the fill factor:

$$FF = \frac{V_{MPP} \times J(V_{MPP})}{V_{oc} \times J_{sc}} \quad (3.2)$$

The FF is a measure for field dependent loss mechanisms in a solar cell. In the absence of any field dependence the fill factor approaches unity and in the case of a strong field dependence of the photocurrent it can be reduced considerably. With the help of these three figures of merit the power conversion efficiency can be expressed by factors that can easily be read from a current voltage characteristic:

$$PCE = \frac{P_{el}}{P_{opt}} = \frac{J_{sc} \times V_{oc} \times FF}{P_{opt}} \quad (3.3)$$

For measuring JV characteristics under standard operating conditions in a nitrogen filled glovebox, a solar simulator (K.H. Steuernagel Lichttechnik GmbH, Germany) was employed for illumination and a Keithley 236 source measure unit (SMU) was used for applying voltage and recording the current flow through the solar cells to be tested. For temperature dependent experiments the samples were housed in a home-built, temperature-controlled cryostat and kept under dynamic vacuum better than  $10^{-5}$  mbar. The illumination was provided by a green LED (center wavelength 530 nm) tuned

to the intensity at which the JV characteristics matched the ones measured under AM1.5G illumination.

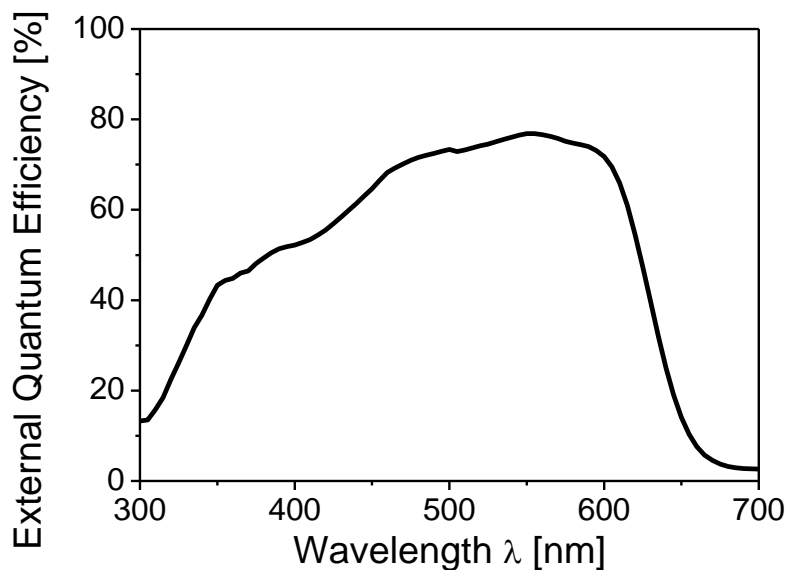
### 3.1.2 External quantum efficiency

The external quantum efficiency (EQE) describes how efficiently photons of a given wavelength are absorbed and create extractable charge carriers in a solar cell. It is calculated from the ratio of extracted electrons to incident photons measured at short circuit conditions. An example EQE curve is shown in **Figure 22**. The EQE is especially interesting for solar cells with active layers consisting of blends of materials with complementary absorption spectra. In this case it can give insight into the contribution of charge generation of each of the components.

The EQE can also be used to calculate an estimate of the short circuit current of a solar cell under solar illumination:

$$J_{sc} = \frac{e}{hc} \int \lambda \times EQE(\lambda) \times P_{AM1.5G}(\lambda) d\lambda . \quad (3.4)$$

Here  $h$  is Planck's constant and  $P_{AM1.5G}$  corresponds to the AM1.5G spectrum. It should be noted however that the EQE spectrum is measured by scanning a



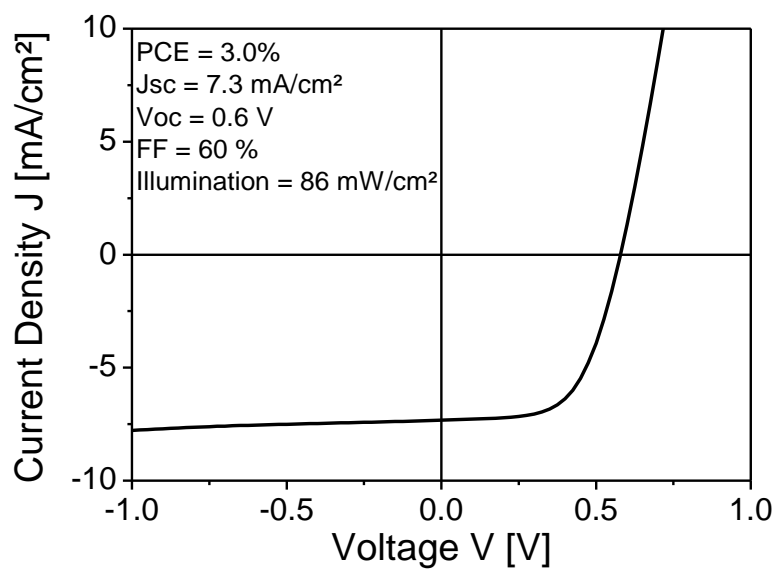
**Figure 22.** Schematic of an external quantum efficiency (EQE) curve of a P3HT:PCBM solar cell device.

low power monochromatic light source through the spectral range of interest. As a consequence the charge carrier density in a device is much lower than under illumination intensities of 1 sun. Loss mechanisms that depend on the charge carrier density can lead to considerable deviations between the estimation of the short circuit current from the EQE and the actually measured short circuit current under AM1.5G illumination.

For EQE measurements monochromatic light was provided by a tungsten halogen lamp and a TRIAX 180 monochromator. The number of incident photons for each wavelength was determined using a calibrated silicon photodiode and the short circuit current was measured with a Keithley 236 SMU.

#### **3.1.3 Device preparation**

Solar cell devices were prepared on indium tin oxide (ITO) coated glass substrates (Präzisions Glas&Optik GmbH, Germany) that were patterned by wet etching and subsequently cleaned by an ultrasonic treatment of multiple steps with various solvents. In between each step the substrates were blown dry with nitrogen. The clean ITO substrates were plasma etched in an argon plasma for 15 minutes before spin-coating of the PEDOT:PSS (Clevios P VP AI 4083, H.C. Starck) hole-transport layer. After applying the PEDOT:PSS layer, the samples were transferred to a nitrogen filled glovebox and dried on a hot plate at 120 °C for 20 min. Also inside the glovebox, P3HT and PCBM were dissolved separately (18 mg/ml) in chlorobenzene and stirred at 70 °C for at least ten hours. For spin-coating of the active layer the P3HT and PCBM solutions were mixed in a 3:2 ratio and filtered onto the substrates with a 0.45 µm PTFE filter. The spincoating was performed at 1000 rpm for 60s. Subsequently, 100 nm thick aluminum electrodes were evaporated on top of the active layer under dynamic vacuum better than  $2 \times 10^{-6}$  mbar (also inside the glovebox). Finally, the devices were completed by annealing at 120 °C for 20 min. Devices prepared from 98% RR-P3HT:PCBM (Sepiolid P200, vide infra) in this manner resulted in power conversion efficiencies of 2.9 - 3.1%. A current voltage characteristic of such a device is shown in **Figure 23**.



**Figure 23.** Exemplary current voltage characteristic of an annealed RR-P3HT:PCBM solar cell with power conversion efficiency of 3.0% under simulated AM1.5G illumination with reduced intensity of 86 mW/cm<sup>2</sup> (instead of 100 mW/cm<sup>2</sup>).

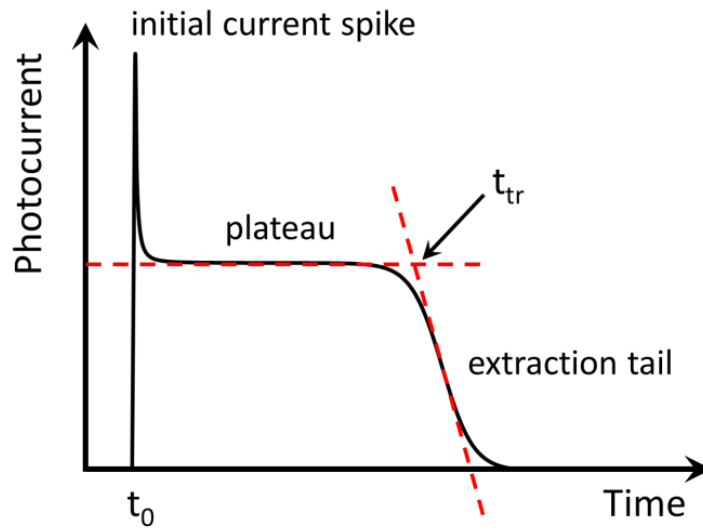
This device fabrication scheme was optimized for the concentrations of the P3HT and PCBM solutions, the spin-coating frequency and the annealing conditions.

### 3.2 The Time-Of-Flight Technique

As introduced above the time-of-flight technique (TOF) can be used to study the transport of a charge carrier package through a material that is sandwiched between two electrodes of which at least one has to be semitransparent to allow photogeneration of charge carriers.

The migration of a photogenerated charge carrier package through a sample causes a typical transient current flow in an external circuit connected to the sample. An example of a typical TOF transient for non-dispersive transport is shown in **Figure 24**. At time  $t_0$  electrons and holes are generated in the sample by a short (ns) laser pulse. The electric field applied through the electrodes causes electrons and holes to drift in opposite directions. Depending on the direction of the electric field holes are extracted from the sample immediately and electrons are transported through the sample or vice versa. In any case the fast extraction of charge carriers at the adjacent electrode causes a drop of the current in the external circuit that manifests itself in the transient as an initial current spike. Furthermore, relaxation processes of the charge carrier package can also contribute to this initial current spike. Once only one type of relaxed, i.e. moving with constant velocity, charge carriers is left, and if the number of these charge carriers is constant, i.e. in the absence of recombination, the current is also constant, which causes a plateau region in the transient. As soon as the first charge carriers of the package reach the counter electrode, they are extracted and the current transient starts to decay. This part of the transient is marked as extraction tail in **Figure 24**. Even though some attempts have been made [98,99], to date there is no analytic description available that universally allows the extraction of an average charge carrier transit time from a TOF transient. Instead the transit time  $t_{tr}$  can be estimated from the intersection of linear fits to the plateau region and the extraction tail of the transient. With knowledge about the thickness  $d$  and assuming a constant electric field  $F = U/d$  across the sample, the mobility can be calculated as follows:



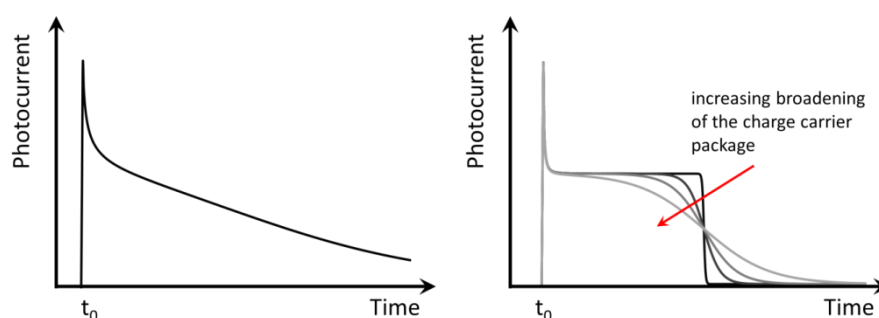


**Figure 24.** Scheme of a typical non-dispersive TOF transient. At time  $t_0$  electrons and holes are created near one electrode. Figure adapted from reference [100]. Used with permission from F. Laquai.

$$\mu = \frac{d}{t_{tr} \times F} = \frac{d^2}{t_{tr} \times U}. \quad (3.5)$$

As pointed out in the introduction to the Gaussian disorder model the field and temperature dependences of the charge carrier mobility can be used to determine quantitative information about the disorder present in the material. Additionally, it is possible to gain some qualitative insight into the role of disorder by analyzing the shape of the TOF transient. As already indicated above, the initial current spike can be influenced by the relaxation of the charge carrier package within the density of states. If the relaxation time is longer than the transit time, than the plateau completely vanishes and the spike merges with the extraction tail, as shown on the left side of **Figure 25**. This is a typical sign of dispersive transport that can be observed when the transit time is shorter than the relaxation time which is generally true in thin samples or at low temperatures. In this case it is not possible to determine an unambiguous transit time from the transient. Furthermore, the disorder influences the shape of the extraction tail. During the drift through the sample the charge carrier package broadens, because the mobility of each charge carrier strongly depends on its position in the DOS and consequently the width

of the charge carrier package depends on the exact shape of the DOS. As can be seen on the right side of **Figure 25**, an increase in the broadening of the charge carrier package has a strong influence on the extraction tail [101]. For this reason it is important to make sure that the initial width of the charge carrier package is much smaller than the thickness of the sample. At a typical absorption coefficient of  $2 \times 10^5 \text{ cm}^{-1}$  approximately 50 % (90 %) of the incoming light is absorbed within the first 35 nm (100 nm) of the sample, so a sample should be much thicker than 100 nm.



**Figure 25.** Left: Scheme of a dispersive TOF transient resulting from a slow relaxation time. Right: Influence of the width of the charge carrier package on the extraction tail.

Sample preparation and experimental setup for the TOF measurements have been described in reference [76]. Samples were generally prepared by spin-coating a solution of the material to be studied on top of a pre-cleaned indium tin oxide (ITO) coated glass substrate (Präzisions Glas & Optik GmbH, Germany). The concentrations of the solutions were adjusted to yield the desired film thicknesses and were in the range of 50 – 150 mg/mL. The solvent used was always chlorobenzene. The solutions were heated to 70 °C for more than 12 h in a nitrogen-filled glovebox to obtain complete dissolution of the materials and were filtered through 0.45  $\mu\text{m}$  PTFE filters. After spin-coating the samples were transferred to an evaporation chamber inside the glovebox and kept at high vacuum ( $< 3 \times 10^{-6}$  mbar) during the evaporation of a 10 nm thick aluminum electrode. For the experiments, the samples were housed in a temperature-controlled, custom-built cryostat under a dynamic vacuum of better than  $10^{-5}$  mbar. The wavelength of the excitation pulse was

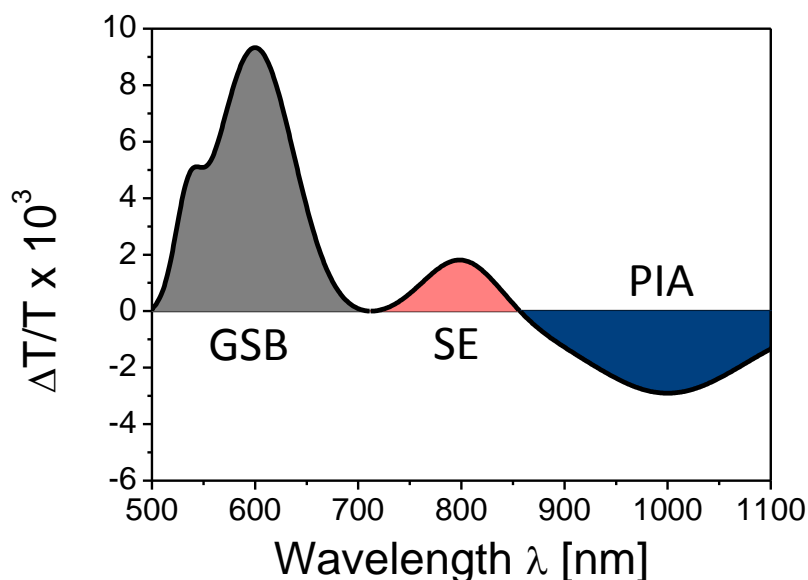
controlled by an optical parametric oscillator (GWU Lasertechnik GmbH, Germany) pumped by the third harmonic of a Nd:YAG laser and was chosen to match the absorption of the respective material. For the measurement of electron (hole) mobilities, the samples were illuminated through the ITO (aluminum) electrode. The polarity of the applied voltage was not changed between measuring electron and hole mobilities and was always chosen to be in reverse-bias in order to prevent charge injection through the electrodes. Current transients were recorded with a digital oscilloscope (Tektronix TDS 524A) triggered by the laser pulse.

### 3.3 Transient Absorption Spectroscopy

Transient absorption spectroscopy is a time-resolved optical pump-probe technique that can be used to study the evolution of excited states populations after a short excitation pulse by tracking the change of the transmission of a sample due to the presence of excited states. For this purpose a sample is illuminated by a first broadband light pulse that is used to determine the ground state transmission spectrum of the sample. Next a short pulse of a wavelength that is strongly absorbed by the sample creates excited states and a second broadband pulse probes the transmission spectrum of the excited sample. By varying the time delay between the excitation pulse (pump) and the second probe pulse the evolution of the transmission spectrum due to relaxation, transition and recombination processes of excited states can be observed. A transient absorption spectrum at any given delay time can be calculated by subtracting the ground state absorption spectrum  $T_{GS}(\lambda)$  from the excited state spectrum  $T_{EXC}(\lambda)$ :

$$\frac{\Delta T}{T}(\lambda, t) = \frac{T_{EXC}(\lambda, t) - T_{GS}(\lambda)}{T_{GS}(\lambda)}. \quad (3.6)$$

Excited species can change the transmission of a sample by three different mechanisms: ground state bleaching (GSB), stimulated emission (SE) and photoinduced absorption (PIA). Ground state bleaching occurs whenever the ground state of a sample is partially depopulated so that the total number of sites taking part in the (ground state) absorption is reduced. This leads to an increase of the transmission in the wavelength region of the ground state absorption spectrum, which corresponds to a positive  $\Delta T/T$  signal. If the excited states have an emissive transition to the ground state, as is typically the case for singlet excitons, the second probe pulse can induce stimulated emission from these states. This causes a positive  $\Delta T/T$  signal in the spectral region of the emission spectrum of the sample. Furthermore, excited species can absorb light and be excited to a higher lying state. The absorption spectra of excited species differ from the ground state absorption spectrum of a sample. Such photoinduced absorption spectra decrease the transmission of



**Figure 26.** Exemplary transient absorption spectrum featuring a ground state bleach (GSB), stimulated emission (SE) and photoinduced absorption (PIA) signals.

the sample in spectral regions characteristic of the respective species and give rise to negative  $\Delta T/T$  signals. An exemplary transient absorption spectrum featuring all of these mechanisms is shown in **Figure 26**. Transient absorption signals are much smaller than ground state transition signals. Typically, excited states can change the transmission of a sample by not more than a few percent even at very high initial excitation densities.

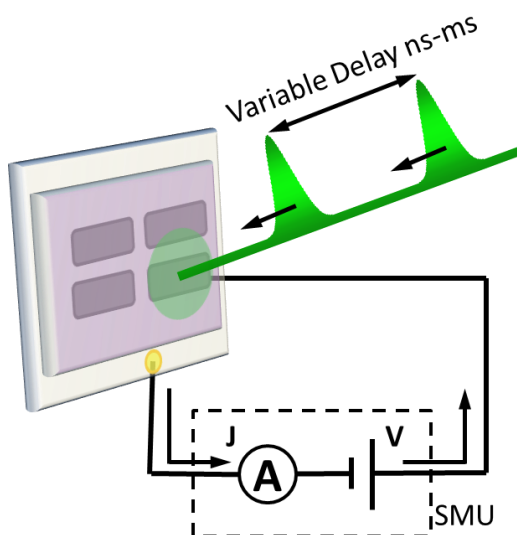
The experimental setup for the TA spectroscopy has been described in reference [31] and [64]. Two different setups were used to cover the time ranges up to 4 ns with a resolution of  $\sim 100$  fs (short delay setup) and up to 1 ms with a resolution of  $\sim 600$  ps (long delay setup). For the short delay setup the output of a commercial titanium:sapphire amplifier (Coherent LIBRA HE, 3.5 mJ, 1 kHz, 100 fs, 800 nm) was split with one portion used to generate a 532 nm excitation pulse in an optical parametric amplifier (Coherent OPerA Solo) and another portion used to generate a white light probe pulse in a home-built two-stage broadband non-collinear optical parametric amplifier (NOPA) for white light generation and amplification in the visible ( $\sim 480$ -850 nm) and with a c-cut 3 mm thick sapphire window for white light generation in

the visible and near-infrared spectral range (~600-1100 nm). The variable delay of up to 4 ns between excitation and probe was introduced by a broadband retro-reflector mounted on a mechanical delay stage. Only reflective optics were used to guide the probe beam to the sample to minimize chirp. The excitation pulse was chopped at 500 Hz with a mechanical chopper, while the sample was probed with a repetition rate of 1 kHz. For the long delay setups the excitation pulse was provided by a frequency doubled (532 nm) actively Q-switched Nd:YVO<sub>4</sub> laser (AOT Ltd. MOPA) triggered by a 500 Hz signal from an electronic delay generator (Stanford Research Systems DG535), that was used to control the delay time between the excitation and the probe. For both setups each probe pulse was dispersed onto a linear silicon photodiode array which was read out after every pulse. Adjacent diode readings corresponding to the transmission of the sample after an excitation pulse and without an excitation pulse were used to calculate  $\Delta T/T$ . TA measurements were performed at room temperature or liquid nitrogen temperature under dynamic vacuum at pressures  $< 10^{-5}$  mbar. Samples were prepared analogous to solar cell devices in order to guarantee the best possible comparability of results. The only differences are that all films were spin-coated directly onto pre-cleaned quartz substrates instead of ITO/PEDOT:PSS coated glass slides and that no aluminum electrodes were applied.

### 3.4 Time Delayed Double Pulse Experiment

The newly developed time delayed double pulse experiment can be used to study the electric field dependence of non-geminate recombination and charge extraction kinetics in organic solar cells. The basic idea of this experiment is to create a first charge carrier package that is subject to recombination and extraction. After a variable delay time a second package is generated in the sample that interacts with the remaining charges from the first package and thus probes the dwell time of the charge carriers in the solar cell. This interaction can be observed by a reduction of the current  $J$  flowing in a connected external circuit. By varying the applied voltage  $V$  a direct observation of the field-dependence of non-geminate recombination and charge extraction in solar cell devices is possible. A schematic of the setup of this experiment is shown in **Figure 27**.

The case if the two charge carrier packages do not interact, because the delay time between the packages is much longer than the lifetime of the first package, is schematically shown on the left side of **Figure 28**. The evolution of



**Figure 27.** Schematic of the setup of the time delayed double pulse experiment. A solar cell is illuminated by two pulsed lasers with a variable delay between the pulses. The resulting current  $J$  flowing in an external circuit is measured for various delay times and applied voltages  $V$ . [102] Reprinted with permission from Mauer et al. *The Journal of Physical Chemistry Letters* 2011, 2, 1736. Copyright 2011 American Chemical Society.

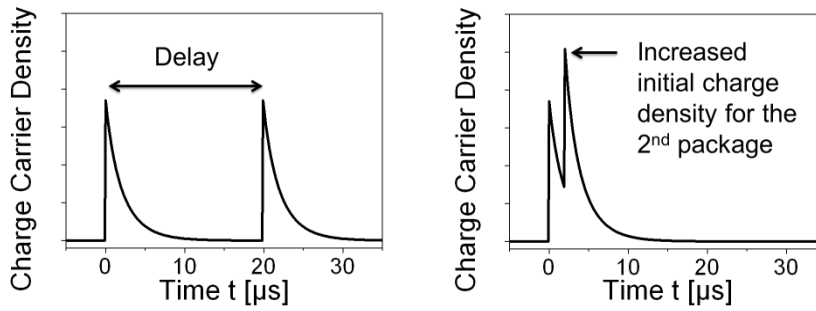
both charge carrier packages can be described with a rate equation considering a linear extraction rate and a Langevin type non-geminate recombination rate:

$$\frac{dn}{dt} = -k_{extr}n - \gamma n^2. \quad (3.7)$$

This means, that for both packages a certain fraction of charges is extracted and the rest recombine. The exact ratio of extraction to recombination depends on the values of the rate constants  $k_{extr}$  and  $\gamma$  and, for now more importantly, on the charge carrier density. Extraction is assumed to be linear in intensity, while recombination is superlinear. Consequently, at higher charge carrier densities the fraction of recombining charges will increase and the fraction of extracted charges decrease. As the delay time between the generation of the two packages is decreased, the initial charge density of the second pulse is increased by the amount of charge carriers remaining in the sample from the first package. Assuming that each laser pulse generates the same charge carrier density  $n_0$  the initial conditions of the two charge carrier packages are  $n_1(0) = n_0$  and  $n_2(t_{del}) = n_0 + n_1(t_{del})$  for the first package being generated at time  $t = 0$  and the second at time  $t = t_{del}$ . This increase in the initial charge carrier density of the second pulse leads to a higher non-geminate recombination rate and thus reduces the number of charge carriers that can be extracted from the device. This is shown on the right hand side of **Figure 28**. In other words, the second charge carrier package interacts with the charge carriers remaining from the first pulse, leading to a reduction in the extractable current from the solar cell due to non-geminate recombination.

As is shown in reference [102] this rate equation can be solved analytically to allow easy fitting of the obtained data with the extraction and recombination rate constants as well as the initial charge carrier densities as fitting parameters. The extraction rate and the active layer thickness  $d$  can be used to estimate the charge carrier mobility  $\mu = k_{extr}d^2/2V$ . It is however not possible to assign this mobility to either electrons or holes as this represents an average value only.





**Figure 28.** Left: Two charge carrier packages generated with a delay long enough to prevent interaction between the packages. Right: At short delay times the remaining charges from the first package increase the initial charge density of the second package, leading to additional non-geminate recombination losses.

With the parameters determined by fitting the data an extrapolation of the importance of non-geminate recombination to standard operating conditions of a solar cell can be performed. At steady-state conditions the charge generation rate  $G$  equals the sum of extraction and recombination rate:

$$G = k_{extr}n + \gamma n^2. \quad (3.8)$$

The generation rate can be estimated from the product of the external quantum efficiency of the cell and the photon flux of the solar AM1.5G illumination. From this equation the steady-state charge carrier density in the device can be estimated and used to calculate the extraction and recombination current densities in a working solar cell:

$$J = \frac{1}{A} \frac{dQ}{dt} = e \frac{V}{A} \frac{dn}{dt} = -ed(k_{extr}n + \gamma n^2) = J_{extr} + J_{rec}. \quad (3.9)$$

As the extraction rate depends on the applied voltage, so does the extraction current so that the voltage dependence of the photocurrent in the external circuit can be estimated from this calculation.

It should be noted that for this data analysis scheme the charge carrier density dependence of the charge carrier mobility has not been taken into account. It would lead to a density dependence of the extraction and recombination rate constants as already pointed out in the section on non-geminate recombination. This additional density dependence renders the equations no

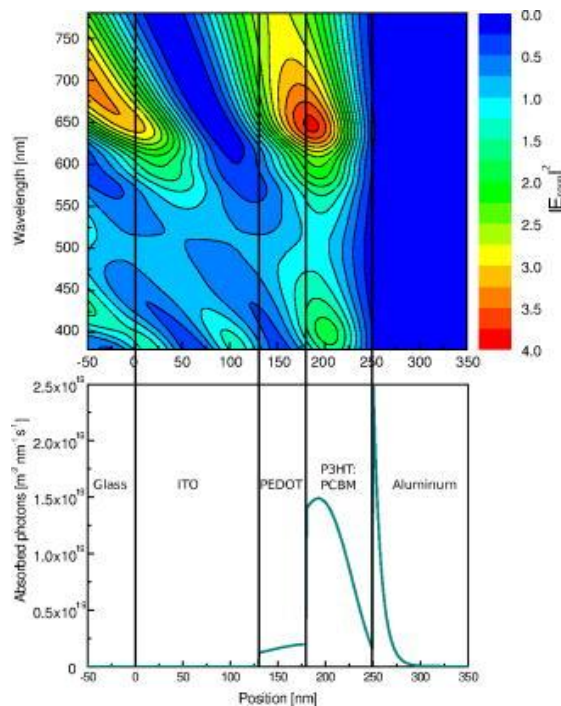
longer analytically solvable, which considerably hinders the data analysis. While some discrepancy between the data and the fits can be expected due to this negligence it is only a minor effect and does not significantly influence the main findings of this data analysis.

The experimental setup for the time delayed double pulse experiment has been described in reference [102]. For measuring current-voltage characteristics under illumination by two pulsed lasers, a Keithley 2400 source measure unit was used to source voltage and measure current. For the first laser a commercial titanium:sapphire laser (Coherent LIBRA HE) was used to pump a home-built narrowband non-collinear optical parametric amplifier to generate pulses with a center wavelength of 530 nm, a typical pulse length of  $<1$  ps, and a repetition rate of 1 kHz. The second laser used was a frequency doubled (532 nm) actively Q-switched Nd:YVO<sub>4</sub> laser (AOT Ltd. MOPA) with a pulse length of  $\sim 600$  ps and a repetition rate of 1 kHz. The variable delay time between both lasers was controlled by an electronic delay generator (Stanford Research Systems DG535). All measurements were performed at room temperature under dynamic vacuum at pressures  $< 10^{-5}$  mbar.

### 3.5 Device Simulations

Simulations of photovoltaic devices can be a useful tool for testing physical device models based on experimental observations. The aim of simulations of solar cell devices is to calculate current-voltage characteristics assuming a certain set of physical models to describe the optical and electrical properties of a cell and to compare it to experimentally determined current-voltage characteristics. As very different physical effects can have similar influences on the shape of a current-voltage characteristic it is often not enough to just study devices under standard conditions, but also under varying conditions like temperature or light intensity changes to test certain assumptions.

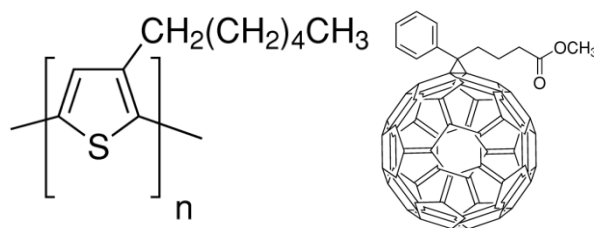
Simulations were performed with the commercially available software Setfos (Fluxim AG, Switzerland). The simulation schemes, algorithms and available physical models have been described in references [103] and [104] in great



**Figure 29.** Electromagnetic field penetration plot (top) is calculated using a transfer matrix formalism. This field penetration is then used to derive the photon absorption rate profile (bottom). The device simulated here consists of a glass substrate, a  $\sim 125$  nm thick ITO electrode, a 50 nm thick PEDOT:PSS hole-transport layer, a 75 nm thick active layer and a 100 nm thick aluminum electrode [103]. Reprinted with permission from Häusermann et al. Journal of Applied Physics 2009, 106, 104507. Copyright 2009, American Institute of Physics.

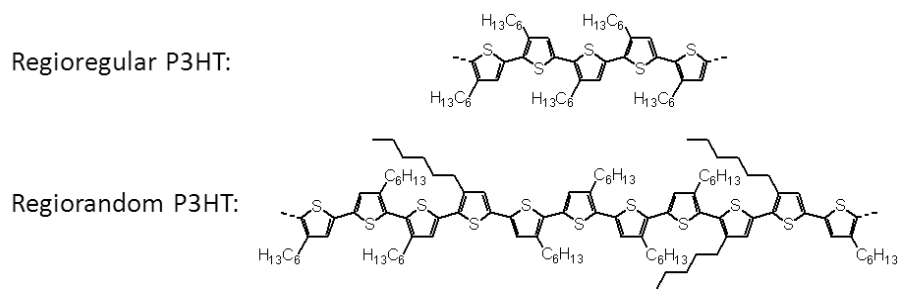
detail. In short, Setfos combines a transfer matrix formalism for optical and drift-diffusion calculations for electrical simulations of solar cell devices consisting of a multilayer stack of thin films. With the transfer matrix formalism the photon absorption rate and from that the exciton generation rate can be determined at any position in a device under illumination by an arbitrary spectrum, e.g. an AM1.5G spectrum (see **Figure 29**). Once the exciton generation rate profile is known, the charge generation rate can be determined for different models of charge generation. Setfos treats the active layer of a solar cell as an effective medium and its microscopic details are not considered explicitly. This means that the active layer is defined as a medium with the HOMO and the hole mobility of the donor and the LUMO and the electron mobility of the acceptor and the optical properties of a blend film. Charge generation in such an effective medium is assumed to be either instantaneous or via charge-transfer excitons according to the Onsager-Braun model. In order to consider interface effects like incomplete exciton quenching an additional loss factor can be applied. With knowledge about the charge generation rate profile drift-diffusion calculations can be performed to simulate current-voltage characteristics. These involve charge transport models that can be chosen from constant mobilities over Poole-Frenkel like field dependent mobilities up to field, temperature, and charge density dependent transport in a Gaussian density of states. Non-geminate recombination is assumed to be of Langevin type with a reduction factor to account for interface effects as introduced above. Finally, injection of charge carriers is assumed to be thermionic which means that the injected current depends on the temperature and on the charge carrier mobility.

### 3.6 Materials – P3HT:PCBM



**Figure 30.** Chemical structures of P3HT (left) and PCBM (right).

In this work the material system poly(3-hexylthiophene-2,5-diyl) (P3HT) and [6,6]-phenyl C<sub>61</sub> butyric acid methyl ester (PCBM) was studied. In P3HT the addition of the hexyl-chain at the three position renders the otherwise symmetrical thiophene monomer asymmetrical. Consequently, 3-hexylthiophene monomers can couple with different orientations of the side chains. The position between the sulfur atom and the hexyl chain (i.e. on the right side of the sulfur atom in **Figure 30**) is called head, the position on the other side of the sulfur atom is called tail of the monomer. Monomers can couple either in a head-head, tail-tail or head-tail coupling. If the type of coupling of a polymer chain is exclusively head-tail coupling, it is called regioregular (RR). The P3HT used for investigations in this work was supplied by BASF with three different degrees of regioregularity, ranging from almost exclusive head-tail coupling (Sepiolid P200, RR > 98%), over slightly lower regioregularity (Sepiolid P100, RR = 94%) to a completely random distribution of all three types of coupling, i.e. regiorandom (RRa) P3HT (compare also **Figure 31**). PCBM with a purity better than 99% was purchased from Sigma-Aldrich. All materials were used as received.



**Figure 31.** Sections from a regioregular (top) and a regiorandom (bottom) P3HT chain.

**Table 1.** Molecular weight  $M_w$ , polydispersity index (PDI) and regioregularity of the studied materials.

<b>Material</b>	<b><math>M_w</math> [kg/mol]</b>	<b>PDI</b>	<b>Regioregularity [%]</b>
Regiorandom P3HT	unknown	unknown	random
Sepiolid P100	60.00	2.2	94 %
Sepiolid P200	25.00	1.6	>98 %
PCBM	1.03	n/a	n/a







# 4

## Results and Discussion

In this chapter the experimental results collected with the techniques introduced in chapter 3 are presented and discussed in the context of the recent literature. As the results and discussions within the framework of this thesis were all published in peer reviewed journals, this chapter is simply a collection of all relevant published articles.<sup>3</sup> A complete list of scientific contributions can be found on page 157.

---

<sup>3</sup> In accordance with the MPGC examination regulations §11.1.

## 4.1 Charge Transport

The article “The Impact of Polymer Regioregularity on Charge Transport and Efficiency of P3HT:PCBM Photovoltaic Devices” was published in the journal *Advanced Functional Materials* by WILEY-VCH on July 9<sup>th</sup>, 2010.

From Mauer, R.; Kastler, M.; Laquai, F. *Advanced Functional Materials* 2010, 20, 2085. Copyright © 2010 by John Wiley & Sons, Inc. Reprinted by permission of John Wiley & Sons, Inc.

# The Impact of Polymer Regioregularity on Charge Transport and Efficiency of P3HT:PCBM Photovoltaic Devices

By Ralf Mauer, Marcel Kastler, and Frédéric Laquai\*

The charge transport in pristine poly(3-hexylthiophene) (P3HT) films and in photovoltaic blends of P3HT with [6,6]-phenyl C61 butyric acid methyl ester (PCBM) is investigated to study the influence of charge-carrier transport on photovoltaic efficiency. The field- and temperature dependence of the charge-carrier mobility in P3HT of three different regioregularities, namely, regiorandom, regioregular with medium regioregularity, and regioregular with very high regioregularity are investigated by the time-of-flight technique. While medium and very high regioregularity polymers show the typical absorption features of ordered lamellar structures of P3HT in the solid state even without previous annealing, films of regiorandom P3HT are very disordered as indicated by their broad and featureless absorption. This structural difference in the solid state coincides with partially non-dispersive transport and hole mobilities  $\mu_h$  of around  $10^{-4}$  and  $10^{-5}$   $\text{cm}^2 \text{V}^{-1} \text{s}^{-1}$  for the high and medium regioregularity P3HT, respectively, and a slow and dispersive charge transport for the regiorandom P3HT. Upon blending the regioregular polymers with PCBM, the hole mobilities are typically reduced by one order of magnitude, but they do not significantly change upon additional post-spincoating annealing. Only in the case of P3HT with high regioregularity are the electron mobilities similar to the hole mobilities and the charge transport is, thus, balanced. Nonetheless, devices prepared from both materials exhibit similar power conversion efficiencies of 2.5%, indicating that very high regioregularity may not substantially improve order and charge-carrier transport in P3HT:PCBM and does not lead to significant improvements in the power-conversion efficiency of photovoltaic devices.

poly(3-hexylthiophene) (P3HT) and [6,6]-phenyl C61 butyric acid methyl ester (PCBM). Power-conversion efficiencies (PCE) in excess of 5% for single-layer devices<sup>[1,2]</sup> and more than 6% in tandem cell configurations have been reported for this particular system, despite its limited spectral overlap with solar radiation.<sup>[3]</sup> Meanwhile, novel materials with enhanced overlap with the solar radiation spectrum, especially in the red to infrared part, better control of charge-carrier photogeneration and recombination, and eventually higher charge-carrier mobilities and efficiencies have been developed. However, P3HT:PCBM remains of high interest, as it represents a prototypic photovoltaic donor-acceptor system, and, more importantly, it is readily available.<sup>[4]</sup> Although most of the advances in efficiency have been the result of empirical variations in the multiple processing parameters, for instance by adding co-solvents, changing annealing conditions, optimizing the interlayer, and fine tuning the blend ratios, a conclusive picture of the influence of these parameters on the photophysics of the blend system is still lacking. The situation for polymer-based devices is further complicated since the photophysical properties of polymers are also dependent on the molecular weight,

polydispersity and, as is the case for P3HT, regioregularity of the polymer.

In this work we report on charge-carrier mobility measurements of a set of structural isomers of P3HT with very high regioregularity ( $rr > 98\%$ ), medium regioregularity ( $rr = 94\%$ ), as well as a regiorandom P3HT (i.e., entirely statistical coupling of head to tail, head to head, or tail to tail connection sites) by the time-of-flight technique (TOF). The charge-carrier mobility was measured as a function of the applied electric field and temperature of the system for samples consisting of the pristine polymers as well as for blends of the polymers with PCBM in annealed and non-annealed films. Finally, we demonstrate photovoltaic devices prepared using the two regioregular polymers and try to correlate the influence of regioregularity on charge-carrier mobility and device efficiency.

## 1. Introduction

Organic solar cells are on the way to become large-area, low-cost, flexible, and light-weight sources of renewable energy. One of the most prominent material systems, which have been investigated for bulk heterojunction (BHJ) solar cells, is a blend of regioregular

[\*] Dr. F. Laquai, R. Mauer, Dr. M. Kastler  
Max Planck Research Group for Organic Optoelectronics  
Max Planck Institute for Polymer Research  
Ackermannweg 10, D-55128 Mainz (Germany)  
E-mail: laquai@mpip-mainz.mpg.de

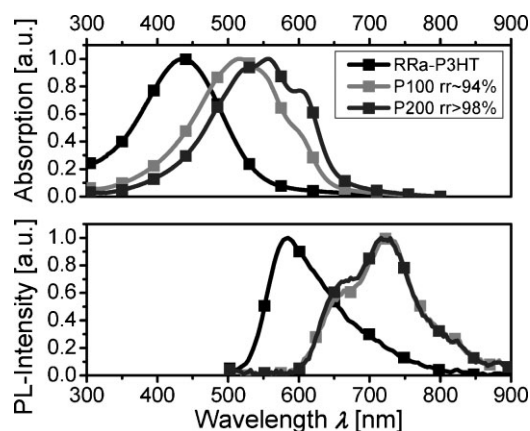
DOI: 10.1002/adfm.201000320

## 2. Results and Discussion

### 2.1. Absorption and Photoluminescence of P3HT

The upper part of Figure 1 depicts the absorption spectra of regiorandom P3HT (RRa-P3HT), P3HT of medium regioregularity (Sepiolid P100,  $rr \sim 94\%$ ), and P3HT of high regioregularity (Sepiolid P200,  $rr > 98\%$ ). The absorption spectrum of Sepiolid P200 features three vibronic bands located at 530 nm (2.34 eV), 560 nm (2.21 eV) and 610 nm (2.03 eV). The same vibronic structure can be observed in the spectrum of Sepiolid P100 with a weak hypsochromic shift of about 10 nm and a different distribution of oscillator strengths in the individual vibronics compared to Sepiolid P200. These vibrational bands are typically attributed to well-ordered regions of P3HT polymer chains with lamellar structures.<sup>[5]</sup> In contrast, the spectrum of RRa-P3HT does not show the signatures of any vibronic structures and instead exhibits one featureless and blue-shifted absorption peak with its maximum at 436 nm (2.84 eV). This in turn resembles the absorption of a highly diluted solution of regioregular P3HT, that is, under conditions that suppress intermolecular interactions that lead to ordering of polymer chains and interchain interactions.<sup>[5]</sup> It appears that the steric hindrance induced by the randomly oriented side-chains in the RRa-P3HT leads to twisted polymer chains, which suppresses the interaction of chains to such an extent, that no residual features of stacking of the polythiophene chains can be observed anymore. Additionally, we note that the extinction coefficient of the materials increases with higher regioregularity, giving values of  $1.6 \times 10^5$ ,  $2.0 \times 10^5$ , and  $2.6 \times 10^5 \text{ cm}^{-1}$  at the respective maxima of absorption for RRa-P3HT, Sepiolid P100, and Sepiolid P200, respectively.

These findings are consistent with the photoluminescence (PL) spectra shown in the lower part of Figure 1. Again the spectrum of RRa-P3HT is featureless and blue-shifted compared to the spectra of Sepiolid P100 and Sepiolid P200 with an emission maximum at 584 nm (2.12 eV), similar to the PL of a highly diluted solution of the regioregular material. The PL spectra of Sepiolid P100 and Sepiolid P200 are virtually identical with two vibronic bands at 662 nm (1.87 eV) and 724 nm (1.71 eV) and a very weak shoulder at



**Figure 1.** Absorption and photoluminescence spectra of regiorandom P3HT (RRa-P3HT) in comparison to rr-P3HT of medium regioregularity (Sepiolid P100,  $rr \sim 94\%$ ) and high regioregularity (Sepiolid P200,  $rr > 98\%$ ).

830 nm (1.49 eV). Furthermore, the emission intensity of the regioregular polymers is much lower than that of RRa-P3HT as a consequence of the strong intermolecular interaction in the ordered regions of Sepiolid P100 and Sepiolid P200 leading to an enhanced intermolecular delocalization of the excited state, which in turn causes a weaker radiative coupling to the ground state.<sup>[6]</sup> However, among the regioregular polymers Sepiolid P200 shows a slightly higher emission intensity than Sepiolid P100.

The fluorescence decay of Sepiolid P100 and Sepiolid P200 was found to be quasi single exponential and independent of the emission wavelength indicating the existence of a single emissive species, the first excited singlet exciton, in these polymers. In contrast, the fluorescence lifetime of RRa-P3HT is wavelength dependent and the fluorescence shows a strong spectral relaxation indicated by a red shift of the emission maximum in time. This suggests that the excited states are subject to fast relaxation within a broad density of states by successive energy transfer processes to segments with larger conjugation, and, thus, lower energy. The fluorescence lifetimes were determined to be  $(576 \pm 2)$  ps and  $(486 \pm 2)$  ps for Sepiolid P200 and Sepiolid P100, respectively. In RRa-P3HT no mean value for the lifetime could be determined. We found that the fluorescence lifetime at an emission wavelength of 640 nm was  $(389 \pm 4)$  ps and this was even shorter for smaller wavelengths most probably because of spectral relaxation of the excited states towards the low energy part of the density of states (see Supporting Information, Fig. S1).

We conclude from these observations that a substantial fraction of the polymer chains in films of Sepiolid P100 and Sepiolid P200 form well-ordered structures, whereas the films of RRa-P3HT remain disordered with strongly decreased interchain interactions.

### 2.2. Hole Transport in Pristine P3HT

We measured the hole-transport properties of pristine films of Sepiolid P100, Sepiolid P200, and RRa-P3HT by the time-of-flight (TOF) technique. The TOF technique probes the charge-carrier transport through the bulk of the material, which is typically sandwiched between two electrodes, after photogeneration of a charge-carrier package at one electrode by excitation with a short laser pulse. The charges are driven through the bulk by the applied external electric field and give rise to a specific current-transient pattern, from which the transit time  $t_T$  of the charges through the bulk can be extracted. From this transit time, the charge-carrier mobility  $\mu$  can be calculated using the relation

$$\mu = d^2 / (V \times t_T) \quad (1)$$

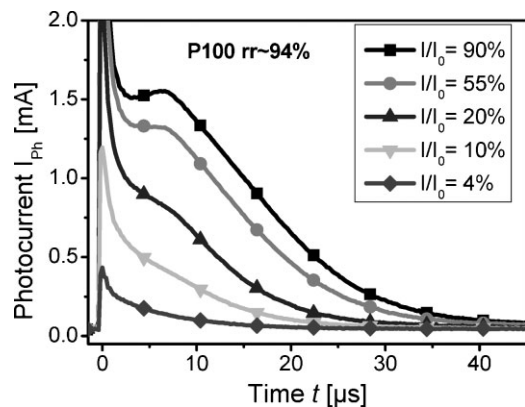
where  $V$  equals the applied voltage and  $d$  is the sample thickness. Although this technique allows measurements at charge-carrier densities similar to those in solar-cell devices, namely,  $10^{15}$ – $10^{17} \text{ cm}^{-3}$ , the layer thickness is usually about one order of magnitude larger, which may sometimes result in different morphologies of the active layer of TOF samples compared to that in solar cells. Since most of the TOF measurements on P3HT presented in the literature show dispersive transport of charges in P3HT, we followed the common practice in the field and determined the transit time of the charge carriers through the

sample from a double logarithmic plot for a better comparison with already published results.<sup>[7–9]</sup> The obtained results were further analyzed using the Gaussian disorder model (GDM) proposed by Bässler and coworkers.<sup>[10]</sup> Within the framework of this model, the field- and temperature dependence of the charge-carrier mobility  $\mu$  is given by

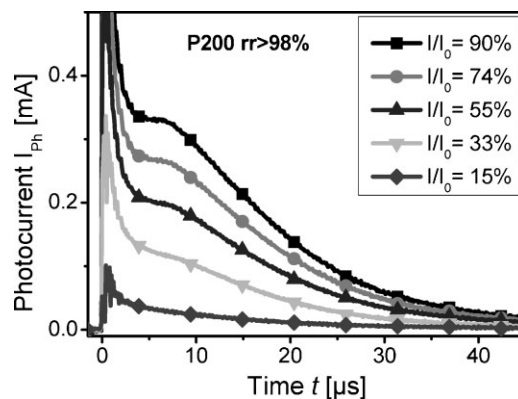
$$\mu(F, T) = \mu_0 \exp \left[ - \left( \frac{2\sigma}{3kT} \right)^2 \right] \exp \left[ C\sqrt{F} \left( \left( \frac{\sigma}{kT} \right)^2 - \Sigma^2 \right) \right] \quad (2)$$

where  $\mu_0$  is the zero-field, infinite temperature value of the mobility (mobility prefactor),  $k$  is the Boltzmann constant,  $T$  the temperature,  $\sigma$  the width of the density of states (energetic disorder) and  $\Sigma$  the positional-disorder parameter,  $C$  is an empirical constant, and  $F$  the applied electric field. From this equation follows that the temperature dependence of the mobility is mainly determined by the energetic disorder, while the field dependence is given by the difference between the energetic disorder normalized to the thermal energy often referred to as the energetic disorder parameter  $\hat{\sigma} = \sigma/kT$  and the positional disorder parameter  $\Sigma$ . If both contributions are similar, the dependence of the mobility on the electric field vanishes. However, if the energetic disorder dominates over the positional disorder, the mobility will increase with increasing electric field as long as the measurements are performed at high enough electric fields. This is the case for many of the previously investigated conjugated polymers and small molecules, which form amorphous glassy films in the solid state.<sup>[11]</sup> Since the GDM was derived for charge transport in these systems, the validity and applicability of the model for charge transport in partially crystalline and ordered systems such as P3HT is indeed questionable. However, its straightforward applicability to experimental data makes it easy to use for data analysis. Because of the above-mentioned limitations, in the following discussion we only use the GDM to extract the energetic disorder, since it allows for a better comparability with previous reports on charge transport in P3HT and P3HT:PCBM.

Figures 2 and 3 show the current transients of Sepiolid P100 and Sepiolid P200 recorded at various excitation intensities. The signals show an initial spike caused by the charge-carrier photogeneration followed by a current decay. Clearly, the shape



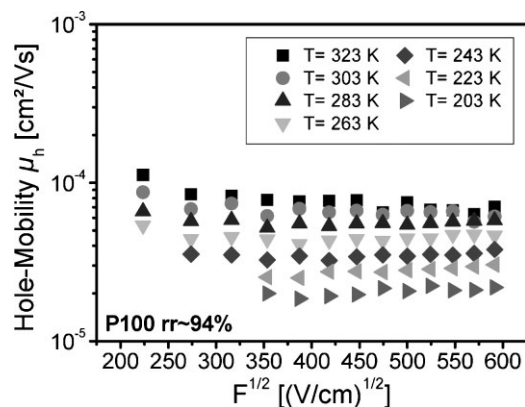
**Figure 2.** Time-of-flight hole transients in pristine Sepiolid P100 ( $rr \sim 94\%$ ) parametric in light intensity.



**Figure 3.** Time-of-flight hole transients in pristine Sepiolid P200 ( $rr > 98\%$ ) parametric in light intensity.

of the signals depends on the excitation intensity. The signals at high excitation intensities exhibit a clear plateau after the initial charge-generation peak indicative of non-dispersive charge transport. Furthermore, in the case of Sepiolid P100 the plateau turns into a cusp at very high excitation intensities. This cusp is also observed for Sepiolid P200 at high excitation intensities, elevated temperatures, and high electric fields, thus, in situations where the ratio of photogenerated charges with respect to charges stored on the sample electrodes is large. Pivrikas et al. assigned this cusp to space-charge perturbed charge transport.<sup>[12]</sup> However, in addition to the findings of Pivrikas et al. we observed that towards lower excitation intensities the plateau in the transients vanishes and transport becomes dispersive. This could indicate a transition from a transport regime, where traps are filled by excess charge carriers and a large fraction of charges drifts through the bulk unaffected by the traps, to a trap-limited dispersive transport regime. The concentration of charge carriers at which this turnover occurs is on the order of  $10^{-16} \text{ cm}^{-3}$ , which is in good agreement with recently published results of Clarke et al.<sup>[13]</sup> They showed that in P3HT:PCBM blends bimolecular recombination can be described by a model containing an exponential density of trap states, which is caused by structural distortions. The change in dispersivity was found to neither have an effect on the determined transit times nor on the dependence of the charge-carrier mobility on the applied electric field, suggesting that there was no rearrangement of the electric field because of the number of charges created within the sample during the time-of-flight experiment.<sup>[14]</sup>

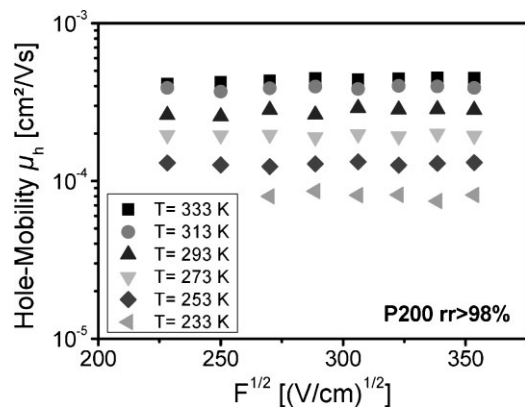
The field dependencies of the obtained hole mobilities at temperatures between 323 and 223 K are plotted in Figures 4 and 5 for Sepiolid P100 and Sepiolid P200, respectively. The hole mobility of Sepiolid P100 was on the order of  $10^{-5} \text{ cm}^2 \text{ V}^{-1} \text{ s}^{-1}$  and decreased at lower temperatures. It was only very weakly dependent on the electric field with a tendency towards a stronger dependence at lower temperatures. In the framework of the Gaussian disorder model this dependency is observed in systems in which the positional disorder  $\Sigma$  is comparable to the energetic disorder  $\sigma$  normalized to the thermal energy  $kT$ .<sup>[15]</sup> In this case, the term containing the field dependence in Equation 2 vanishes. From the temperature dependence of the mobility we estimated the energetic disorder of Sepiolid P100 to  $\sigma = (56 \pm 2) \text{ meV}$ . The hole-mobility of Sepiolid P200 was substantially higher than that of Sepiolid P100 and on the order of  $10^{-4} \text{ cm}^2 \text{ V}^{-1} \text{ s}^{-1}$ . This increase



**Figure 4.** Field dependence of hole mobility in pristine Sepiolid P100 at different temperatures.

in mobility can possibly be caused by two effects. On the one hand, Kim et al.<sup>[16]</sup> observed somewhat higher hole-mobilities in P3HT of higher regioregularity. On the other hand, Sepiolid P100 and Sepiolid P200 do not only differ in regioregularity, but also in molecular weight, with values for the weight averaged molecular weight  $M_w$  of approximately 60 000 g mol<sup>-1</sup> for Sepiolid P100 and 25 000 g mol<sup>-1</sup> for Sepiolid P200, respectively. Ballantyne et al.<sup>[7]</sup> studied the influence of molecular weight on charge transport in P3HT by the TOF technique and found that upon changing the molecular weight from 18 000 g mol<sup>-1</sup> to 56 000 g mol<sup>-1</sup> the hole mobility decreased by roughly one order of magnitude from  $2 \times 10^{-4}$  to  $3 \times 10^{-5}$  cm<sup>2</sup> V<sup>-1</sup> s<sup>-1</sup> at room temperature. Since they did not quote the regioregularity of their materials, a direct comparison of the absolute values of the mobilities is not entirely possible. However, the general trend described by them is similar to our findings. Unfortunately, it is not possible to obtain higher molecular weights for the high regioregularity polymer to get a direct comparison, since the polymer becomes gradually less soluble with increasing degree of polymerization because of its high regioregularity and tendency to stack in solution preventing a further increase of the molecular weight during synthesis.

The dependence of the hole mobility on the electric field and temperature in Sepiolid P200 was comparable to that in Sepiolid



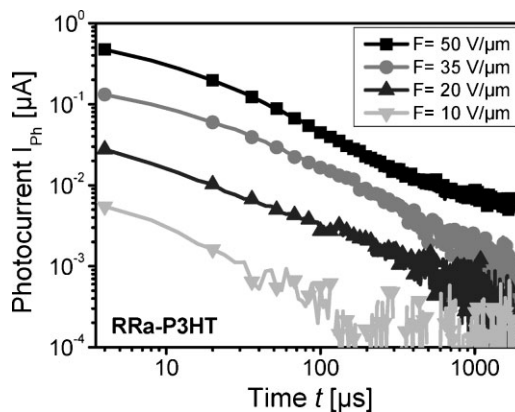
**Figure 5.** Field dependence of hole mobility in pristine Sepiolid P200 at different temperatures.

P100. The energetic disorder of  $\sigma = (58 \pm 1)$  meV for Sepiolid P200 was within the experimental error of that of Sepiolid P100. This value is somewhat lower than that reported by Ballantyne et al.,<sup>[7,8]</sup> who found the energetic disorder in regioregular P3HT to be  $\sigma = 71$  meV for molecular weights comparable to the materials in our study. In addition to TOF measurements, the Sepiolid P200 sample was also investigated using the dark-injection space-charge limited-current (DI-SCLC) technique.<sup>[17]</sup> This technique is complementary to TOF and allows mobilities to be determined at very low electric fields, where field-induced photogeneration of charges is not sufficient to detect a TOF transient. The results of these measurements are in good agreement with those of the TOF measurements at higher electric fields with mobilities on the order of  $10^{-4}$  cm<sup>2</sup> V<sup>-1</sup> s<sup>-1</sup>, which again only marginally depend on the applied electric field (see Supporting Information Figs. S2 and S3).

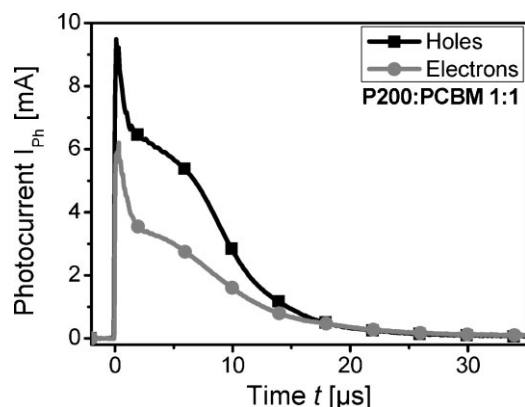
The TOF transients of RRa-P3HT measured at various electric fields are depicted in Figure 6. All transients feature an entirely dispersive decay of the current transient within a few hundred microseconds. It was not possible to extract meaningful transit times from these measurements and the charge transport remained dispersive even at elevated temperatures (60 °C). However, it is clear that the charge carriers are transported much slower in this polymer, since the current transient is extending into the hundred microseconds time range indicating multiple trapping of charge carriers during the transport. In the previous section we reported that the randomly oriented side chains of RRa-P3HT suppress the formation of lamellar ordered regions in the solid state and strongly increase the disorder of the material. It appears that the disorder in films of RRa-P3HT is increased to a large extent resulting in a broadened density of states, which in turn leads to dispersive charge transport. We also tried to obtain electron-current transients from the pristine P3HT samples, but we could not measure meaningful electron transients for any of the P3HT samples.

### 2.3. Charge Transport in P3HT:PCBM Blends

Unlike for the pristine P3HT samples, we found both hole and electron transients in 1:1 blends of Sepiolid P200 and PCBM

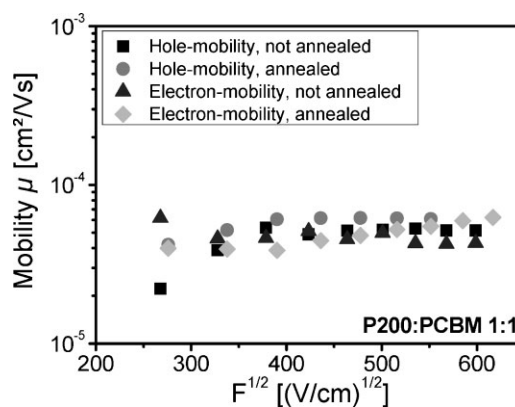


**Figure 6.** Time-of-flight hole transients in pristine RRa-P3HT at multiple electric fields.



**Figure 7.** Time-of-flight electron and hole transients in a 1:1 blend of Sepiolid P200 and PCBM.

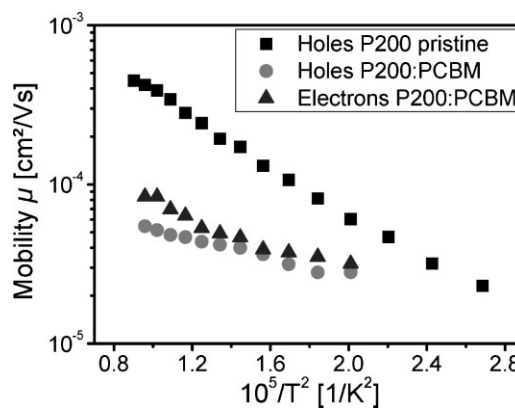
(Fig. 7). However, the hole transient was more dispersive than in the case of the pristine material (compare to Fig. 3). This could partially be caused by the decreased absorption of the blend compared to the pristine polymer film, as a reduced absorption leads to an increased penetration depth of the excitation pulse and, thus, to a broader local distribution of photogenerated charge carriers (i.e., a wider charge-carrier package). In addition, according to Clarke et al.,<sup>[13]</sup> PCBM can induce structural distortions in the P3HT phase leading to an increased density of trap states. For a 1:1 blend of P3HT and PCBM they found that the charge-carrier density threshold for a transition between trap-limited and trap-free transport is on the order of  $10^{-18} \text{ cm}^{-3}$ . The charge-carrier densities determined from our TOF transients are on the order of  $10^{-17} \text{ cm}^{-3}$  and, thus, it can be expected that traps have a strong influence on our results. Nevertheless, a distinct kink in the transients could be detected for all measurements so that a clear assignment of the transit times could be made. As we could not measure the electron transients in pristine P3HT, we assume that in the blend electrons are transported through the PCBM phase and holes are transported through the P3HT. The mobilities of both charge-carrier types were determined to be on the order of  $10^{-5} \text{ cm}^2 \text{ V}^{-1} \text{ s}^{-1}$ , which is about one order of magnitude lower than the hole mobility in pristine Sepiolid P200. While Ballantyne et al.,<sup>[7]</sup> Baumann et al.,<sup>[18]</sup> and Yang et al.<sup>[19]</sup> found almost no difference in hole mobilities of pristine P3HT and blends with PCBM over a large range of molecular weights and P3HT:PCBM blending ratios, Mihailetchi et al.<sup>[20]</sup> observed a reduction in hole mobility by more than three orders of magnitude when they blended a P3HT of similar regioregularity as Sepiolid P200 with PCBM. Additionally, when they annealed the blends, they were able to recover the value of the hole mobility to that of pristine P3HT within the blend. However, this is not the case for our material. As shown in Figure 8, neither hole- nor electron mobility were affected by the thermal annealing. In their study Mihailetchi et al.<sup>[20]</sup> reported an increase in mobility along with a red-shift and decreasing vibronic line-width of the absorption spectra of the blends, resulting in an absorption spectrum that, except for the PCBM contribution, is almost identical to that of pristine P3HT. The absorption spectra of our non-annealed blends of Sepiolid P200 and PCBM (see SI, Fig. S4) already resembled those of pristine Sepiolid P200 and annealing caused an increase in



**Figure 8.** Room-temperature hole- and electron mobilities in annealed and non-annealed blends of Sepiolid P200 and PCBM.

oscillator strength only, neither a red-shift nor a narrowing of the vibronic features was observed. Hence, it appears that the as-cast Sepiolid P200:PCBM film already has a morphology that is similar to the annealed blend reported by Mihailetchi et al. and consequently annealing does not have such a pronounced influence on the charge-carrier mobility. The cause for the discrepancy between our observations and those of Mihailetchi et al. is most probably caused by the fact that we used chlorobenzene as a solvent whereas they used chloroform, which results in different morphologies because of the much faster drying of the film during the spin-coating process. This implies that a change in the hole mobility in P3HT:PCBM blends upon annealing is not the main reason for the increase in solar-cell efficiency observed upon annealing of the devices. It appears that additional effects have to be considered, which could be weak changes in the thermodynamics of the blend resulting in an increased ratio of charge generation over charge recombination as reported by Clarke et al.<sup>[21]</sup> In fact, we observed that the number of charge carriers extracted from the sample during a TOF measurement is larger in the annealed blend than in the non-annealed blend by a factor of 2.25.

Figure 9 compares the hole mobility in pristine Sepiolid P200 with the hole- and electron-mobilities in the annealed blend as a



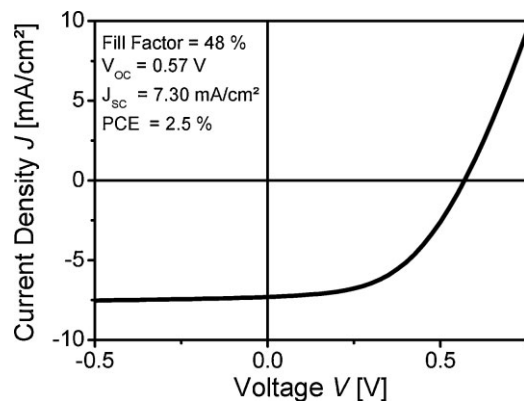
**Figure 9.** Temperature dependence of hole mobility in pristine Sepiolid P200 and hole- and electron mobility in an annealed blend of Sepiolid P200 and PCBM.

function of temperature. Clearly, the hole mobility in pristine Sepiolid P200 depends much stronger on temperature than the electron- and hole-mobilities in the blend. The energetic disorder determined from Equation 2 was  $\sigma_h = (33 \pm 2)$  meV for the holes and  $\sigma_e = (43 \pm 2)$  meV for the electrons. Thus, the energetic disorder for hole transport was reduced by about 40% when blending Sepiolid P200 with PCBM. The reason for this cannot be easily understood. As already mentioned above, a comparison of the absorption spectra of pristine Sepiolid P200 and blends with PCBM does not show any significant differences. This suggests that the formation of well-ordered aggregates, as discussed in section 2.1, is not disturbed by the presence of PCBM and that the morphology of P3HT in pristine and in blend films is rather similar possibly because of the phase separation between the two rather immiscible materials.

In blends of Sepiolid P100 and PCBM the electron mobility was found to be similar to that in Sepiolid P200:PCBM. The hole mobility however could not be determined as the transients were very dispersive and did not show a clear sign of a transit time. Probably, the increased dispersivity, caused by the reduced absorption coefficient combined with a lower hole mobility in Sepiolid P100 compared to that in Sepiolid P200, prevented us from resolving the charge transport with our experimental setup. Thus, we can only assume that in the Sepiolid P100:PCBM blends the hole mobility is lower than that in Sepiolid P200:PCBM blends and consequently the charge-carrier mobility is not as well balanced.

#### 2.4. Photovoltaic Characteristics

Bulk heterojunction solar cells with blends of both regioregular polymers with PCBM were prepared and characterized. Typical current voltage ( $I$ - $V$ ) characteristics of a Sepiolid P200:PCBM (1:1) blend solar cell measured under illumination with an AM1.5G spectrum at  $80 \text{ mW cm}^{-2}$  is shown in Figure 10. The power-conversion efficiency of the device was found to be 2.5% with a fill factor of  $FF = 48\%$ , an open circuit voltage of  $V_{OC} = 0.57 \text{ V}$  and a short-circuit current density of  $J_{SC} = 7.30 \text{ mA cm}^{-2}$ . The device efficiency was increased in steps to about 2.5% for Sepiolid P100 and Sepiolid P200 by varying only the annealing conditions and the



**Figure 10.** Typical  $I$ - $V$  characteristics of a Sepiolid P200:PCBM solar cell under AM1.5 solar illumination.

solvents. We did not change the other parameters to try and increase the efficiency of the blends even further, since this would have been out of the scope of the present study. We realize that as such the preparation conditions have not yet been entirely optimized as can be deduced from the lower fill factor and lower short-circuit currents of our cells compared to literature reports showing record efficiencies for P3HT:PCBM bulk heterojunction solar cells. However, a trend towards reproducible power-conversion efficiencies of about 3% with P3HT:PCBM solar cells seems to have been established in recent literature.<sup>[22–26]</sup>

Devices prepared with Sepiolid P100 in general exhibited lower short-circuit current densities than devices using Sepiolid P200, but they had comparable fill factors and slightly higher open-circuit voltages resulting in similar power-conversion efficiencies for both blend systems. Hence, the observed difference in charge-transport properties described above only results in small changes in device performance and does not seem to play a very crucial role in the measured range of power-conversion efficiencies. A tendency towards lower open-circuit voltages at higher polymer regioregularities had already been reported by others.<sup>[27]</sup> Veldman et al.<sup>[28]</sup> found that in donor-acceptor blends like P3HT:PCBM the open-circuit voltage is linearly dependent on the energetic difference between the highest molecular orbital (HOMO) of the donor and the lowest unoccupied molecular orbital (LUMO) of the acceptor with a slope close to one. Thus, it appears that the change in open-circuit voltage could be caused by a lower HOMO in Sepiolid P100 compared to Sepiolid P200, which is compliant with the overall red-shift of the absorption spectrum of Sepiolid P200 with respect to Sepiolid P100 (Fig. 1). In addition, Kirchartz et al.<sup>[29]</sup> suggested that under certain conditions, for instance through non-ideal recombination of charge carriers at the electrodes or an energetic distribution of charge-transfer states at the heterojunction, an increase in charge-carrier mobility could lead to a reduction of the open-circuit voltage. This would be consistent with our findings reported in section 2.3.

### 3. Conclusions

The regioregularity of P3HT was shown to have a pronounced impact on the packing of its polymer chains in pristine P3HT and P3HT:PCBM blend films. P3HT with very high regioregularity (Sepiolid P200,  $rr > 98\%$ ) exhibited a well-ordered solid-state structure as indicated by the pronounced vibronic features of the absorption spectrum and the further red-shifted absorption compared to P3HT with medium regioregularity (Sepiolid P100,  $rr \sim 94\%$ ). Regiorandom P3HT, however, did not show any signs of ordering as a consequence of the steric repulsion of the side chains. The solid-state order was found to influence the charge-carrier transport in films of the pristine polymers as well as in blends with PCBM typically used for solar-cell devices. Whereas in pristine regiorandom P3HT charge transport was very slow and dispersive, very high regioregularity led to a faster ( $\mu \sim 5 \times 10^{-5} \text{ cm}^2 \text{ V}^{-1} \text{ s}^{-1}$ ) and almost balanced charge transport of the holes and electrons, and medium regioregularity resulted in lower hole mobilities and unbalanced charge transport in the blends. Both regioregular materials demonstrated virtually no dependence of the charge-carrier mobility on the applied electric



field and only a weak dependence on temperature. The charge transport was only marginally influenced by annealing, suggesting that the materials were already optimized in the as-cast films. Consequently, we conclude that a change in charge-carrier mobility can be ruled out as a reason for the improvement of power-conversion efficiencies of devices upon annealing. In spite of the differences caused by the different regioregularities, solar cells prepared from both regioregular polymers in combination with PCBM showed comparable power-conversion efficiencies of about 2.5% without a full empirical optimization of the processing parameters. It, thus, appears that increasing the order and charge-carrier mobility in P3HT films by using very high regioregular polymers does not significantly help to improve the device efficiency.

## 4. Experimental

**Materials:** Sepiolid P100, Sepiolid P200, and RRA-P3HT were supplied by BASF SE, Germany. PCBM was purchased from Sigma Aldrich. All materials were used as received.

**Sample Preparation:** For TOF samples the indium tin oxide (ITO)-coated glass substrates (Präzisions Glas&Optik GmbH, Germany) were patterned by wet etching and subsequently cleaned by an ultrasonic treatment of multiple steps with different solvents. In between each step the substrates were blown dry with nitrogen gas. The clean ITO substrates were plasma etched in argon plasma for 20 min before spin-coating of the organic films. For pristine films, Sepiolid P200 or P100 (RRA-P3HT) was dissolved in chlorobenzene at a concentration of 100 (160) mg mL<sup>-1</sup> and stirred at 70 °C for more than 12 h in a nitrogen-filled glovebox. For blend films, Sepiolid P200 or P100 (30 mg) and PCBM (30 mg) were dissolved separately in dichlorobenzene (600 µL). All solutions were filtered through PTFE filters (0.45 µm) directly before spin-coating inside the glovebox. On top of these films a layer of semitransparent aluminum (*d* of about 10 nm) was deposited as counter electrode. The samples were directly loaded into the evaporation chamber from the glovebox and kept in high vacuum (<3 × 10<sup>-6</sup> mbar) during evaporation of the aluminum electrodes. All annealed samples were treated by solvent-vapor annealing in a dichlorobenzene atmosphere for 25 min before deposition and by thermal annealing at 150 °C for 5 min after deposition of the aluminum electrodes. For solar-cell devices a layer of poly(3,4-ethylenedioxythiophene) poly(styrenesulfonate) (PEDOT:PSS) (Clevios P VP Al 4083, H.C. Stark) was spin-coated onto the cleaned ITO. Blend films of Sepiolid P100 or Sepiolid P200 and PCBM were prepared in the same way as for the TOF samples, but at concentrations of 20 mg mL<sup>-1</sup>. The devices were completed by deposition of a layer of aluminum (*d* ~ 100 nm). The annealing conditions were the same as for the TOF samples. The active area of the devices as determined by the overlap between the aluminum and the patterned ITO was 10 mm<sup>2</sup>.

**TOF Measurements:** For the TOF measurements the samples were housed in a temperature-controlled, custom-built cryostat under a dynamic vacuum of better than 10<sup>-5</sup> mbar. The wavelength of the excitation pulse was controlled by an optical parametric oscillator (OPO) (GWU Lasertechnik GmbH, Germany) pumped by the third harmonic of a Nd:YAG laser that was chosen to match the absorption of the respective material. For the measurement of electron- (hole-) mobilities, the samples were illuminated through the ITO (aluminum) electrode. The sign of the applied voltage was not changed between measuring electron- and hole mobilities and was always chosen to be in reverse-bias in order to prevent charge injection through the electrodes. Current transients were detected with a Tektronix oscilloscope (TDS 524A) triggered by the laser pulse.

**Time-Resolved Spectroscopy:** Samples for time-resolved spectroscopy and further characterization methods were prepared on cleaned quartz substrates using the method described above. Ultrafast time-resolved fluorescence spectroscopy was performed using a Hamamatsu C4742

Streak Camera system. The samples were excited using a frequency-doubled mode-locked Ti:sapphire laser, producing approximately 100 fs pulses at a repetition rate of 80 MHz. The excitation wavelength could be tuned in a range from 380–420 nm to match the absorption of the polymer. The emitted light was collected by a telescope and dispersed by a 0.25 m monochromator with a 50 lines mm<sup>-1</sup> grating before detection with the Streak Camera. Most spectra were accumulated over 500 measurements to increase the signal-to-noise ratio. The samples were placed in a cryostat with a dynamic vacuum better than 10<sup>-5</sup> mbar.

**Further Characterization Methods:** Absorption spectra were recorded using a Perkin-Elmer Lambda 25 spectrophotometer. For the detection of photoluminescence spectra a custom-built setup consisting of a halogen light source, a monochromator, and a USB spectrometer was used. Layer thicknesses were determined by a Tencor P10 surface profilometer. Solar-cell device characterization was performed with a solar simulator (K.H. Steuernagel Lichttechnik GmbH, Germany) inside a nitrogen-filled glovebox.

## Acknowledgements

R. Mauer thanks the Max Planck Graduate Center Mainz for support. F. Laquai acknowledges financial support from the Max Planck Society (Max Planck Research Group) and from the International Research Training Group "Self-organized Materials for Optoelectronics" (IRTG 1404) funded by the Deutsche Forschungsgemeinschaft (DFG). All authors thank I.A. Howard for helpful discussions and C. Klose for assistance with device preparation. Technical assistance from A. Becker and D. Richter is also gratefully acknowledged. Supporting Information is available online from Wiley InterScience or from the authors.

Received: February 16, 2010  
Published online: May 25, 2010

- [1] W. L. Ma, C. Y. Yang, X. Gong, K. Lee, A. J. Heeger, *Adv. Funct. Mater.* **2005**, *15*, 1617.
- [2] M. Reyes-Reyes, K. Kim, J. Dewald, R. Lopez-Sandoval, A. Avadhanula, S. Curran, D. L. Carroll, *Org. Lett.* **2005**, *7*, 5749.
- [3] J. Y. Kim, K. Lee, N. E. Coates, D. Moses, T. Q. Nguyen, M. Dante, A. J. Heeger, *Science* **2007**, *317*, 222.
- [4] K. M. Coakley, M. D. McGehee, *Chem. Mater.* **2004**, *16*, 4533.
- [5] J. Clark, C. Silva, R. H. Friend, F. C. Spano, *Phys. Rev. Lett.* **2007**, *98*, 206 406.
- [6] G. Rumbles, I. D. W. Samuel, L. Magnani, K. A. Murray, A. J. DeMello, B. Crystall, S. C. Moratti, B. M. Stone, A. B. Holmes, R. H. Friend, *Synth. Met.* **1996**, *76*, 47.
- [7] A. M. Ballantyne, L. Chen, J. Dane, T. Hammant, F. M. Braun, M. Heeney, W. Duffy, I. McCulloch, D. D. C. Bradley, J. Nelson, *Adv. Funct. Mater.* **2008**, *18*, 2373.
- [8] A. M. Ballantyne, J. S. Wilson, J. Nelson, D. D. C. Bradley, J. R. Durrant, M. Heeney, W. Duffy, I. McCulloch, presented at *Organic Photovoltaics VII*, San Diego, CA August **2006**.
- [9] S. A. Choulis, Y. Kim, J. Nelson, D. D. C. Bradley, M. Giles, M. Shkunov, I. McCulloch, *Appl. Phys. Lett.* **2004**, *85*, 3890.
- [10] H. Bässler, *Phys. Status Solidi B* **1993**, *175*, 15.
- [11] F. Laquai, G. Wegner, H. Bässler, *Phil. Trans. R. Soc. A* **2007**, *365*, 1473.
- [12] A. Pivrikas, G. Juska, R. Osterbacka, M. Westerling, M. Viliunas, K. Arlauskas, H. Stubb, *Phys. Rev. B* **2005**, *71*, 125 205.
- [13] T. M. Clarke, F. C. Jamieson, J. R. Durrant, *J. Phys. Chem. C* **2009**, *113*, 20 934.
- [14] G. Juska, K. Genevicius, K. Arlauskas, R. Osterbacka, H. Stubb, *Phys. Rev. B* **2002**, *65*, 233 208.
- [15] P. M. Borsenberger, L. Pautmeier, H. Bässler, *J. Chem. Phys.* **1991**, *94*, 5447.
- [16] Y. Kim, S. Cook, S. M. Tuladhar, S. A. Choulis, J. Nelson, J. R. Durrant, D. D. C. Bradley, M. Giles, I. McCulloch, C. S. Ha, M. Ree, *Nat. Mater.* **2006**, *5*, 197.
- [17] W. Helfrich, P. Mark, *Z. Physik* **1962**, *166*, 370.

- [18] A. Baumann, J. Lorrmann, C. Deibel, V. Dyakonov, *Appl. Phys. Lett.* **2008**, 93.
- [19] J. S. Huang, G. Li, Y. Yang, *Appl. Phys. Lett.* **2005**, 87.
- [20] V. D. Mihailetchi, H. X. Xie, B. de Boer, L. J. A. Koster, P. W. M. Blom, *Adv. Funct. Mater.* **2006**, 16, 699.
- [21] T. M. Clarke, A. M. Ballantyne, J. Nelson, D. D. C. Bradley, J. R. Durrant, *Adv. Funct. Mater.* **2008**, 18, 4029.
- [22] A. Pivrikas, P. Stadler, H. Neugebauer, N. S. Sariciftci, *Org. Electron.* **2008**, 9, 775.
- [23] M. Lenes, S. W. Shelton, A. B. Sieval, D. F. Kronholm, J. C. Hummelen, P. W. M. Blom, *Adv. Funct. Mater.* **2009**, 19, 3002.
- [24] Y. Kim, A. M. Ballantyne, J. Nelson, D. D. C. Bradley, *Org. Electron.* **2009**, 10, 205.
- [25] G. Dennler, *Mater. Today* **2007**, 10, 56.
- [26] J. K. Lee, Y. M. Wang, S. Cho, F. Wudl, A. J. Heeger, *Org. Electron.* **2009**, 10, 1223.
- [27] C. H. Woo, B. C. Thompson, B. J. Kim, M. F. Toney, J. M. J. Fréchet, *J. Am. Chem. Soc.* **2008**, 130, 16 324.
- [28] D. Veldman, S. C. J. Meskers, R. A. J. Janssen, *Adv. Funct. Mater.* **2009**, 19, 1939.
- [29] T. Kirchartz, B. E. Pieters, K. Taretto, U. Rau, *Phys. Rev. B* **2009**, 80.

## **4.2 Charge Generation and Recombination**

The article “Effect of Morphology on Ultrafast Free Carrier Generation in Polythiophene:Fullerene Organic Solar Cells” was published in the Journal of the American Chemical Society by the American Chemical Society on October 5<sup>th</sup>, 2010.

Reprinted with permission from Howard, I. A.; Mauer, R.; Meister, M.; Laquai, F. Journal of the American Chemical Society 2010, 132, 14866. Copyright 2010 American Chemical Society.

## Effect of Morphology on Ultrafast Free Carrier Generation in Polythiophene:Fullerene Organic Solar Cells

Ian A. Howard,\* Ralf Mauer, Michael Meister, and Frédéric Laquai\*

Max Planck Research Group for Organic Optoelectronics, Max Planck Institute for Polymer Research, Ackermannweg 10, D-55128 Mainz, Germany

Received June 16, 2010; E-mail: ian.howard@mpip-mainz.mpg.de; laquai@mpip-mainz.mpg.de

**Abstract:** Despite significant study, the precise mechanisms that dictate the efficiency of organic photovoltaic cells, such as charge separation and recombination, are still debated. Here, we directly observe efficient ultrafast free charge generation in the absence of field in annealed poly(3-hexylthiophene):methanofullerene (P3HT:PCBM). However, we find this process is much less efficient in unannealed and amorphous regiorandom blends, explaining the superior short-circuit current and fill-factor of annealed RR-P3HT:PCBM solar cells. We use transient optical spectroscopy in the visible and near-infrared spectral region covering, but not limited to, the previously unobserved and highly relevant time scale spanning 1 to 100 ns, to directly observe both geminate and nongeminate charge recombination. We find that exciton quenching leads directly (time scale less than 100 fs) to two populations: bound charges and free charges. The former do not lead to photocurrent in a photovoltaic cell; they recombine geminately within 2 ns and are a loss channel. However, the latter can be efficiently extracted in photovoltaic cells. Therefore, we find that the probability of ultrafast free charge formation after exciton quenching directly limits solar cell efficiency. This probability is low in disordered P3HT:PCBM blends but approaches unity in annealed blends.

### 1. Introduction

Organic photovoltaic cells (OPVs) are based on partially demixed blends of electron-donating and electron-accepting materials. They have the advantage over their inorganic counterparts of the potential for low-cost, large-area fabrication and have reached power conversion efficiencies of over 7%.<sup>1</sup> The efficiency with which they convert sunlight into electrical power depends on the product of two factors: their quantum efficiency (current generated per photon absorbed) and their energy efficiency (fraction of photon energy retained by an extracted charge). The quantum efficiency itself is determined by the product of the efficiencies of a cascade of events: photon absorption, exciton quenching, charge separation, and charge extraction. These events occur over highly disparate time and length scales. Although various methods of altering the morphology, from thermal and solvent-vapor annealing,<sup>2,3</sup> to deposition from solvent mixtures,<sup>4,5</sup> have been used to optimize the quantum efficiency in many OPV blends, the complexity and widely ranging time and length scales of the quantum efficiency cascade mean that firm understanding of the precise structure–function relationship is still developing.

Recently, detailed morphological and time-resolved optical studies have begun to clarify this structure–function relationship. Direct observation with sub-10 nm resolution of the blend morphology over 100 nm thickness and a micrometer size area has recently been achieved for the benchmark P3HT:PCBM blends using electron tomography, with the key finding that annealing develops ordered P3HT nanorods with widths around 15 nm, thicknesses of a few nanometers, and lengths on the scale of micrometers.<sup>6</sup> Furthermore, Ohkita et al. recently demonstrated that the annealing and order in the P3HT phase strongly enhances the generation of separated charges and suppresses loss during carrier collection.<sup>7</sup> By extending the observation of charge recombination to cover its entire progress (200 fs to 10  $\mu$ s), including the previously unobserved but critically relevant intermediate time scale of 3–100 ns, we gain physical insight into how the transition from amorphous to better ordered P3HT domains affects both the generation of free charges and their recombination. We directly observe that annealing of P3HT:PCBM blends leads to ultrafast free charge generation. This prompt generation process is inconsistent with theoretical models based on an Onsager–Braun type charge separation through a Coulombically bound pair and elucidates why parameters for the charge-pair lifetimes in such models had to exceed experimentally observed values by several orders of magnitude.<sup>8</sup> Our work therefore highlights not only the critical role of local order in the high quantum efficiency of P3HT:

(1) Liang, Y.; Xu, Z.; Xia, J.; Tsai, S.-T.; Wu, Y.; Li, G.; Ray, C.; Yu, L. *Adv. Mater.* **2010**, *xx*, in press.

(2) Padinger, F.; Rittberger, R. S.; Sariciftci, N. S. *Adv. Funct. Mater.* **2003**, *13*, 85.

(3) Li, G.; Yao, Y.; Yang, H.; Shrotriya, V.; Yang, G.; Yang, Y. *Adv. Funct. Mater.* **2007**, *17*, 1636.

(4) Zhang, F.; Jespersen, K. G.; Björström, C.; Svensson, M.; Andersson, M. R.; Sundström, V.; Magnusson, K.; Moons, E.; Yartsev, A.; Inganäs, O. *Adv. Funct. Mater.* **2006**, *16*, 667.

(5) Campbell, A. R.; Hodgkiss, J. M.; Westenhoff, S.; Howard, I. A.; Marsh, R. A.; McNeill, C. R.; Friend, R. H.; Greenham, N. C. *Nano Lett.* **2008**, *8*, 3942.

(6) Van Bavel, S. S.; Sourty, E.; De With, G.; Loos, J. *Nano Lett.* **2009**, *9*, 507.

(7) Guo, J. M.; Ohkita, H.; Benten, H.; Ito, S. *J. Am. Chem. Soc.* **2010**, *132*, 6154.

(8) Deibel, C.; Strobel, T.; Dyakonov, V. *Phys. Rev. Lett.* **2009**, *103*, 036402.

PCBM solar cells but also the need to develop a better theoretical understanding, perhaps encompassing correlated disorder,<sup>9</sup> of charge separation at junctions between organic semiconductors.

As model systems we use regiorandom (RRa) P3HT and highly (>98%) regioregular (RR) P3HT (BASF Sepiolid P200) blended with PCBM. Transient changes of the excited state absorption of pristine polymers as well as blends are monitored in the visible and in the near-infrared spectral region (500–1100 nm), and spectra are compared with those obtained by quasi-steady-state photoinduced absorption spectroscopy. This allows us to clearly assign the contribution of the individual excited states to the absorption spectra that we observe and also assemble in a stepwise fashion a clear and quantitative understanding of the population transitions.

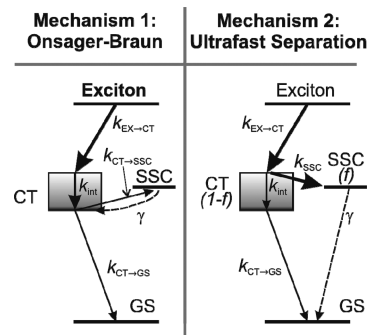
## 2. Models of Charge Separation and Recombination

Before presenting our experimental results, we briefly outline two theoretical frameworks for considering the quantum efficiency loss mechanisms in organic solar cells that we will later compare with our data. However, first we briefly discuss the charge recombination reactions that play a role in these models.

**2.1. Monomolecular and Bimolecular Charge Recombination.** A first important distinction between loss mechanisms in organic solar cells is whether they follow monomolecular or bimolecular kinetics. Monomolecular processes occur with the same rate (and probability) irrespective of the illumination intensity, while bimolecular processes occur more quickly at higher excited state densities created by more intense illumination. Therefore, monomolecular processes cause a fixed loss of quantum efficiency at all intensities, while bimolecular processes cause a variable loss that becomes more severe at higher illumination.

When an electron and hole generated by the quenching of a single exciton recombine with one another it is termed geminate recombination.<sup>10–12</sup> Geminate recombination may repopulate the ground state, or, in high open-circuit voltage blends, populate an energetically accessible triplet exciton state.<sup>12,13</sup> In either case, it is a monomolecular terminal loss mechanism and reduces the quantum efficiency by a fixed factor at all illumination intensities.

When two free opposite charges recombine it is called nongeminate recombination. The rate of nongeminate recombination depends on the density of the spatially separated (or free) charges, and therefore the rate of nongeminate recombination depends on the intensity of the light excitation. In previous investigations of P3HT:PCBM blends, the nongeminate recombination rate was usually observed to have an order greater than 2 (which is the order theoretically expected for 3D Langevin recombination).<sup>14–16</sup> This stronger dependence on charge density could imply that the mobility depends on charge



**Figure 1.** Illustrations of the two limiting cases for the mechanism of charge generation and separation. CT stands for charge-transfer state, SSC for spatially separated (free) charges, and GS for ground state. In mechanism 1 the thermal relaxation of the charge-transfer state is much faster than separation; consequently charge separation and recombination are mediated by the relaxed charge-transfer state. An Onsager–Braun type description of charge separation should be applicable and separation times of certainly >1 ns are expected. In the second limiting case, the spatial separation of charges in hot charge-transfer states created directly after exciton quenching rivals or exceeds the rate of internal conversion in the CT manifold. In this case, free, spatially separated charges are generated on a very fast time scale (<100 fs). See text for further details.

density,<sup>17,18</sup> the morphology restricts the dimensionality of charge diffusion,<sup>19</sup> a trap density alters recombination dynamics,<sup>20</sup> or a combination of these factors. In any case, the amount of loss this type of recombination causes depends on the illumination intensity. In P3HT:PCBM solar cells at short circuit conditions under solar illumination intensity, nongeminate recombination is so low as to be negligible.<sup>18,21</sup>

When one free carrier is caught in an immobile trap state and then subsequently recombines with another free carrier it is called trap-assisted recombination. Depending on whether or not the trap density can be approximated as constant, trap-assisted recombination can follow density-dependent or -independent kinetics.

**2.2. Onsager–Braun Charge Separation.** Two limiting cases for the mechanism of charge generation and recombination can be considered.<sup>22,23</sup> These are schematically illustrated in Figure 1. The first mechanism, like the Onsager–Braun model, considers that charge separation occurs in kinetic competition with recombination from an equilibrated geminate pair. In this mechanism a hot charge-transfer state created by exciton quenching first quickly relaxes (~100 fs time scale) to its lowest excited electronic and vibrational level. Thereafter, on a longer ~5 ns time scale, the charges held in such relaxed charge-

- (9) Groves, C.; Blakesley, J. C.; Greenham, N. C. *Nano Lett.* **2010**, *10*, 1063.  
 (10) Clarke, T.; Ballantyne, A.; Jamieson, F.; Brabec, C.; Nelson, J.; Durrant, J. *Chem. Commun.* **2009**, 89.  
 (11) De, S.; Pascher, T.; Maiti, M.; Jespersen, K. G.; Kesti, T.; Zhang, F. L.; Inganas, O.; Yartsev, A.; Sundstrom, V. *J. Am. Chem. Soc.* **2007**, *129*, 8466.  
 (12) Westenhoff, S.; Howard, I. A.; Hodgkiss, J. M.; Kirov, K. R.; Bronstein, H. A.; Williams, C. K.; Greenham, N. C.; Friend, R. H. *J. Am. Chem. Soc.* **2008**, *130*, 13653.  
 (13) Ohkita, H.; Cook, S.; Astuti, Y.; Duffy, W.; Heeney, M.; Tierney, S.; McCulloch, I.; Bradley, D. D. C.; Durrant, J. R. *Chem. Commun.* **2006**, 3939.

- (14) Shuttle, C. G.; O'Regan, B.; Ballantyne, A. M.; Nelson, J.; Bradley, D. D. C.; Durrant, J. R. *Phys. Rev. B* **2008**, *78*, 113201.  
 (15) Shuttle, C. G.; O'Regan, B.; Ballantyne, A. M.; Nelson, J.; Bradley, D. D. C.; de Mello, J.; Durrant, J. R. *Appl. Phys. Lett.* **2008**, *92*, 093311.  
 (16) Clarke, T. M.; Jamieson, F. C.; Durrant, J. R. *J. Phys. Chem. C* **2009**, *113*, 20934.  
 (17) Pasveer, W. F.; Cottaar, J.; Tanase, C.; Coehoorn, R.; Bobbert, P. A.; Blom, P. W. M.; de Leeuw, D. M.; Michels, M. A. J. *Phys. Rev. Lett.* **2005**, *94*, 206601.  
 (18) Shuttle, C. G.; Hamilton, R.; Nelson, J.; O'Regan, B. C.; Durrant, J. R. *Adv. Funct. Mater.* **2010**, *20*, 698.  
 (19) Juska, G.; Genevicius, K.; Nekrasas, N.; Sliuzys, G.; Osterbacka, R. *Appl. Phys. Lett.* **2009**, *95*, 013303.  
 (20) Nelson, J.; Choulis, S. A.; Durrant, J. R. *Thin Solid Films* **2004**, *451–452*, 508.  
 (21) Marsh, R. A.; McNeill, C. R.; Abrusci, A.; Campbell, A. R.; Friend, R. H. *Nano Lett.* **2008**, *8*, 1393.  
 (22) Brédas, J. L.; Norton, J. E.; Cornil, J.; Coropceanu, V. *Acc. Chem. Res.* **2009**, *42*, 1691.  
 (23) Clarke, T. M.; Durrant, J. R. *Chem. Rev.* **2010** *xx*, in press.

transfer states hop, either to become spatially separated (a process that is endothermic or at least goes through a higher energy intermediate because the charge-transfer state still has a significant binding energy),<sup>22</sup> or to come into such close proximity that they recombine geminately. A key feature of this first mechanism is that the rate (and therefore also yield) of carrier separation is increased by the drift of charges caused by the electric field inside the device. This means that as the field in the device increases, the charge-transfer states separate more quickly and therefore their lifetime and luminescence decreases, while at the same time the quantum efficiency of the device increases.<sup>24</sup> In a blend in which the charge-transfer state is emissive, the charge-transfer state lifetime can be directly monitored by temporally resolving its emission. This method has been used to show that the charge-transfer state lifetime in fluorene:PCBM OPVs does indeed decrease with increasing field,<sup>25</sup> showing the relevance of the Onsager–Braun type mechanism of charge separation. Also in P3HT:PCBM solar cells, wherein CT emission is difficult to temporally resolve, recent bias-dependent transient absorption measurements,<sup>26</sup> and correlation of the above- and below-bandgap absorption and photocurrent,<sup>27</sup> are interpreted to support this mechanism of charge generation, with the latter also suggesting excess energy does not increase the probability of charge separation. Also, Monte Carlo simulations based on these assumptions have provided reasonable descriptions of the morphological effects of blend structure on charge separation.<sup>28</sup> However, the support for this model is by no means universal. Neher and co-workers have recently demonstrated that charge-transfer state separation cannot account for all of the photocurrent observed, and that at low fields the photocurrent must come from a different source.<sup>29</sup> Furthermore, in order to explain the field dependence of photocurrent using such a model, exceedingly long charge-transfer state lifetimes ( $\sim 7 \mu\text{s}$ ) that are inconsistent with experimental observations ( $\sim 10 \text{ ns}$ ) must be used.<sup>24</sup>

The rate equations that describe the population evolutions in this mechanism are shown in eq 1, wherein CT is the charge-transfer state population, SSC is the spatially separated electron population, GS is the population returned to the ground state,  $k_{i \rightarrow j}$  is a characteristic rate for monomolecular flow from population  $i$  to population  $j$ ,  $\gamma$  is the density-dependent recombination rate constant, and  $\lambda + 1$  is the order of the density-dependent (“bimolecular”) recombination. For 3D isotropic Langevin recombination with a time and carrier-density independent mobility  $\lambda = 1$ , as mentioned earlier  $\lambda$  can exceed 1 if the morphology limits the dimensionality of diffusion or the charge mobility is time- or density-dependent. In this first mechanism, the fraction of geminate recombination is given by  $k_{\text{CT} \rightarrow \text{GS}} / (k_{\text{CT} \rightarrow \text{GS}} + k_{\text{CT} \rightarrow \text{SSC}})$ , the total depletion rate of the initially formed charge-transfer states is  $k_{\text{tot}} = k_{\text{CT} \rightarrow \text{SSC}} + k_{\text{CT} \rightarrow \text{GS}}$ , the fraction of nongeminate recombination is  $k_{\text{CT} \rightarrow \text{SSC}} / (k_{\text{CT} \rightarrow \text{GS}} +$

$k_{\text{CT} \rightarrow \text{SSC}})$ , and the effective rate of nongeminate recombination is  $\gamma k_{\text{CT} \rightarrow \text{GS}} / (k_{\text{CT} \rightarrow \text{GS}} + k_{\text{CT} \rightarrow \text{SSC}})$ . Here we see that when separation is much more likely than recombination ( $k_{\text{CT} \rightarrow \text{SSC}} \gg k_{\text{CT} \rightarrow \text{GS}}$ ), the effective bimolecular recombination rate will be strongly reduced, which would be consistent with the experimentally observed bimolecular recombination rates being much lower than that predicted by the Langevin equation.<sup>30</sup> To summarize, in this mechanism the charge-transfer state is a key intermediate state, with the rate of separation versus recombination determining the amount of geminate vs nongeminate recombination and also mediating the rate of the bimolecular recombination.

$$\begin{aligned} d\text{CT}/dt &= -k_{\text{CT} \rightarrow \text{GS}}\text{CT} - k_{\text{CT} \rightarrow \text{SSC}}\text{CT} + \gamma\text{SSC}^{\lambda+1} \\ d\text{SSC}/dt &= k_{\text{CT} \rightarrow \text{SSC}}\text{CT} - \gamma\text{SSC}^{\lambda+1} \\ d\text{GS}/dt &= k_{\text{CT} \rightarrow \text{GS}}\text{CT} \end{aligned} \quad (1)$$

**2.3. Ultrafast Charge Separation.** The second mechanism involves direct spatial separation of charges from excited (“hot”) charge-transfer states before they thermally relax and predicts different yields and kinetics for geminate and nongeminate recombination compared to the Onsager–Braun model. The precise mechanism for the charge separation is still unclear; it is proposed that the excess energy of the strongly exothermic exciton quenching can be directly translated into kinetic energy of the electron and hole<sup>31</sup> or that, similar to charge formation from highly excited singlet excitons in a pristine material, a greater separation of electron and hole in the wave function of higher excited CT states leads directly to separated charges.<sup>22</sup> Nonetheless, the key feature of this mechanism is that on an ultrafast time scale after exciton quenching either free charges or a thermally relaxed charge-transfer state is produced. The thermalization of the charge-transfer state by internal conversion places an upper limit on the time scale for charge separation in this model. As the process of internal conversion in organic materials is extremely fast, occurring within several hundred femtoseconds both in singlet<sup>32</sup> and triplet manifolds,<sup>33</sup> we assume that it will occur at a similarly fast rate in the charge-transfer manifold. Therefore, in this second mechanism, the rate of spatial separation from the hot charge-transfer state must be fast on the time scale of hundreds of femtoseconds in order for device efficiency to be appreciable.<sup>34</sup> This is faster than the instrument response of our experiment, and therefore we can consider that in this model the number of free (spatially separated) and bound (charge-transfer state) charges can be taken as an initial condition. The rate equations describing the second mechanism are shown in eq 2, which have the initial conditions that a fraction  $f$  of the excitons create spatially separated charges (via a hot charge-transfer state) within the pulse length of the excitation and the remaining  $(1 - f)$  of the excitons create charge-transfer states that decay monomolecularly. Analytic solutions can be found for the rate equations. These are shown in eq 3. The nomenclature remains as introduced for eq 1.

(24) Blom, P. W. M.; Mihailetchi, V. D.; Koster, L. J. A.; Markov, D. E. *Adv. Mater.* **2007**, *19*, 1551.

(25) Veldman, D.; Ipek, O.; Meskers, S. C. J.; Sweelssen, J.; Koetse, M. M.; Veenstra, S. C.; Kroon, J. M.; van Bavel, S. S.; Loos, J.; Janssen, R. A. J. *J. Am. Chem. Soc.* **2008**, *130*, 7721.

(26) Marsh, R. A.; Hodgkiss, J. M.; Friend, R. H. *Adv. Mater.* **2010**, *22*, 3672.

(27) Lee, J.; Vandewal, K.; Yost, S. R.; Bahlke, M. E.; Goris, L.; Baldo, M. A.; Manca, J. V.; Voorhis, T. V. *J. Am. Chem. Soc.* **2010**, *132*, 11878.

(28) Groves, C.; Marsh, R. A.; Greenham, N. C. *J. Chem. Phys.* **2008**, *129*.

(29) Inal, S.; Schubert, M.; Sellinger, A.; Neher, D. *J. Phys. Chem. Lett.* **2010**, *1*, 982.

(30) Pivrikas, A.; Juška, G.; Mozer, A. J.; Scharber, M.; Arlauskas, K.; Sariciftci, N. S.; Stubbs, H.; Österbacka, R. *Phys. Rev. Lett.* **2005**, *94*, 176806.

(31) Peumans, P.; Forrest, S. R. *Chem. Phys. Lett.* **2004**, *398*, 27.

(32) Virgili, T.; Marinotto, D.; Manzoni, C.; Cerullo, G.; Lanzani, G. *Phys. Rev. Lett.* **2005**, *94*, 117402.

(33) Yang, X. D.; Lee, C. L.; Westenhoff, S.; Zhang, X. P.; Greenham, N. C. *Adv. Mater.* **2009**, *21*, 916.

(34) The term ‘spatially-separated charge’ is slightly misleading at high excitation intensities, as in these cases the average separation between charges can remain small due to their very high density. In this case what we mean by ‘spatially-separated’ charge are those charges that have lost any preferential association with their geminate pair, i.e., they are free to interact with any nearby opposite charge.

$$\begin{aligned}
 dCT/dt &= -k_{CT-GS}CT \\
 dSSC/dt &= -\gamma SSC^{\lambda+1} \\
 dGS/dt &= k_{CT-GS}CT + \gamma SSC^{\lambda+1}
 \end{aligned}
 \quad (2)$$

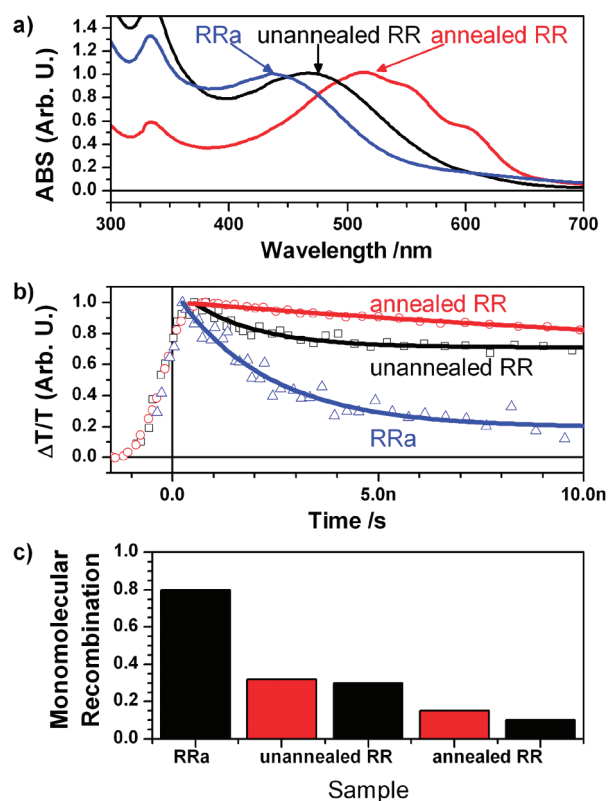
$$\begin{aligned}
 CT(t) &= N_0(1-f)\exp(-k_{CT-GS}t) \\
 SSC(t) &= (\lambda\gamma t + (fN_0)^{-\lambda})^{-1/\lambda} \\
 GS(t) &= N_0(1-f)(1 - \exp(-k_{CT-GS}t)) + \\
 &\quad N_0f - ((\lambda\gamma t + (fN_0)^{-\lambda})^{-1/\lambda})
 \end{aligned}
 \quad (3)$$

### 3. Results

Familiar with the possible kinetics of charge separation, and geminate and nongeminate recombination, we now examine our experimental results. In this section we first present a brief overview of how the intermolecular order and charge recombination changes through the sample series we present. We then proceed with a detailed and stepwise analysis in order to interpret the features presented in the overview, starting with RRa-P3HT, then unannealed RR-P3HT, and finally annealed RR-P3HT results. As the photophysics change with increasing P3HT order, we discuss the mechanisms for the changes and what they imply for device performance.

**3.1. Effect of P3HT Order on Recombination.** In Figure 2a we present the steady-state absorption spectrum of the RRa, unannealed, and annealed P3HT:PCBM blends. As expected, the absorption steadily red-shifts, due to the increased contribution to the absorption of weakly interacting H-aggregates in the regions of P3HT with high intermolecular order.<sup>35</sup> The intermolecular order increases from the RRa, to the unannealed and finally to the annealed RR-P3HT:PCBM blends.

Figure 2b shows the mean induced absorption from 750 to 850 nm of each sample for the first 10 ns after low intensity excitation where, as we will later confirm, monomolecular processes dominate the early time decay. We will later find that in this region, charge-transfer states and spatially separated charges have the same mean cross-section, and therefore that the transient absorption signal here is proportional to the total number of charge-transfer states plus spatially separated charge pairs. Thus, we can use this region to directly watch how the total number of charges, free and bound, changes with time. We can see that this decay changes significantly between the samples. In the RRa-P3HT:PCBM blend a large portion of the population decays within 2 ns. In the unannealed RR-P3HT:PC13M blend there is a decay component with a similar lifetime, but the weight of this component is much smaller, and consequently it results in a much smaller population loss. In the annealed RR-P3HT:PCBM blend the decay is slower, it does not exhibit the 2 ns component observed in the other two samples. Furthermore, its population loss is the least. We will find later that, at these low excitation intensities, the decay on this time scale is almost entirely monomolecular, so the amount of geminate recombination and/or monomolecular trap-assisted recombination can be approximated by the fraction of the signal that has decayed in the first 10 ns. We show these estimates of the geminate recombination losses in Figure 2c, alongside values that we extract later from a complete global model of the data. These geminate losses will directly reduce OPV performance at all light intensities, and therefore we can already hypothesize that this directly observed reduction of monomolecular recombination with increasing P3HT order is responsible for the



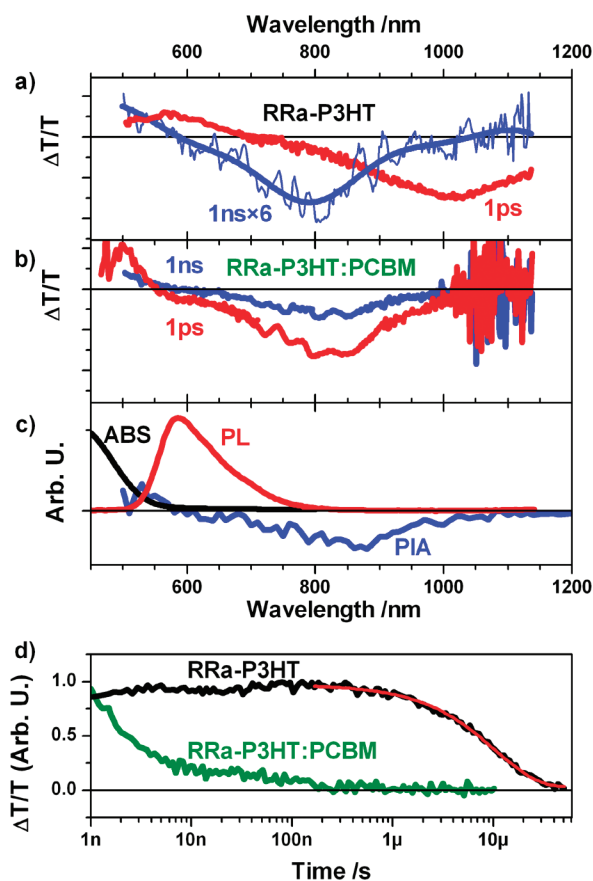
**Figure 2.** Comparison of RRa-P3HT:PCBM (labeled RRa), unannealed chloroform-cast RR-P3HT:PCBM (unannealed RR), and annealed chlorobenzene-cast RR-P3HT:PCBM (annealed RR) blends. Panel a shows the shift of the absorption spectra between samples due to differing interchain ordering. Panel b shows the kinetics of the charge-induced absorption over the first 10 ns at the lowest excitation intensities. The solid lines show fits to a monomolecular decay described in the text. Panel c shows the fraction of recombination that is intensity independent for each sample obtained by qualitatively examining the low-fluence decay (black bars) or from the global fit described in the text (red bars).

improvements of OPV device performance with annealing. In the following sections, we will examine this more closely and learn more about what the kinetics imply about the processes of exciton quenching, charge separation, and charge recombination. We will also discover that the effect of morphology on these processes is clearly evident in the kinetics, and that the kinetics are consistent with the development of pure P3HT ordered regions that are only on the order of a few nanometers in their most constrained dimension but much longer than this in their other dimensions.

**3.2. RRa-P3HT and RRa-P3HT:PCBM.** In this first subsection we start the detailed examination of the data looking at the amorphous regiorandom P3HT alone and blended 1:1 with PCBM. We find that in the pure P3HT film (no PCBM added) singlet excitons decay within 1 ns, with some fraction intersystem crossing to long-lived triplet states that decay with a lifetime of 10  $\mu$ s. In contrast, we find that when PCBM is added to the blend, excitons are quenched within 100 fs and therefore no triplets are formed. The exciton quenching results predominantly in charge-transfer states which decay geminately (i.e., independent of fluence) with a characteristic inverse rate of 2 ns. This fast geminate decay explains the poor performance of amorphous P3HT:PCBM blends in solar cells.

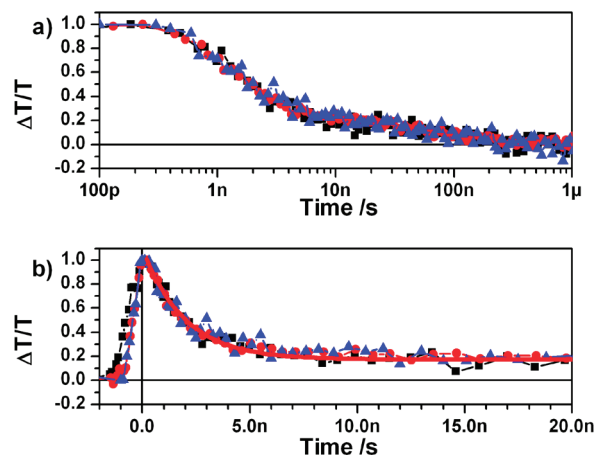
**3.2.1. Absence of Triplets in RRa-P3HT:PCBM.** Recent work has demonstrated that long-lived triplet excitons are formed in

(35) Clark, J.; Silva, C.; Friend, R. H.; Spano, F. C. *Phys. Rev. Lett.* **2007**, *98*, 206406.



**Figure 3.** Panels a and b show the transient absorption spectra of regiorandom P3HT alone and blended with PCBM, respectively. The spectrum after 1 ns is multiplied by 6 for clarity in panel a. Panel c shows the absorption and photoluminescence of a RRa-P3HT film and the quasi-steady-state photoinduced absorption spectrum of a RRa-P3HT:PCBM blend (at 80 K). Panel d shows the normalized mean transient absorption of each film from 700 to 900 nm; the red line is a single exponential fit to the triplet lifetime (10  $\mu$ s). The laser excitation intensity was 7  $\mu$ J/cm<sup>2</sup>.

RRa-P3HT.<sup>36</sup> In order to determine the charge kinetics in a RRa-P3HT:PCBM blend, we must first ascertain whether triplet states also contribute to the observed long-lived transient absorptions in the blend. In order to do this, we compare the transient absorption of RRa-P3HT and a RRa-P3HT:PCBM blend. Figure 3a shows transient absorption spectrum of RRa-P3HT 1 ps and 1 ns after excitation (the spectrum after 1 ns is multiplied by 6 for clarity). One picosecond after photoexcitation, the excited state population is dominated by singlet excitons. The positive  $\Delta T/T$  signal in the region of photoluminescence (compare red lines in Figure 3a,c) is due to stimulated emission from singlet excitons. The photoinduced absorption (negative  $\Delta T/T$  signal) peaks at approximately 1000 nm, consistent with the PIA of the singlet state observed in previous work.<sup>36</sup> Also as found in previous work,<sup>36</sup> the singlet excitons decay quickly, within 1 ns, with some fraction intersystem crossing into triplet excitons which have a photoinduced absorption peaking at 800 nm (see blue line in Figure 2a). Under low fluence conditions, these triplet excitons are the dominant photoexcited state after 1 ns. The decay of these triplets is shown in Figure 3d by the black line. The red line is a fit to a monoexponential decay, from which a lifetime of 10  $\mu$ s is extracted. This is slightly longer



**Figure 4.** Panel a shows the normalized charge-induced absorption from 750–900 nm as a function of time in the RRa-P3HT:PCBM blend film after 7 (black squares), 15 (red circles), and 60 (blue triangles)  $\mu$ J/cm<sup>2</sup> excitation pulses. Panel b shows the first 20 ns of the same data on a linear scale; the red line is a monoexponential fit yielding a geminate recombination lifetime of 2 ns.

than the lifetime of 7  $\mu$ s recently reported in the literature,<sup>36</sup> but this discrepancy could be explained by slightly fewer triplet quenching sites (for example oxygen molecules) being present in our sample.

Figure 3b shows the transient absorption spectrum of RRa-P3HT:PCBM after 1 ps and 1 ns. No stimulated emission is observed, even at times less than 1 ps. Rather, the signal is dominated by a photoinduced absorption which is broad but peaks between 850 and 900 nm. This is the same spectrum that is observed with quasi-steady-state photoinduced absorption at low temperature (blue line in Figure 3c) and is assigned to the product of exciton quenching. This indicates that excitons are quenched much faster (in less than 100 fs) than they intersystem cross in the pristine film, and that therefore the number of triplets formed in the blend should be negligible. This is further supported by the fact that the shape of the transient spectrum in a blend does not evolve with time. Furthermore, comparing the quasi-steady-state PIA of the pristine film and the blend, the blend has an infrared absorption growing toward 2  $\mu$ m typical of a charge-induced absorption, while the pristine blend does not (see Supporting Information). We therefore conclude that the products of exciton quenching dominate the excited state population of the blend, and any contribution of triplet excitons to the dynamics is exceedingly negligible.

This conclusion is supported by the dynamics presented in Figure 3d. The green line showing the induced absorption of RRa-P3HT:PCBM blend traces a much faster decay than that of the triplets observed in pristine RRa-P3HT. This clearly indicates that charges, rather than triplet excitons, dominate the excited state population in the blend and that charge recombination is faster than triplet decay.

**3.2.2. Geminate Recombination in RRa-P3HT:PCBM.** In order to examine how the recombination of the charges generated in RRa-P3HT:PCBM blend depends on the charge density, i.e., to investigate the roles of geminate and nongeminate processes in charge recombination, we investigate the transient absorption as a function of the excitation pulse intensity. By comparing the normalized traces of the recombination kinetics over a series of excitation intensities, the presence (or absence) of intensity-dependent recombination can be analyzed. In Figure 4a we present such a plot showing the time dependence of the

(36) Guo, J. M.; Ohkita, H.; Bente, H.; Ito, S. *J. Am. Chem. Soc.* **2009**, *131*, 16869.



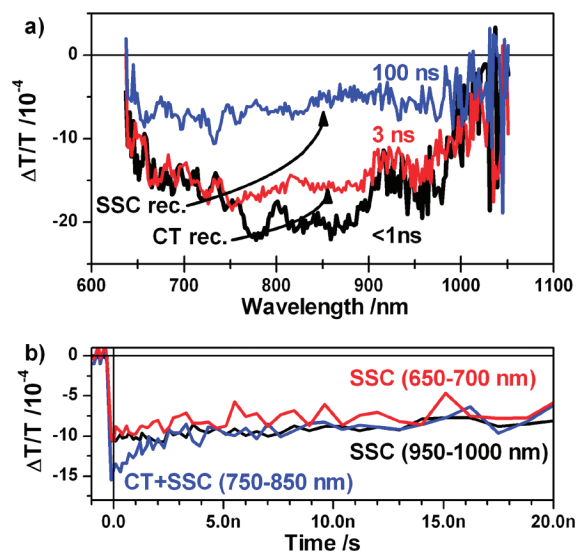
normalized charge-induced absorption from 750 to 900 nm in RRa-P3HT:PCBM for a sequence of excitation pulse fluences. The decay in each case is the same, with approximately 80% of the population decaying within the first couple of nanoseconds and the remaining 20% of the population decaying on the time scale of 200 ns. This observation, that the rate of the 80% majority component of the recombination does not depend on fluence, indicates that this recombination is monomolecular and geminate. Figure 4b focuses on the major component of the recombination, showing only the first 20 ns. Fitting a single monoexponential decay to all of the curves yields the red line shown with an inverse rate for this initial geminate charge-transfer state recombination of 2 ns (rate =  $5 \times 10^8/s$ ). Therefore, the majority of the quenched excitons (80%) in the RRa-P3HT blend form charge-transfer states that decay within 2 ns. Previously, it has been shown that the charges bound in charge-transfer states in polymer:polymer photovoltaic blends are immobile.<sup>12</sup> Our observation that the charge-transfer states do not interact even at the highest excitation intensity, which corresponds to an average separation of only 3.5 nm between charge-transfer states, provides strong indirect evidence that their mobility is low. Therefore, these likely immobile, quickly decaying states are not likely to be efficiently split under the internal field of a photovoltaic cell and explain a loss mechanism of up to 80% of the absorbed photons that correlates with the poor performance of RRa-P3HT:PCBM photovoltaic devices.<sup>37</sup>

The inverse rate we find for geminate recombination is somewhat longer than that of 800 ps found by Ohkita et al. who measured on a 3 ns window.<sup>7</sup> Repeating their measurement and fitting only on a 3 ns window, we extract an inverse rate constant of 1.5 ns (see Supporting Information). This can be explained by considering there is some heterogeneity in the rate of geminate recombination, dependent on the precise interfacial alignment.<sup>38</sup> So although there is not complete agreement for the characteristic geminate recombination rate, we can say with certainty that it typically occurs on a time scale less than 2 ns. Finally, we ascribe the 20% of the signal that decays on a much longer time scale to nongeminate, perhaps trap-assisted, recombination of spatially separated charges.

**3.3. Geminate and Nongeminate Recombination in Unannealed RRa-P3HT:PCBM.** With the understanding that charge recombination in the amorphous RRa-P3HT:PCBM is dominated by fast geminate recombination of charge-transfer states, we now turn to examine the photophysics of an unannealed RRa-P3HT:PCBM blend. We will find that one-third of the quenched excitons produce geminate pairs that decay with the same rate as those observed in the previous section while the remaining two-thirds generate free charges, that in our test films undergo bimolecular recombination but in solar cells could be extracted.

On a time scale less than 1 ns we find that the kinetics are broadly similar to those in the RRa-P3HT:PCBM blend. Again, no stimulated emission is observed, which indicates that in the unannealed blend, exciton quenching is again essentially immediate. Hence, we begin our analysis of this blend by investigating the products of exciton quenching and their decay.

In Figure 5a we present the mean induced absorption spectrum of the unannealed RRa-P3HT blend <1, then 3, and finally 100 ns after excitation. At an early time, the spectrum



**Figure 5.** Panel a shows the average induced absorption spectrum of unannealed RRa-P3HT:PCBM at the indicated times. CT state recombination in the first 2 ns reduces the peak at 850 nm, and then subsequent SSC recombination reduces the remaining broad induced absorption. Panel b shows the kinetics in spectral regions where the CT cross-section is much smaller than the SSC cross-section (black and red curves), and also the region where the CT state and SSC have the same mean cross-section (blue curve).

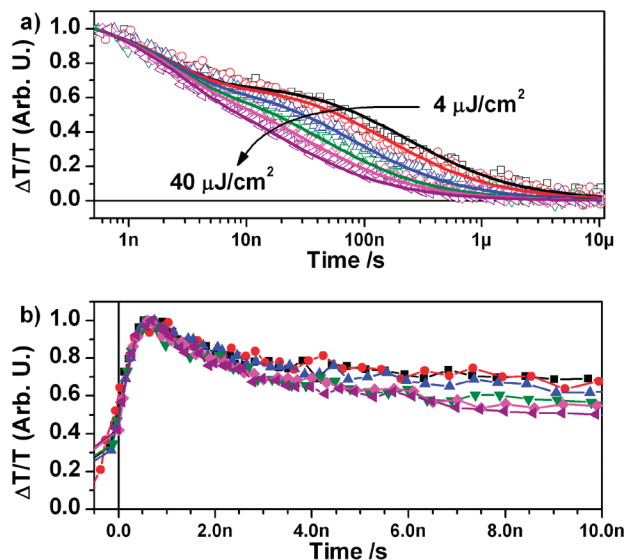
peaks at 850 nm, the peak wavelength of CT absorption observed in the previous section. We will see that this peak decays with exactly the same rate as the geminate pairs in RRa-P3HT:PCBM, leaving a broader induced absorption that decays on a time scale of hundreds of nanoseconds. Therefore, Figure 5 immediately suggests that two populations are created concurrently by exciton ionization: charge transfer states that have a peaked absorption at 850 nm and decay within 2 ns, and free charges that have a broad induced absorption and do not (at least at low to moderate fluence) decay within the first 3 ns.

In order to extract the population dynamics of charge-transfer states and spatially separated charges from the observed transient absorption signals we must know the relative cross-section of each species over the observed wavelength range. Fortunately, the analysis is greatly simplified by the observation that the CT states and SSC pairs have the same average cross-section of  $5 \times 10^{-17} \text{ cm}^2$  in the wavelength range 750–850 (see Supporting Information for details). In this region the transient absorption is simply proportional to the total of number charges (CT states and SSCs). Consequently, the recombination of a CT state decreases the signal by the same amount as the recombination of a SSC pair (in essence we create an artificial isobestic ‘point’ by averaging a deliberately selected appropriate wavelength range). Figure 5b compares the transient absorption kinetics in regions wherein the CT cross-section is much smaller than the SSC cross-section, and therefore the transient absorption signal tracks exclusively the SSC population, with the transient absorption kinetics in the 750–850 nm region wherein the transient absorption kinetics show, with equal weighting, the kinetics of the CT states plus the kinetics of the SSC pairs. Comparing the initial value of the 750–850 nm region with the value of the plateau, we can simply estimate that one-third of the initial population are CT states while two-thirds are promptly generated free SSCs.

We now investigate the fluence dependence of the mean PIA from 750 to 850 nm in an unannealed RRa-P3HT:PCBM blend.

(37) Campoy-Quiles, M.; Kanai, Y.; El-Basaty, A.; Sakai, H.; Murata, H. *Org. Electron.* **2009**, *10*, 1120.

(38) Huang, Y. S.; Westenhoff, S.; Avilov, I.; Sreearunothai, P.; Hodgkiss, J. M.; Deleener, C.; Friend, R. H.; Beljonne, D. *Nat. Mater.* **2008**, *7*, 483.



**Figure 6.** Panel a shows the mean induced absorption decay (750–850 nm) in an unannealed RR-P3HT:PCBM blend at various excitation intensities (open symbols), alongside global fits (solid lines) described in the text. Panel b presents the first 10 ns of the data on a linear scale to highlight the intensity independent geminate charge-transfer recombination. Excitation intensities 4, 6.5, 13, 20, 26, and 40  $\mu\text{J}/\text{cm}^2$ .

Figure 6a illustrates that in the unannealed sample a portion of the charge recombination becomes more rapid with higher intensity excitation, but also that a monomolecular, intensity-independent, component is visible that dominates the recombination in the first 2 ns. This monomolecular component is highlighted by the linear scale graph of early time shown in Figure 6b. Such mixed decay is completely consistent with our observations in Figure 5 and moreover our hypothesis that charge-transfer state recombination accounts for the decay on a time scale of less than 2 ns and that the recombination of spatially separated charges account for the remaining longer-time decay.

Let us now quantitatively consider what these observed kinetics imply about the mechanism of charge separation. Of the two mechanisms introduced in section 2, the first cannot explain a major feature of the data, namely that although the fraction of separation has substantially increased between the RRA and unannealed RR blends, the CT lifetime remains unchanged. From our observation of geminate charge-transfer state recombination in RRA-P3HT PCBM we know that  $k_{\text{CT-GS}} \approx 5 \times 10^8/\text{s}$ . We observe that two-thirds of the decay in the unannealed sample is bimolecular, so two-thirds of the charge-transfer states must spatially separate. In this case  $k_{\text{CT-GS}}/(k_{\text{CT-SSC}} + k_{\text{CT-GS}}) = 1/3$ , and therefore  $k_{\text{CT-SSC}} + k_{\text{CT-GS}} = k_{\text{tot}} \approx 1.5 \times 10^9/\text{s}$ . Therefore, for this model to be self-consistent, the CT state should decay in the unannealed RR blend in less than 1 ns. However, the CT state decay is not this fast, in fact fitting a single exponential to the early time decay results in a time constant of approximately 2 ns, unchanged from the value observed in the RRA blend. Therefore, the high yield of spatial separation is not consistent with the Onsager–Braun type model of charge generation; however, it is consistent with an ultrafast mechanism of charge generation. Given that the cross-sections of the CT and SSC are the same in the region considered, the normalized transient absorption is given by  $[N_0(1 - f)\exp(-k_{\text{CT-GS}}t) + (\lambda\gamma t + (fN_0)^{-\lambda})^{-1/2}]/N_0$ . Using the calculated values for  $N_0$ , (see Supporting Information) the parameters  $f$ ,  $k_{\text{CT-GS}}$ ,  $\lambda$ , and  $\gamma$  are extracted by globally fitting the entire

**Table 1.** Parameters along with Standard Error Extracted from Global Fit of Model from Section 2.3 to the Data for Unannealed RR-P3HT:PCBM and Annealed RR-P3HT:PCBM Shown in Figures 6a and 9a

parameter	unannealed	annealed
$1 - f$ (fraction monomolecular recombination)	$0.32 \pm 0.01$	$0.15 \pm 0.01$
$f$ (fraction nongeminate recombination)	$0.68 \pm 0.01$	$0.85 \pm 0.01$
$k_{\text{CT-GS}}/\text{s}$ (geminate recombination rate)	$4.9 \pm 0.2 \times 10^8$	$2.5 \pm 0.2 \times 10^8$
$\lambda + 1$ (order of nongeminate decay)	$2.18 \pm 0.01$	$2.45 \pm 0.01$
$\gamma$ ( $\text{cm}^3$ ) $^{\lambda} \text{s}^{-1}$ (nongeminate decay rate)	$2.3 \pm 0.5 \times 10^{-15}$	$1.9 \pm 0.3 \times 10^{-20}$

intensity series. Fits are performed using Origin 8 (Originlab Corporation). The data are well described by this model, as illustrated by the solid lines overlaying the data in Figure 6a). The extracted parameters along with their standard error are summarized in Table 1. To summarize, the observations of immediate bimolecular recombination and an unchanged rate of geminate recombination in the unannealed RR-P3HT:PCBM blend are inconsistent with a model of free charge formation through a charge-transfer state. They imply that quenched excitons immediately form either charge-transfer states or free charges. In the absence of field, charge-transfer states recombine geminately with the same rate as those in the amorphous RRA-P3HT:PCBM blend.

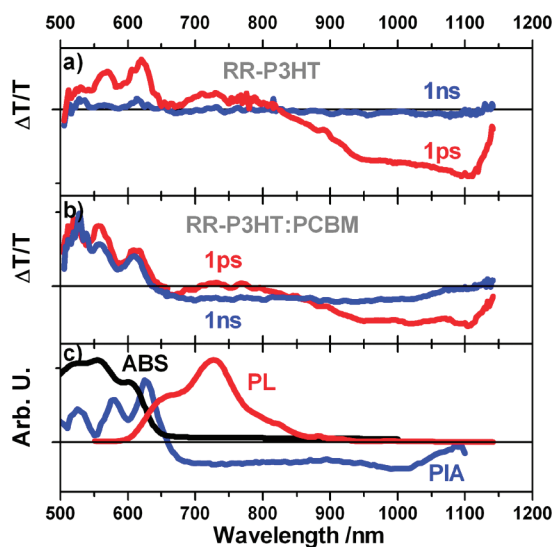
In order to compare the recombination we observe with 3D Langevin recombination, we use the charge carrier mobility of these samples measured using the time-of-flight technique,<sup>39</sup> to calculate a 3D Langevin coefficient ( $\gamma_{3D}$ ) on the order of  $10^{-10} \text{cm}^{-3} \text{s}^{-1}$ . Then, to compare the recombination rate at specific densities between 3D Langevin recombination where  $\lambda = 1$  (a pure second-order process) and extracted nongeminate recombination where  $\lambda = 1.18$ , we use the relation:  $(dC/dt)_a/(dC/dt)_b = \gamma_a/\gamma_b C^{(\lambda_a - \lambda_b)}$ . For carrier densities spanning the range from those typical in a photovoltaic device under solar illumination to the highest intensities used in this work, i.e.,  $10^{15}$ – $10^{19}/\text{cm}^3$ , the observed rate in the unannealed sample varies from 1/10th to 1/20th of the rate predicted by Langevin recombination. This slower-than-Langevin recombination is consistent with previous measurements<sup>30</sup> and has been ascribed to morphological effects decreasing the probability of charge pairs meeting.<sup>40,41</sup>

**3.4. Nongeminate Recombination in Annealed RR-P3HT:PCBM.** In this section the photophysics of the annealed P3HT:PCBM blend is studied and contrasted to the previous results. We find that a portion of the exciton quenching is no longer instantaneous, indicating that some excitons must now diffuse through regions of highly pure P3HT before encountering an interface. We also find that, unlike the less efficient amorphous and unannealed blends, there is no geminate recombination in the annealed blend. Essentially all quenched excitons immediately generate free charges even in the absence of field, explaining the high short-circuit current and fill factor of annealed P3HT:PCBM devices. The order of the recombination also changes, and although change in the carrier density dependence of the mobility and trap distributions likely plays a role in this alteration, we also raise the possibility that restricted

(39) Mauer, R.; Kastler, M.; Laquai, F. *Adv. Funct. Mater.* **2010**, *20*, 2085.

(40) Koster, L. J. A.; Mihailetschi, V. D.; Blom, P. W. M. *Appl. Phys. Lett.* **2006**, *88*, 052104.

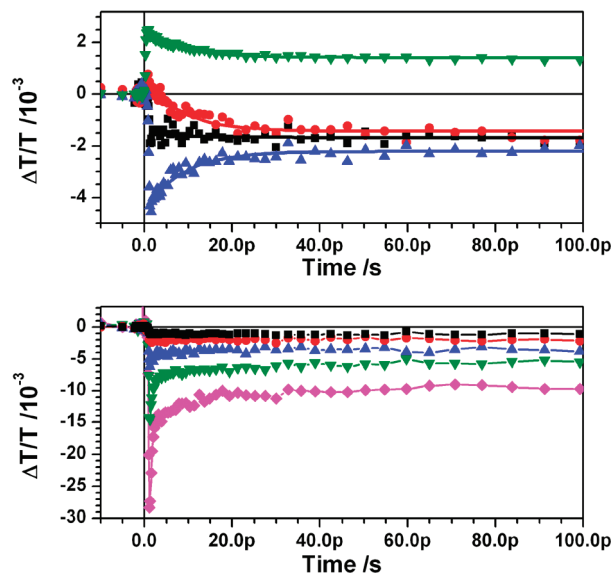
(41) Groves, C.; Greenham, N. C. *Phys. Rev. B* **2008**, *78*, 155205.



**Figure 7.** Panels a and b show the transient absorption spectra of regioregular P3HT alone and in an annealed blend with PCBM. Panel c shows the absorption and photoluminescence of a RR-P3HT film and the quasi-steady-state photoinduced absorption spectrum of a RR-P3HT:PCBM blend (at 80 K). The excitation fluence was  $\sim 7 \mu\text{J}/\text{cm}^2$ .

diffusion due to 2D morphological constraint of charges in the pure P3HT regions (that caused the diffusion limited exciton quenching) could be partially responsible.

**3.4.1. Diffusion Limited Exciton Quenching.** In the previous two samples, the exciton quenching occurred in less than 100 fs after excitation, indicating that the excitons did not need to diffuse to reach a PCBM molecule. This is not the case in the annealed blend, in which stimulated emission from excitons similar to that in pure P3HT is observed for a few picoseconds after excitation, indicating that some excitons in the annealed blend must travel significantly further in order to be quenched. Figure 7a) shows the transient absorption spectrum for pure RR-P3HT. After 1 ps (red line) the excited state population is dominated by singlet excitons. The positive  $\Delta T/T$  signal in the region of the P3HT photoluminescence (red line in Figure 7c) is due to stimulated emission from the excitons. After 1 ns (blue line) the singlet excitons have decayed back into the ground state and, at the low fluences considered, the excited state population is completely diminished. Figure 7b) shows the transient absorption spectrum for an annealed RR-P3HT:PCBM blend. In this case, after 1 ps (red line) the spectrum is a mixture between the exciton spectrum seen in the pure polymer and the long-lived charge signal seen in the quasi-steady-state PIA experiment (blue line in Figure 7c). The stimulated emission peaked around 720 nm is still clearly visible in the 1 ps spectrum in Figure 7b, but it is superimposed on the negative offset of charge-induced absorption from promptly generated charges. This stimulated emission in the annealed blend is a clear indication that, contrary to initial reports,<sup>42</sup> the exciton quenching does not occur entirely within 120 fs. This will be examined in the next section and is in agreement with recent literature.<sup>7,43</sup> We see that between 500 and 620 nm the absorption bleach of the singlet state is greater than the net bleach of the charge, consistent with the singlet exciton being more delocalized than



**Figure 8.** Panel a shows the change in transient absorption in an annealed RR-P3HT:PCBM blend over the first 100 ps for the bleach between 550 and 600 nm (green down-triangles), the region of stimulated emission between 725 and 775 nm (red circles), the isosbestic point at  $\sim 860$  nm (black squares), and the region of 900–1000 nm (blue up-triangles). The solid lines show the global fit to a monoexponential decay, indicating that all the transitions are described by a 9 ps inverse rate. Panel b shows the evolution of the transient absorption at the isosbestic point after an excitation pulse with fluences of 2 (black squares), 4 (red circles), 10 (green down-triangles), and 40  $\mu\text{J}/\text{cm}^2$  (pink diamonds). At low fluence the population remains constant over the whole time range; however, at high fluences annihilation in the first 10 ps reduces the population.

the charge or the charge causing overlapping induced absorption in this region. Therefore, transition of the excited state population from singlet excitons to charges decreases the bleach in this region. In the region of the stimulated emission, from 650 to 840 nm, the induced absorption of the charges is greater than that of the exciton, and consequently the transition from exciton to charge is here accompanied by a growth in the induced absorption. In the small region roughly between 840 and 860 nm we find an isosbestic point, where the induced absorption of the singlet excitons and the charges are the same, meaning that the kinetics in this wavelength range are affected only by decay into the ground state and are unchanged by exciton quenching. Finally, we note that at longer wavelengths the induced absorption of the exciton state is greater than the induced absorption of the charge, and therefore a transition from exciton to charge is accompanied by a decrease in induced absorption. By briefly examining the kinetics in these four regions, we will determine the rate of diffusion-limited charge generation.

In Figure 8 we present the kinetics in an annealed RR-P3HT:PCBM blend on a time scale less than 100 ps. Figure 8a shows the kinetics in the region of the bleach, in the region of stimulated emission from the exciton, at the isosbestic point, and in the region of induced absorption after a low fluence excitation pulse. The black squares show the kinetics at the isosbestic point and are therefore directly proportional to the total excited state population. The invariance of the signal at the isosbestic point indicates that the total excited state population remains constant on this time scale at this low fluence. Therefore, on this time scale, there can be a conversion of excited state population from one pool to another but no recombination to the ground state. Previously, the kinetics on this time scale were ascribed to conversion of charge-transfer

(42) Hwang, I. W.; Moses, D.; Heeger, A. J. *J. Phys. Chem. C* **2008**, *112*, 4350.

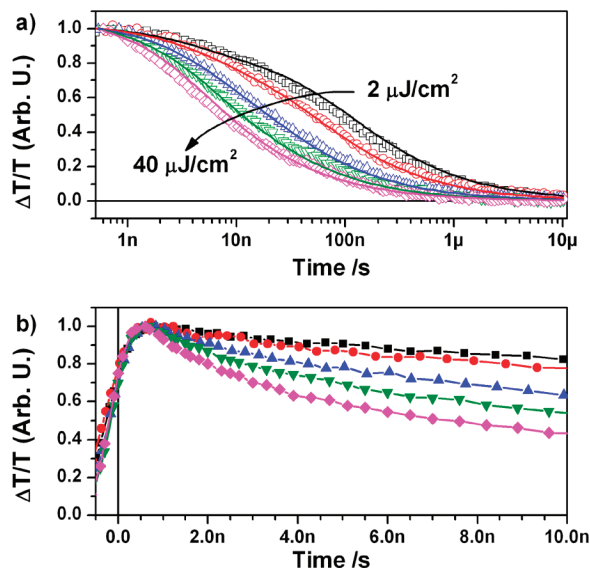
(43) Marsh, R. A.; Hodgkiss, J. M.; Albert-Seifried, S.; Friend, R. H. *Nano Lett.* **2010**, *10*, 923.

states to spatially separated charges.<sup>42</sup> However, the continued observation of stimulated emission (red circles) unequivocally demonstrates that these dynamics involve exciton states. In order to estimate the characteristic rate with which these excitons diffuse to the interface and form charges we globally fit the kinetics to a single exponential decay. The resulting fit is shown as the solid lines in Figure 8a. An inverse rate of 9 ps is obtained, and it is clear that this single rate describes the kinetics at all regions. Therefore, these early kinetics can all be assigned to diffusion-limited exciton quenching and are comparable to those observed in polymer:polymer blends.<sup>44</sup> If the exciton diffusion coefficient is known, then the rate of diffusion-limited exciton quenching provides an estimate of the polymer domain size.<sup>44</sup> The diffusion coefficient of excitons in P3HT has recently been measured to be  $1.8 \times 10^{-3} \text{ cm}^2/\text{s}$ ,<sup>45</sup> from which the diffusion length in 10 ps can be calculated as  $d = (Dt)^{1/2} \approx 1 \text{ nm}$ . Therefore, on average, excitons must only diffuse 1 nm before they are ionized in the P3HT:PCBM blend, indicating that even after annealing the smallest dimension of the pure P3HT domains is on the order of a few nanometers, allowing exciton quenching to remain very efficient.

One problem that can hinder the interpretation of transient absorption data is the emergence of second-order processes due to the high photon flux during the short excitation pulses. Figure 8b shows the kinetics at the isosbestic point for a sequence of excitation pulse fluences. At low fluence there is no change in population over the entire time range. However, starting with the  $10 \mu\text{J}/\text{cm}^2$  fluence, a population loss in the first 10 ps starts occurring. This indicates that an annihilation mechanism starts to compete with charge-transfer at high fluences, and that therefore, at high fluences, some excitons are returned to the ground state via a second-order interaction rather than diffusing to an interface and creating charges. The most likely candidate for this interaction is exciton-charge annihilation, which has been observed to be important in similar systems.<sup>46,47</sup> This second-order process is observed in annealed samples because it can compete with the diffusion-limited rate of exciton quenching but not in unannealed samples because here the quenching remains faster than the second-order process (see Supporting Information). In order to assign kinetics relevant to solar cell operation, it is important to observe the transient absorption at a variety of fluences, because high fluence excitation can, as in this case, introduce second-order effects that completely mask the relevant low excitation density process.

### 3.4.2. Bimolecular Recombination in Annealed P3HT:PCBM.

In the previous section we observed that a portion of exciton quenching in annealed RR-P3HT is diffusion limited, indicating that highly pure regions of P3HT are formed, which have a thickness on the order of a few nanometers. In this section we find that in the annealed RR-P3HT:PCBM blend no nanosecond geminate recombination remains, indicating that free charge generation is much more efficient than in the amorphous RR-P3HT:PCBM blend and also significantly better than in the unannealed blend. The charge-density dependence of the recombination is also altered, which is usually attributed to a



**Figure 9.** Panel a shows the charge induced absorption decay (750–850 nm) in an annealed RR-P3HT:PCBM blend at various excitation intensities (open symbols), alongside global fits according to mechanism 2 described in section 2 (solid lines). Panel b presents the first 10 ns of the data on a linear scale, showing that the early time decay becomes intensity independent at low intensities. Excitation intensities were 2, 4, 10, 20, and  $40 \mu\text{J}/\text{cm}^2$ .

change in the carrier-density dependence of the mobility or variations in the individual microstructure of devices. We observe that, in addition to these factors, a shift to more restricted diffusion in the annealed samples due to faster motion of charges in 2D ribbons could also contribute to this change in density dependence.

In Figure 9a we present the fluence dependence of the mean induced absorption from 750 to 850 nm for the annealed RR-P3HT:PCBM blend. It is clearly altered from that of the unannealed blend presented in Figure 6, and on the basis of these alterations, we can make two qualitative observations. First, the absence of a clear, 2 ns, monomolecular decay component (see Figure 9b) indicates that charge-transfer state formation has been strongly suppressed by annealing, meaning that annealing has increased the generation of free carriers. Second, as Figure 9b highlights, the decay is affected by intensity from the very earliest time, even in the first nanosecond it is increased, again providing strong evidence that the generation of free carriers must happen directly following exciton quenching. Qualitatively examining Figure 9b slightly more closely, we note that at the lowest two fluences measured, which differ by a factor of 2 in pump intensity, there is little difference in the early time decay, with both signals decaying similarly to approximately 0.9 after 5 ns. This indicates that a monomolecular process is responsible for a fraction of the charge recombination at low charge densities; however, the decay is significantly slower than the charge-transfer state recombination. This suggests that, in the case of annealed P3HT:PCBM, the monomolecular charge recombination may be due to a trap or morphology-assisted process rather than geminate charge-transfer state recombination.<sup>16,48</sup>

In order to quantitatively examine the data, we fit it to the second mechanism for charge separation in the same way we did the unannealed data. Again, the data are well described by

(44) Westenhoff, S.; Howard, I. A.; Friend, R. H. *Phys. Rev. Lett.* **2008**, *101*, 016102.

(45) Shaw, P. E.; Ruseckas, A.; Samuel, I. D. W. *Adv. Mater.* **2008**, *20*, 3516.

(46) Howard, I. A.; Hodgkiss, J. M.; Zhang, X.; Kirov, K. R.; Bronstein, H. A.; Williams, C. K.; Friend, R. H.; Westenhoff, S.; Greenham, N. C. *J. Am. Chem. Soc.* **2010**, *132*, 328.

(47) Hodgkiss, J. M.; Tu, G. L.; Albert-Seifried, S.; Huck, W. T. S.; Friend, R. H. *J. Am. Chem. Soc.* **2009**, *131*, 8913.

(48) Tong, M. H.; Coates, N. E.; Moses, D.; Heeger, A. J.; Beaupre, S.; Leclerc, M. *Phys. Rev. B* **2010**, *81*, 125210.

the model, as illustrated by the solid lines overlaying the data in Figure 9a (the kinetics cannot be described by mechanism 1, see Supporting Information). The extracted parameters are again shown in Table 1. Comparison with the parameters extracted for the unannealed blend confirms our qualitative observations that the rate of monomolecular decay and the branching ratio between monomolecular and bimolecular recombination are changed. Fifteen percent of the charge recombination in the annealed sample is monomolecular but with a time scale twice as long as that in the unannealed and RRa blends. Given the alteration in rate, we propose this monomolecular component is not geminate charge-transfer state recombination but rather a mechanism similar to that proposed by Sundstrom and co-workers,<sup>11</sup> in which some charge pairs separate but are constrained by the blend morphology to stay in reasonably close proximity and recombine monomolecularly. This would indicate that roughly 15% of heterojunction sites in annealed RR-P3HT blends hinder complete spatial separation of charge and consequently lead charge pairs generated at these sites to stay close enough together that they recombine monomolecularly on a time scale under 10 ns. It is not impossible that these carriers could be separated by applied field and therefore contribute to the field dependence of the transient absorption recently observed by Friend and co-workers.<sup>26</sup>

The 85% majority of the free charges generated undergo density-dependent “bimolecular” recombination. However, the order of this bimolecular reaction is changed significantly, taking on a value close to 2.5 compared to that of 2.2 for the unannealed sample. Recombination in annealed RR-P3HT:PCBM solar cells with a reaction order greater than 2 has recently been correlated with a density-dependent carrier mobility,<sup>18</sup> which can be caused by an exponential tail of localized subgap states.<sup>20</sup> The order has also been observed to vary between devices<sup>18</sup> and has previously been found (on a longer time scale) to decrease with annealing.<sup>16</sup> A decrease in the reaction order after annealing is consistent with traps becoming more shallow.

On the shorter time scales we observe here, we see the opposite effect; the reaction order increased with annealing. Although carrier density dependence is likely to play a key role in determining the reaction order, and variation of the crystallinity between unannealed samples can lead to variations in the order between devices,<sup>16</sup> we here draw attention to the possibility that restriction of charge diffusion in 2D pure P3HT domains could contribute to an increase in reaction order with annealing. As the dimensionality of the diffusion that limits recombination is reduced, the order of the reaction is increased. For a 2D case, the reaction order expected is 2.5.<sup>19</sup> In the case of 2D Langevin recombination, the recombination coefficient,  $\gamma$ , can be calculated theoretically expressed as  $\gamma_{2D} = 3\pi^{1/2}\gamma_{3D}l^{3/2}/4$ , where  $l$  is the thickness of the constrained dimension.<sup>19</sup> With our estimate of  $10^{-10} \text{ cm}^{-3} \text{ s}^{-1}$  for  $\gamma_{3D}$  based on TOF measurements, and the value for  $\gamma$  of  $1.9 \pm 0.3 \times 10^{-20}$  extracted from the fit of the observed data, we can solve this expression to estimate the thickness of the constrained dimension: we obtain a value for  $l$  of 4 nm. This is consistent with the length that we previously estimated in which excitons diffuse before being quenched in the annealed film. It is also consistent with the thickness of the 2D crystalline domains recently observed using electron tomography.<sup>6</sup> Restriction of diffusion by the nanomorphology has previously been observed to play a key role in determining second-order interactions in polymer:polymer blends,<sup>46</sup> and the opportunity in this P3HT:PCBM system to couple direct experimental observation with electron tomography of the blend

morphology over orders of magnitude in length scale (from the nanometer to multimicrometer) with the observation of reaction kinetics over orders of magnitude in time (from the femtosecond to multimicrosecond) offers exciting prospects to develop a fully rigorous understanding of the processes underpinning the performance of devices based on complex organic heterostructures.

#### 4. Summary and Implications for Photovoltaic Device Performance

The key finding of our experiments in terms of photovoltaic device performance is that exciton quenching in annealed RR-P3HT:PCBM blends immediately produces free charges, even in the absence of field. This explains their high quantum efficiency and fill factor in solar cells. The ultrafast generation of free charges depends strongly on morphology. The yield of free charges is lower in unannealed blends, and very small in blends of amorphous RRa-P3HT. In these cases charge-transfer states that decay geminately within nanoseconds are also formed and will be much harder to extract in a solar cell, explaining reductions in quantum efficiency as well as fill factor. Interestingly, although the exciton energy is the highest in the RRa-P3HT and therefore the excess energy generated by exciton quenching the greatest, the free charge yield is the lowest. Therefore, contrary to suggestions that excess energy is the key criterion for free charge generation,<sup>49</sup> our results suggest that the ultrafast generation of free charges is more strongly related to structural order. This suggestion is consistent with results demonstrating efficient solar cells with significantly less excess energy lost at the heterojunction,<sup>50,51</sup> and also with recent observations that demonstrate efficient free carrier generation in annealed P3HT:PCBM devices even when an interfacial state is created without excess energy.<sup>27</sup>

In the unannealed blends we find 32% of quenched excitons form geminately decaying charge-transfer states. However, the IQE of unannealed devices is only around 30%,<sup>52</sup> which implies that the extraction of the free charges must also be rather inefficient in the unannealed blend.

In the annealed blend there is a 15% component of monomolecular decay on a time scale of  $\sim 5$  ns that we attribute to spatially separated charges generated in regions of the film where further spatial separation is morphologically hindered, i.e., where one charge is trapped at or near an interface. If we assume that all exciton quenching proceeds with an inverse rate of  $\sim 10$  ps and use 300 ps as the unquenched exciton lifetime (see Supporting Information), we find that 5% of excitons can decay before being quenched. Such recombination and incomplete quenching accounts for the roughly 80% IQE of annealed devices.<sup>52</sup> Scaled down to charge densities of  $10^{16} \text{ cm}^{-3}$ , approximately those expected in a solar cell, our results suggest the time scale for nongeminate recombination is  $\sim 3$  ms. This is much longer than the charge extraction time and therefore consistent with the observation that bimolecular recombination plays little role in the device efficiency.

We therefore conclude that the key to the high efficiency of annealed P3HT:PCBM solar cells lies in their ability to directly

(49) Ohkita, H.; Cook, S.; Astuti, Y.; Duffy, W.; Tierney, S.; Zhang, W.; Heeney, M.; McCulloch, I.; Nelson, J.; Bradley, D. D. C.; Durrant, J. R. *J. Am. Chem. Soc.* **2008**, *130*, 3030.

(50) Lenes, M.; Wetzelaer, G.; Kooistra, F. B.; Veenstra, S. C.; Hummelen, J. C.; Blom, P. W. M. *Adv. Mater.* **2008**, *20*, 2116.

(51) Piliago, C.; Holcombe, T. W.; Douglas, J. D.; Woo, C. H.; Beaujuge, P. M.; Fréchet, J. M. J. *J. Am. Chem. Soc.* **2010**, *132*, 7595.

(52) Burkhard, G. F.; Hoke, E. T.; Scully, S. R.; McGehee, M. D. *Nano Lett.* **2009**, *9*, 4037.

generate free charges upon exciton quenching. This ultrafast free charge generation is strongly related to the sample morphology, with the samples with increased order showing far greater free charge generation. This can explain the morphologically dependent charge yields previously measured after longer delay times.<sup>16,53</sup> However, neither the role of excess energy in this process nor the exact role of ordered regions on charge generation is completely clear. Therefore, although we clearly demonstrate that fast generation of free charges is possible and underlies the high quantum efficiency and fill-factor of annealed P3HT:PCBM solar cells, the mechanism for this generation remains a question for further research.

## 5. Methods

Regioregular (RR) P3HT (Sepiolid P200,  $M_w = 25,000 \text{ g mol}^{-1}$ , PDI = 1.6, regioregularity >98%) and regiorandom (RRa) P3HT were obtained from BASF SE. PCBM (~99%) was purchased from Aldrich. All materials were used as received. The polymers and PCBM were separately dissolved in chlorobenzene or chloroform, the solutions were mixed and then spin-cast onto precleaned quartz substrates in a nitrogen-filled glovebox. The annealed sample was heated to 120 °C for 20 min in a nitrogen-filled glovebox.

Transient absorption (TA) measurements were performed with a home-built pump–probe setup. To measure in the time range of 1–4 ns with a resolution of ~100 fs, the output of a commercial titanium:sapphire amplifier (Coherent LIBRA HE, 3.5 mJ, 1 kHz, 100 fs) was split with one portion used to generate a 532 nm excitation pulse (output of an optical parametric amplifier (Coherent OPerA Solo)) and another used to generate a white light probe using a home-built two-stage broadband (480–850 nm) noncollinear optical parametric amplifier (NOPA) for white light generation and amplification in the visible and a c-cut 3 mm thick sapphire window for white light generation in the visible to near-infrared spectral range. The variable delay of up to 4 ns between pump and probe was introduced by a broadband retroreflector mounted on a mechanical delay stage. Only reflective optics were used to guide the probe beam to the sample to minimize chirp. The excitation pulse was chopped at 500 Hz, while the white light pulses were dispersed onto a linear photodiode array which was read out at 1

kHz. Adjacent diode readings corresponding to the transmission of the sample after an excitation pulse and without an excitation pulse were used to calculate  $\Delta T/T$ . For measuring in the time range of 1 ns to 1 ms with a resolution of 600 ps, the excitation pulse was provided by an actively Q-switched Nd:YVO<sub>4</sub> laser (AOT Ltd. MOPA). The delay between pump and probe in this case was controlled by an electronic delay generator (Stanford Research Systems DG535). TA measurements were performed at room temperature under dynamic vacuum at pressures <10<sup>-5</sup> mbar.

Quasi-steady-state PIA experiments were performed with monochromatic light (LOT-Oriel Omni- $\lambda$  300 monochromator) generated from a 100 W tungsten halogen light source (Müller XH 100) used as probe and the output of an UV-LED (Hamamatsu LC-L2, 365 nm) used as pump. The transmitted probe light was detected after dispersion by a second identical monochromator by an amplified silicon photodetector (Thorlabs PDA100A) in the wavelength range from 500 to 1100 nm, an InGaAs detector (Thorlabs DET10C) from 900 to 1800 nm, and a second InGaAs detector (Thorlabs DET10D) from 1800 to 2100 nm. The pump light was chopped at approximately 330 Hz by a mechanical chopper, and the change in transmission  $\Delta T$  induced by the pump was extracted by using the lock-in technique (EG&G Princeton Applied Research Model 5210). Prior to the PIA measurement, the total transmission was measured to calculate  $\Delta T/T$ . All PIA measurements were performed in a nitrogen-cooled optical cryostat (Oxford Instruments Optistat CF) at 80 K in helium atmosphere. The total probe area was approximately 1 cm<sup>2</sup>.

**Acknowledgment.** The authors thank M. Kastler (BASF SE) for kind provision of RRa-P3HT and Sepiolid P200, A. Becker for technical support, and the IRTG 1404 for funding. I.A.H. thanks the Alexander von Humboldt Foundation for a postdoctoral fellowship. F.L. thanks the Max Planck Society for funding a Max Planck Research Group. R.M. and M.M. thank the Max Planck Graduate Center (MPGC) for financial support.

**Supporting Information Available:** Additional PIA spectra, kinetic traces, fluence dependence, and fits to Braun–Onsager type charge generation. This information is available free of charge via the Internet at <http://pubs.acs.org/>.

JA105260D

(53) Keivanidis, P. E.; Clarke, T. M.; Lilliu, S.; Agostinelli, T.; Macdonald, J. E.; Durrant, J. R.; Bradley, D. D. C.; Nelson, J. J. *Phys. Chem. Lett.* **2010**, *1*, 734.

### **4.3 Field and Temperature Dependence of Charge Generation and Recombination**

The article “Effect of Nongeminate Recombination on Fill Factor in Polythiophene/Methanofullerene Organic Solar Cells” was published in The Journal of Physical Chemistry Letters by the American Chemical Society on December 3<sup>rd</sup>, 2010.

Reprinted with permission from Mauer, R.; Howard, I. A.; Laquai, F. J. Phys. Chem. Lett. 2010, 1, 3500. Copyright 2010 American Chemical Society.

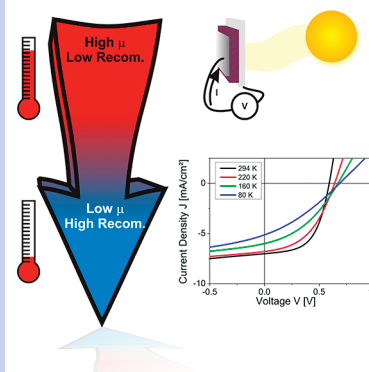
# Effect of Nongeminate Recombination on Fill Factor in Polythiophene/Methanofullerene Organic Solar Cells

Ralf Mauer, Ian A. Howard,\* and Frédéric Laquai\*

Max Planck Research Group for Organic Optoelectronics, Max Planck Institute for Polymer Research, Ackermannweg 10, D-55128 Mainz, Germany

**ABSTRACT** A key factor in solar cell efficiency is the dependence of the photocurrent on applied bias. With respect to organic solar cells, it is often suggested that this factor is governed by the field dependence of charge-transfer state separation. Here, we demonstrate that this is not the case in benchmark polythiophene/methanofullerene solar cells. By examining the temperature and light intensity dependence of the current–voltage characteristics, we determine that (1) the majority of free charge generation is not dependent on the field or temperature and (2) the competition between extraction and recombination of free charges principally determines the dependence of photocurrent on bias. These results are confirmed by direct observation of the temperature dependence of charge separation and recombination using transient absorption spectroscopy and highlight that in order to achieve optimal fill factors in organic solar cells, minimizing free carrier recombination is an important consideration.

**SECTION** Kinetics, Spectroscopy



Organic solar cells with power conversion efficiencies exceeding 7% have recently been demonstrated.<sup>1</sup> However, there is still a debate over the physical mechanisms that limit the figures of merit in organic solar cells and over the directions that should be pursued to further improve device efficiency and stability toward the regime required for commercial relevance.<sup>2</sup> In particular, several contradictory explanations have been proposed for the process that determines the bias dependence of the photocurrent. This is an important issue to resolve because the bias dependence of the photocurrent has a large influence on the solar cell's fill factor, which directly affects its power conversion efficiency (power conversion efficiency is equal to the product of open-circuit voltage, short-circuit current, and fill factor). In this Letter, we provide evidence that, contrary to popular models, it is the bias dependence of separated charge sweep-out rather than the bias dependence of charge-transfer state separation that determines the bias dependence of the photocurrent.

A common explanation of the bias dependence of the photocurrent is that it is determined by the field dependence of the separation of charge-transfer states.<sup>3–7</sup> The photo-physical processes involved in this explanation run as follows. Tightly bound excitons created by photon absorption diffuse to a donor–acceptor interface, at which point a charge-transfer state (or bound charge pair) is created across the heterojunction. This charge-transfer state can then either separate to yield photocurrent or can recombine, causing a loss of quantum efficiency. The branching ratio of the charge-transfer state population between separation and recombination depends on, among other factors, field and temperature

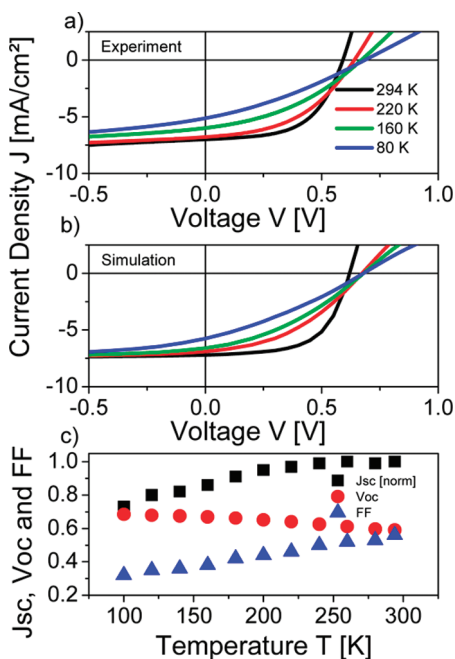
in a manner theoretically approximated by Braun's extension of Onsager theory<sup>8</sup> and further refined by Tachiya.<sup>9</sup> This is asserted to cause the bias dependence of the photocurrent. Importantly, in this explanation, charge recombination occurs between an electron and hole generated by the same photon, termed geminate recombination, and therefore is a monomolecular process (it occurs at the same rate irrespective of the charge density). Recently, such a mechanism has been proposed to explain the bias-dependent transient absorption of a polythiophene/methanofullerene blend.<sup>6</sup> However, other recent results show that the majority (> 80%) of excitons in such a blend form separated free charges directly after they are quenched at the interface even in the absence of field,<sup>10–12</sup> suggesting that the field-dependent suppression of geminate recombination is unlikely to account for the bias dependence of the photocurrent, a position that is also supported by device-based measurements and charge extraction techniques.<sup>13–15</sup> These latter experiments suggest that the bias dependence of the photocurrent is determined by a process that occurs after photo-generated electron–hole pairs have become spatially separated, such as the process of nongeminate recombination (wherein a free charge captures an opposite charge and recombines).<sup>16</sup> This process occurs in competition with the field-dependent sweep out of the photogenerated charges and therefore can cause field dependence in the photocurrent.

**Received Date:** October 27, 2010

**Accepted Date:** November 29, 2010

**Published on Web Date:** December 03, 2010





**Figure 1.** (a) *IV* characteristics of a P3HT/PCBM photovoltaic device at various temperatures under illumination equivalent to  $0.8 \times \text{AM1.5G}$  (see Methods section). (b) Simulations of the *IV* characteristics at the various temperatures demonstrating nongeminate recombination can describe the bias dependence of the photocurrent. The mobility is decreased at lower temperatures. See text for details. (c) Experimentally observed short-circuit current, open-circuit voltage, and fill factor as a function of temperature.

Furthermore, in contrast to geminate recombination, the rate of nongeminate recombination depends on the charge density, and therefore, its effect increases at higher carrier densities caused by higher light intensity, lower carrier mobilities, or low internal fields. Nongeminate recombination has already been observed to be important close to the open-circuit voltage.<sup>17,18</sup>

In order to experimentally clarify the cause of the field dependence of the photocurrent and the underlying charge recombination mechanism, we study devices based on the highly optimized poly(3-hexylthiophene)/methanofullerene (P3HT/PCBM) and combine an investigation of the temperature dependence of the solar cell's current–voltage characteristics with transient absorption measurements. These experiments reveal that ultrafast, temperature- and field-independent charge separation followed by competition between charge extraction and nongeminate recombination explain the device characteristics.

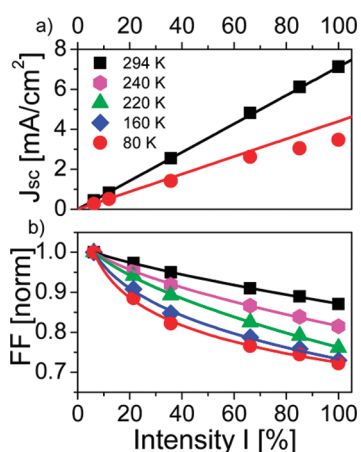
**Temperature and Intensity Dependence of Device Characteristics.** In Figure 1, we present the temperature dependence of the *IV* characteristics of the solar cells. All parameters that describe the power conversion efficiency change with temperature. The open-circuit voltage increases with decreasing temperature. This increase is mainly caused by a decrease in the dark current (Supporting Information) at lower temperatures that is compatible with a reduced thermionic injection<sup>19</sup> and lower mobility<sup>20</sup> of the charge carriers. High dark current reduces the net amount of extracted charge carriers and

simultaneously increases nongeminate recombination, thus leading to a decrease in open-circuit voltage.<sup>18,21</sup> Once the dark current is negligibly small, the open-circuit voltage saturates at 0.7 V, a value which corresponds with the work function difference of the ITO/PEDOT:PSS and aluminum electrodes and is roughly 0.3 V smaller than the energy of the charge-transfer state at the P3HT/PCBM interface.<sup>22</sup>

The fill factor, which is affected by the field dependence of the extraction of photogenerated charge carriers, decreases almost linearly over the temperature range studied. This eventually also leads to a reduction of the short-circuit current at temperatures below 250 K (once the fill factor drops below 50%). There are two possible explanations of why at lower temperature for a fixed electric field fewer charges are extracted from the device. If charge separation were described by the temperature- and field-activated dissociation of charge-transfer states as assumed by Onsager–Braun type models, then at low temperatures, more charge-transfer states would recombine geminately, and fewer would lead to separated charges. To compensate for the reduction in thermally activated splitting at low temperatures, higher fields would be required to generate free charges. Alternatively, if charge separation were unaffected by field and temperature, then an increased nongeminate recombination due to higher charge densities caused by lower mobility at lower temperatures would lead to a reduction in extraction efficiency. In the latter process, the bias dependence of the photocurrent is determined by a competition between nongeminate recombination and charge extraction in accordance with a recently developed model for the open-circuit voltage by Maurano et al.<sup>18</sup> In this context, the charge carrier mobility is the main parameter influencing the bias dependence of the photocurrent as a lower mobility will lead to reduced extraction rates and thus to an increased charge carrier density in the device. As the extraction rate also varies with field, the charge carrier density also increases with the positive applied voltage. A higher charge carrier density in turn leads to a higher nongeminate recombination rate, and thus, the ratio of charge extraction to nongeminate recombination will be shifted in favor of nongeminate recombination. Figure 1b shows the results of numerical simulations (see Methods for details) based on this model of field-independent charge separation followed by nongeminate recombination. The change in the bias dependence of the photocurrent caused by nongeminate recombination causes a fill factor reduction, and the increased probability of nongeminate recombination at higher charge densities caused by more intense illumination or lower mobility recreates the trends observed in the data. It will be shown in the further discussion that only this second model is consistent with all features of the data.

In summary, the central question is whether geminate or nongeminate recombination is the dominating loss mechanism in the devices under study. In the following considerations, we make use of the fact that geminate recombination is independent of the charge carrier density (and, therefore, also excitation intensity) while nongeminate recombination does depend on the density.<sup>23</sup>

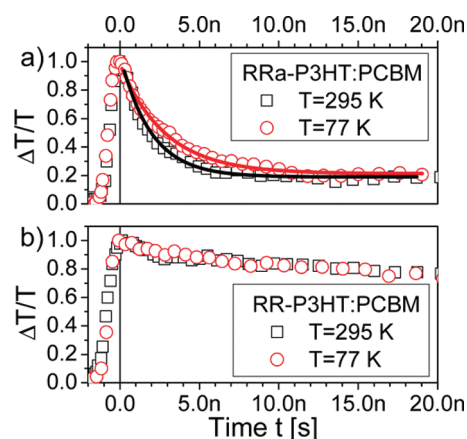
In Figure 2a, the excitation intensity dependence of the short-circuit current density is shown for measurements



**Figure 2.** (a) Short-circuit current density  $J_{sc}$  as a function of excitation intensity  $I$  at 294 and 80 K. The lines represent a linear fit through the origin and the first two data points. (b) Fill factor (FF) as a function of excitation intensity for the series of temperatures indicated in (a). Lines serve as guides to the eye. 100% intensity corresponds to the equivalent of  $0.8 \times \text{AM1.5G}$  illumination (see Methods for details).

performed at room temperature and 80 K. The straight lines are fits through the first two points of the data series plus the origin and represent a linear dependence of  $J_{sc}$  on the intensity. At room temperature,  $J_{sc}$  follows the linear trend up to intensities equivalent to 1 sun conditions. However, at 80 K, the higher-intensity data points systematically deviate from the linear trend, with  $J_{sc}$  lying further below the linear trend with increasing intensity. This suggests that nongeminate recombination at short-circuit conditions is negligible at room temperature (all separated charges can be extracted) but is important at lower temperatures. This is further supported by Figure 2b, in which the intensity dependence of the fill factor is presented. For all temperatures, the fill factor decreases toward higher intensities, with a stronger dependence at lower temperatures. The fill factor is best (64%) at high temperatures and low excitation intensities, that is, at the lowest charge carrier density in the device, and it is worst (33%) at low temperatures and high excitation intensities when the charge carrier density is the highest. Critically, while smaller fill factors at lower temperatures can be expected from a temperature- and field-dependent charge separation model, as mentioned above, a change in the intensity dependence cannot.<sup>24</sup> In contrast, it is completely consistent with nongeminate recombination being the process that determines the fill factor.

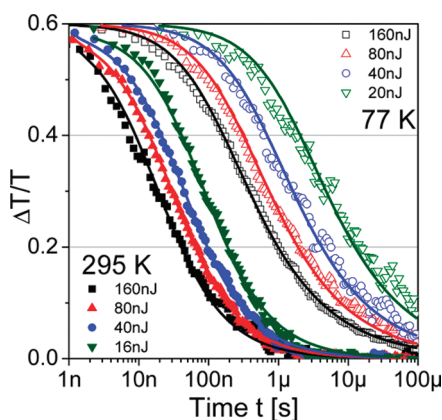
**Temperature Independence of Charge Separation.** To further elucidate whether geminate or nongeminate recombination is responsible for the observed changes, we have conducted transient absorption spectroscopy measurements of P3HT/PCBM blend films on quartz substrates (representative of the kinetics in a device at zero internal field) at room and liquid nitrogen temperature. We wished to monitor the total population of bound charges (which can recombine geminately) and free charges (which recombine nongeminately). Therefore, we searched for an isosbestic point, where the absorption of these two bound and free charges is equal and therefore the induced absorption is proportional to the total number of



**Figure 3.** (a) Normalized induced absorption of free and bound charges integrated over the spectral region of 750–800 nm as a function of time in a RRa-P3HT/PCBM blend film measured at room temperature (black squares) and at liquid nitrogen temperature (red circles) after a  $< 4 \mu\text{J cm}^{-2}$  excitation pulse at 532 nm. (b) Same data for a RR-P3HT/PCBM blend film.

bound plus free charges. In earlier work,<sup>11</sup> we identified that when integrated between 750 and 800 nm, the absorptions of the bound and free charges are equal, allowing the integrated kinetics in this region to be interpreted as representing the total number of bound plus free charges. The difference between geminate and nongeminate recombination lies in the kinetics of their decay. Charge carriers bound in a charge-transfer state recombine geminately in less than 2 ns in the absence of field,<sup>10,11</sup> while separated charges recombine on time scales from nanoseconds up to micro- to milliseconds at room temperature.<sup>10,11,25</sup> The ratio of bound to separated charges depends strongly on morphology,<sup>11,26</sup> with about 80% charge-transfer state formation in amorphous blends containing regiorandom (RRa) P3HT but almost no ( $< 20\%$ ) charge-transfer state formation in well-ordered blends with highly regioregular (RR) P3HT. Figure 3 shows transient absorption data at room and liquid nitrogen temperature for both RRa-P3HT/PCBM and annealed RR-P3HT/PCBM blends taken at very low fluence in order to highlight monomolecular recombination of charge-transfer states. The data reveal that the formation of spatially separated charges is not temperature-dependent and remains close to unity in RR-P3HT even in the absence of field and at low temperature. The recombination dynamics for RRa-P3HT are shown in Figure 3a. In this amorphous blend, the short-lived decay typical of geminate recombination of charge-transfer states reduces the signal by 80% within the first 10 ns at both temperatures. As shown in the Supporting Information, this decay does not depend on the excitation intensity, supporting its assignment to geminate charge-transfer state recombination. The residual 20% long-lived absorption at both temperatures is caused by the longer-lived free charges. As the branching ratio of 4:1 between bound and free charges is not changed by a decrease in temperature of over 200 K, we conclude that the spatial separation of charges is not temperature-activated in RRa-P3HT.

Figure 3b presents the recombination dynamics for RR-P3HT. We have previously found that in this annealed blend at room temperature, there is no geminate decay



**Figure 4.** Kinetics of the normalized charge-induced absorption in RR-P3HT/PCBM integrated over the spectral region of 750–800 nm at room and liquid nitrogen temperature, starting when the signals have decayed to 60% of their initial value. The symbols correspond to various excitation pulse energies.

caused by charge-transfer states.<sup>11</sup> Here, we observe that the dynamics of the decay over the first 10 ns are the same at 295 and 77 K, indicating that again the branching ratio is unaffected by the over 200 K change in temperature. The small fraction of monomolecular decay in this case occurs on a time scale longer than charge-transfer state recombination and is assigned to recombination of a small fraction of charges that become trapped near an interface,<sup>11</sup> and therefore, at low temperature as at room temperature, the yield of free charges even in the absence of applied field is found to be close to unity.

*Temperature Dependence of Nongeminate Recombination.* Our examination of the transient absorption over the first 10 ns revealed that the formation of free charges does not depend on temperature. In Figure 4, we extend our observation of the transient absorption to longer time scales to examine the effect of temperature on nongeminate recombination. The rate of nongeminate recombination can be described by  $(dn/dt) = -k\mu(n,T)n^2$ , where  $n$  is the charge carrier density,  $k$  is a constant, and  $\mu(n,T)$  is the charge-carrier-density- and temperature-dependent mobility. If the density dependence of the mobility can be expressed for a given temperature,  $T$ , as  $\mu(n,T) = \mu_0(T)n^{\beta(T)}$ ,<sup>27</sup> then the nongeminate recombination rate can be expressed as  $(dn/dt) = -\gamma(T)n^{2+\beta(T)}$ , where  $\gamma$  is the temperature-dependent rate prefactor. Many recent reports observe that the nongeminate (bimolecular) recombination at room temperature depends on density with an order greater than 2, indicating that the density dependence of the charge mobility does affect the recombination kinetics of free charges.<sup>11,28,29</sup> At lower temperatures, the mobility will decrease ( $\mu_0$  becomes smaller), and the density dependence of the mobility will increase ( $\beta$  becomes larger). The cause of the increased density dependence of mobility at low temperature is related to the broad density of states (DOS) caused by disorder.<sup>30</sup> It can be understood qualitatively in the following manner: when the temperature is high, charges occupying sites in the low-energy tail of the DOS can still make a thermally assisted hop to a site higher in the DOS and thereby retain a reasonable mobility;

however, at low temperature, the thermal assistance is lost, and the mobility of the tail states becomes significantly lower than that of states higher in the DOS, leading to a strongly density-dependent mobility. Therefore, as we decrease the temperature, we expect the rate of free charge recombination to decrease due to the lower mobility, and we also expect that the stronger density dependence of mobility at lower temperature<sup>31</sup> will mean that the decay rate changes more significantly with excitation fluence. This is what we observe in Figure 4, wherein we investigate the effect of temperature on free charge recombination. In order to present a qualitative comparison between the rates of free charge recombination for a series of excitation fluences at the two temperatures, we focus on the decay of the last 60% of the signal in each case that is exclusively caused by free carrier recombination. All signals were normalized and shifted so that they decayed to 60% at zero time. Comparing the decay of the free charges, it is clear that at both room and low temperature, the decay is density-dependent, with the decay occurring at different rates for the different excitation fluences. The first striking difference is that the recombination is much slower at low temperature, occurring with rates almost two orders of magnitude slower than recombination at room temperature. This indicates that the mobility also decreases by roughly 2 orders of magnitude between room temperature and 77 K. This reduction in mobility agrees well with that used in our simulations (see Methods for details) and that obtained from previous time-of-flight experiments.<sup>32</sup> The second difference between the decays at room and low temperature is the increased density dependence of mobility at lower temperature, as evidenced by the wider spread of recombination rates over the same range of excitation fluences.

In summary, transient absorption experiments reveal that the majority (at least 80%) of quenched excitons form spatially separated carriers on a subnanosecond time scale irrespective of field and temperature. The transient absorption experiments also show that the carrier mobility is strongly reduced at lower temperatures. Measurements of device characteristics at a variety of light intensities for a wide temperature range were collected, and a decrease in fill factor and short-circuit current with decreasing temperature and increasing intensity were observed. Qualitatively, the measurements at low temperature immediately reveal that the bias dependence of the photocurrent cannot be accounted for by bias-dependent charge-transfer state separation because the light intensity dependence is strongly nonlinear. The device characteristics can be described by a model (consistent with the transient absorption results) in which temperature- and field-independent free charge generation is followed by kinetic competition between nongeminate recombination and charge extraction. Implementation of this model in a numerical simulation (see Methods for details and parameters) led to the simulated  $I$ - $V$  curves shown in Figure 1b that reproduce well all of the trends observed in the experimental data. These results provide strong direct evidence that the device performance of annealed P3HT/PCBM solar cells is attributable to fast, field-independent charge separation followed by a competition between nongeminate recombination and charge extraction.

In order to relate our findings to device characteristics at room temperature, we make the following observations. The IQE of high-performance polythiophene/methanofullerene solar cells is approximately 80% at short-circuit,<sup>33,34</sup> which corresponds well to the approximately 20% total of monomolecular losses observed at the zero field in ultrafast measurements of annealed blends.<sup>10,11</sup> Although we note that monomolecular loss processes can be highly morphology-dependent, this rough equality of monomolecular loss at short- and open-circuit conditions supports our assertion that the monomolecular loss mechanisms do not account for the field dependence of the photocurrent. Instead, our results suggest that at room temperature, as at low temperature, it is competition between carrier extraction and nongeminate recombination that determines the bias dependence of the photocurrent. We approximately estimate the theoretical maximum fill factor by subtracting a bias-independent (recombination-free) photocurrent from the measured dark current (see Supporting Information). This results in an approximation for the maximum obtainable fill factor of about 0.7, while that observed is 0.6. Thus, we can roughly estimate that the fill factor reduction due to nongeminate recombination at low biases reduces the efficiency of devices by approximately 15% and therefore has a similar effect on the net power conversion efficiency as the nonunity IQE caused by geminate processes. Therefore, we suggest that an opportunity to increase the power conversion efficiency of organic solar cells by reducing nongeminate recombination at low internal fields exists in parallel to those currently pursued to minimize monomolecular losses related to charge-transfer states.<sup>35</sup>

## METHODS

Regioregular (RR) P3HT (Sepiolid P200, MW = 25 000 g mol<sup>-1</sup>, PDI = 1.6, regioregularity, ~98%) and regiorandom (RRa) P3HT were supplied by BASF SE. PCBM (~99%) was purchased from Sigma Aldrich. All materials were used as received. The polymers and PCBM were dissolved separately in chlorobenzene at 70 °C, and the solutions were mixed and then spin-cast onto precleaned quartz substrates in a nitrogen-filled glovebox. The RR-P3HT samples were annealed on a hot plate at 120 °C for 20 min in a nitrogen-filled glovebox. Solar cells were prepared in the same way by spin-casting the mixed solutions on a PEDOT:PSS (Clevis P VPAI 4083, H.C. Starck) coated ITO substrate with subsequent evaporation of a 100 nm thick layer of aluminum followed by annealing. The power conversion efficiency of the devices measured was 2.9%, with a peak short-circuit external quantum efficiency of 65% between 500 and 530 nm. The discrepancy in efficiency between our device and 4% efficient devices commonly reported in the literature<sup>36</sup> lies in slightly suboptimal layer thicknesses reducing the photon absorption, as supported by optical transfer matrix simulation of our rather thin device. Our results are therefore also applicable to devices with the standard 4% efficiency.

The pump–probe setup used for the transient absorption measurements has been described in great detail elsewhere.<sup>11</sup> In short, a commercial titanium:sapphire laser (Coherent

LIBRA HE) was used to pump a home-built noncollinear optical parametric amplifier for white light probe generation in the visible and near-infrared spectral range. As pump, either the output of an optical parametric amplifier (Coherent OPerA Solo) or an actively Q-switched Nd:YVO<sub>4</sub> laser (AOT Ltd. MOPA) was used. The delay between the pump and probe pulses for the two pump sources was realized by using a mechanical delay stage and an electronic delay generator, respectively. The measurements were performed in a home-built cryostat at room temperature and 77 K under dynamic vacuum at pressures < 10<sup>-5</sup> mbar.

Solar cell devices were first measured using a solar simulator (K.H. Steuernagel Lichttechnik GmbH, Germany) with a 80 mW cm<sup>-2</sup> AM1.5G illumination spectrum inside of a nitrogen-filled glovebox. Then, they were transferred to a temperature-controlled cryostat, where they were kept in dynamic vacuum at pressures < 10<sup>-5</sup> mbar. As an illumination source for the temperature-dependent measurements, a green LED (center wavelength 530 nm) was used. The intensity of the LED was tuned to reproduce the current–voltage characteristics as measured with the solar simulator inside of the glovebox at room temperature. For the intensity-dependent measurements, various neutral density filters were used to adjust the excitation.

Fully coupled optical and electronic simulations were performed using the commercial simulation software setfos 3 by Fluxim AG. For details, see ref 37. The model under study uses an ultrafast, temperature- and field-independent charge generation with an internal quantum efficiency (IQE) that is adjusted to match the IQE of the experimental devices at room temperature (~80%). Recombination is assumed to be bimolecular, following the Langevin recombination formalism. Charge carrier mobilities at each temperature are set to 1.3 × 10<sup>-4</sup>, 1.3 × 10<sup>-5</sup>, 7.5 × 10<sup>-6</sup>, and 3.5 × 10<sup>-6</sup> cm<sup>2</sup>/(V s) for the temperatures of 294, 220, 160, and 80 K, respectively, and are assumed to be independent of the electric field or charge carrier density. The mobility of electrons and holes is assumed to be equal. While the neglect of the electric field dependence should not have a pronounced influence on the results,<sup>32</sup> the neglect of the carrier density dependence is likely a cause of slight error in the calculated current–voltage characteristics.<sup>27,38</sup> However, the calculated curves reproduce well the qualitative form of the data, even neglecting this second-order effect, and as the density dependence of the mobility affects both recombination and extraction, the influence of this omission is expected to be minor. The only parameters varied between the simulations are the temperature, which mainly influences the dark current via a thermionic injection model, and the charge carrier mobility. It should be noted that as the charge carrier mobility is well-known over a broad range of temperatures<sup>32</sup> and the temperatures are easily accessible during experiment, there is no completely free parameter contained in the model.

**SUPPORTING INFORMATION AVAILABLE** Dark current as a function of temperature, fluence dependence of transient absorption data, mobility and temperature dependence of simulated device characteristics, and approximation of maximum fill factor. This material is available free of charge via the Internet at <http://pubs.acs.org>.

## AUTHOR INFORMATION

### Corresponding Author:

\*To whom correspondence should be addressed. E-mail: ian.howard@mpip-mainz.mpg.de (I.A.H.); laquai@mpip-mainz.mpg.de (FL).

**ACKNOWLEDGMENT** We thank M. Kastler (BASF SE) for provision of RRa-P3HT and Sepiolid P200, the IRTG 1404 for funding, and A. Becker for technical support. I.A.H. thanks the Alexander von Humboldt Foundation for a postdoctoral fellowship. F.L. thanks the Max Planck Society for funding a Max Planck Research Group. R.M. thanks the Max Planck Graduate Center (MPGC) for financial support.

## REFERENCES

- Liang, Y.; Xu, Z.; Xia, J.; Tsai, S.-T.; Wu, Y.; Li, G.; Ray, C.; Yu, L. *Adv. Mater.* **2010**, *22*, E135.
- Dennler, G.; Scharber, M. C.; Brabec, C. J. *Adv. Mater.* **2009**, *21*, 1323.
- Mihailetchi, V. D.; Koster, L. J. A.; Hummelen, J. C.; Blom, P. W. M. *Phys. Rev. Lett.* **2004**, *93*, 216601.
- De, S.; Pascher, T.; Maiti, M.; Jespersen, K. G.; Kesti, T.; Zhang, F. L.; Inganas, O.; Yartsev, A.; Sundstrom, V. *J. Am. Chem. Soc.* **2007**, *129*, 8466.
- Marsh, R. A.; McNeill, C. R.; Abrusci, A.; Campbell, A. R.; Friend, R. H. *Nano Lett.* **2008**, *8*, 1393.
- Marsh, R. A.; Hodgkiss, J. M.; Friend, R. H. *Adv. Mater.* **2010**, *22*, 3672.
- Veldman, D.; Ipek, O.; Meskers, S. C. J.; Sweelssen, J.; Koetse, M. M.; Veenstra, S. C.; Kroon, J. M.; van Bavel, S. S.; Loos, J.; Janssen, R. A. J. *J. Am. Chem. Soc.* **2008**, *130*, 7721.
- Braun, C. L. *J. Chem. Phys.* **1984**, *80*, 4157.
- Wojcik, M.; Michalak, P.; Tachiya, M. *Appl. Phys. Lett.* **2010**, *96*, 162102.
- Guo, J. M.; Ohkita, H.; Benten, H.; Ito, S. *J. Am. Chem. Soc.* **2010**, *132*, 6154.
- Howard, I. A.; Mauer, R.; Meister, M.; Laquai, F. *J. Am. Chem. Soc.* **2010**, *132*, 14866.
- Pensack, R. D.; Asbury, J. B. *J. Phys. Chem. Lett.* **2010**, *1*, 2255.
- Inal, S.; Schubert, M.; Sellinger, A.; Neher, D. *J. Phys. Chem. Lett.* **2010**, *1*, 982.
- Street, R. A.; Cowan, S.; Heeger, A. J. *Phys. Rev. B* **2010**, *82*, 121301.
- Hamilton, R.; Shuttle, C. G.; O'Regan, B.; Hammant, T. C.; Nelson, J.; Durrant, J. R. *J. Phys. Chem. Lett.* **2010**, *1*, 1432.
- These measurements also suggest that nongeminate recombination dominates recombination on the time scales shown to have a field dependence in ref 6.
- Shuttle, C. G.; O'Regan, B.; Ballantyne, A. M.; Nelson, J.; Bradley, D. D. C.; Durrant, J. R. *Phys. Rev. B* **2008**, *78*, 113201.
- Maurano, A.; Hamilton, R.; Shuttle, C. G.; Ballantyne, A. M.; Nelson, J.; O'Regan, B.; Zhang, W.; McCulloch, I.; Azimi, H.; Morana, M.; Brabec, C. J.; Durrant, J. R. *Adv. Mater.* **2010**, *22*, 4987–4992.
- Scott, J. C.; Malliaras, G. G. *Chem. Phys. Lett.* **1999**, *299*, 115.
- Shen, Y. L.; Klein, M. W.; Jacobs, D. B.; Scott, J. C.; Malliaras, G. G. *Phys. Rev. Lett.* **2001**, *86*, 3867.
- Shuttle, C. G.; Maurano, A.; Hamilton, R.; O'Regan, B.; de Mello, J. C.; Durrant, J. R. *Appl. Phys. Lett.* **2008**, *93*, 3.
- Vandewal, K.; Tvingstedt, K.; Gadisa, A.; Inganas, O.; Manca, J. V. *Phys. Rev. B* **2010**, *81*, 125204.
- We note that monomolecular nongeminate kinetics can be caused by interface trap recombination. Our results at low temperature show that a density-dependent nongeminate recombination mechanism occurs in our devices, and we therefore approximate that all nongeminate recombination occurs between mobile charges.
- A change in separation yield caused by space-charge effects reducing the efficiency of charge separation is ruled out by the almost quantitative yield of separated charges at zero field observed in the transient absorption experiments.
- Howard, I. A.; Hodgkiss, J. M.; Zhang, X.; Kirov, K. R.; Bronstein, H. A.; Williams, C. K.; Friend, R. H.; Westenhoff, S.; Greenham, N. C. *J. Am. Chem. Soc.* **2009**, *132*, 328.
- Keivanidis, P. E.; Clarke, T. M.; Lilliu, S.; Agostinelli, T.; Macdonald, J. E.; Durrant, J. R.; Bradley, D. D. C.; Nelson, J. *J. Phys. Chem. Lett.* **2010**, *1*, 734.
- Shuttle, C. G.; Hamilton, R.; Nelson, J.; O'Regan, B. C.; Durrant, J. R. *Adv. Funct. Mater.* **2010**, *20*, 698.
- Clarke, T. M.; Jamieson, F. C.; Durrant, J. R. *J. Phys. Chem. C* **2009**, *113*, 20934.
- Shuttle, C. G.; O'Regan, B.; Ballantyne, A. M.; Nelson, J.; Bradley, D. D. C.; de Mello, J.; Durrant, J. R. *Appl. Phys. Lett.* **2008**, *92*, 093311.
- Nelson, J.; Choulis, S. A.; Durrant, J. R. *Thin Solid Films* **2004**, *451–452*, 508.
- Pasveer, W. F.; Cottaar, J.; Tanase, C.; Coehoorn, R.; Bobbert, P. A.; Blom, P. W. M.; de Leeuw, D. M.; Michels, M. A. J. *Phys. Rev. Lett.* **2005**, *94*, 206601.
- Mauer, R.; Kastler, M.; Laquai, F. *Adv. Funct. Mater.* **2010**, *20*, 2085.
- Burkhard, G. F.; Hoke, E. T.; Scully, S. R.; McGehee, M. D. *Nano Lett.* **2009**, *9*, 4037.
- Street, R. A. *Phys. Rev. B* **2010**, *82*, 207302.
- Deibel, C.; Strobel, T.; Dyakonov, V. *Adv. Mater.* **2010**, *22*, 4097.
- Li, G.; Shrotriya, V.; Huang, J.; Yao, Y.; Moriarty, T.; Emery, K.; Yang, Y. *Nat. Mater.* **2005**, *4*, 864.
- Hausermann, R.; Knapp, E.; Moos, M.; Reinke, N. A.; Flatz, T.; Ruhstaller, B. *J. Appl. Phys.* **2009**, *106*, 104507.
- Eng, M. P.; Barnes, P. R. F.; Durrant, J. R. *J. Phys. Chem. Lett.* **2010**, *1*, 3096.

#### **4.4 Charge Extraction**

The article “Effect of External Bias on Nongeminate Recombination in Polythiophene/Methanofullerene Organic Solar Cells” was published in The Journal of Physical Chemistry Letters by the American Chemical Society on June 22<sup>nd</sup>, 2011.

Reprinted with permission from Mauer, R.; Howard, I. A.; Laquai, F. The Journal of Physical Chemistry Letters 2011, 2, 1736. Copyright 2011 American Chemical Society.

# Effect of External Bias on Nongeminate Recombination in Polythiophene/Methanofullerene Organic Solar Cells

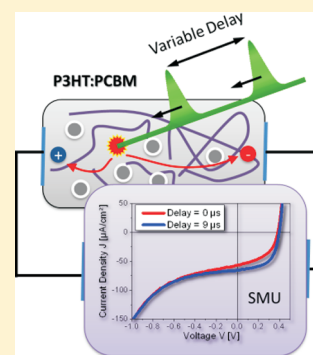
Ralf Mauer, Ian A. Howard,\* and Frédéric Laquai\*

Max Planck Research Group for Organic Optoelectronics, Max Planck Institute for Polymer Research, Ackermannweg 10, D-55128 Mainz, Germany

**S** Supporting Information

**ABSTRACT:** Much recent literature suggests that nongeminate recombination is the loss mechanism that predominantly determines the bias dependence of the photocurrent in efficient organic solar cells. Here, we report a new experimental technique based on measuring the quasi-steady-state current–voltage characteristics during illumination by two pulsed lasers and observing how the current–voltage characteristics change as a function of the time delay between the two pulsed lasers. This technique unequivocally demonstrates a bias dependence of nongeminate recombination and reveals the dwell time of charge carriers in a photovoltaic device. We relate the results of our pulsed experiment to devices under solar illumination and find that the reduction of the charge carrier dwell time with increasing internal electric field explains the observed bias dependence of the device photocurrent under constant illumination and consequently affects the fill factor of high-performance organic solar cells.

**SECTION:** Electron Transport, Optical and Electronic Devices, Hard Matter



Power conversion efficiencies of bulk heterojunction organic solar cells in excess of 7% have recently been reported, in one case on active areas as large as  $1 \text{ cm}^2$ .<sup>1–4</sup> While these values approach the threshold for commercial relevance, there are still some fundamental questions regarding device physics that remain inconclusively answered. For instance, the origin of the bias dependence of the photocurrent (a parameter critical to device performance especially through its influence on the fill factor) can arise from two fundamentally different processes, namely, field-activated splitting of geminately bound charge-transfer (CT) states (also termed polaron pairs) at the interface<sup>5–8</sup> and/or the field dependence of the competition between nongeminate recombination and charge extraction.<sup>9–12</sup> In this Letter, we would like to clarify the discussion of the roles of these two processes with respect to the regioregular poly(3-hexylthiophene) and [6,6]-phenyl C61 butyric acid methyl ester (rr-P3HT/PCBM) reference system by reporting direct observation of the bias dependence of nongeminate recombination and of the dwell time of free charge carriers using a new experimental technique based on measuring the current–voltage characteristics of photovoltaic devices under illumination by two pulsed lasers at various time delays between the pulses.

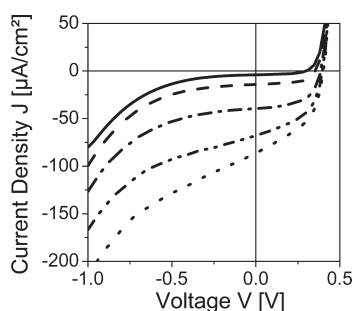
Nongeminate recombination is often studied by techniques using a pulsed laser to create a population of charge carriers at a discrete instant in time and then probing the evolution of that population by either an optical pulse (e.g., transient absorption spectroscopy<sup>13–16</sup>) or a time-varying electrical field (e.g., photo-CELIV,<sup>6</sup> time-delayed collection field,<sup>7</sup> or transient photovoltage<sup>17</sup> experiments). While transient absorption spectroscopy offers a very good time resolution, it

suffers from a limited signal-to-noise ratio. Consequently, in state-of-the-art experimental setups, a charge carrier density of at least  $\sim 5 \times 10^{17} \text{ cm}^{-3}$  must be generated by the excitation pulse in order to achieve a sufficient signal-to-noise ratio to measure the kinetics.<sup>13</sup> This charge density is significantly higher than that in a device at short or open circuit, meaning that nongeminate recombination occurs much more quickly than in a device under solar illumination.<sup>9</sup> We demonstrate the effect that this increased rate of nongeminate recombination has on current–voltage (*JV*) curves in Figure 1 by presenting the quasi-steady-state *JV* curves measured for pulsed laser excitation under conditions typically used for transient absorption, and at lower fluence pulsed excitation (for the *JV* curves under simulated solar illumination, see the Supporting Information). There are several features of the pulsed *JV* curves that are different from those usually observed under standard AM1.5G conditions. The short-circuit current of tens of  $\mu\text{A cm}^{-2}$  is 2–3 orders of magnitude lower than that under standard CW illumination conditions ( $\sim 10 \text{ mA cm}^{-2}$ ). This is a direct consequence of the lower average power of the pulsed illumination. At a pulse fluence of  $100 \text{ nJ cm}^{-2}$  and a pulse repetition rate of 1 kHz, an average power of  $0.1 \text{ mW cm}^{-2}$  ( $10^{14} \text{ photons cm}^{-2} \text{ s}^{-1}$ ) is incident on the sample, which is 3 orders of magnitude lower than the AM1.5G solar power of  $100 \text{ mW cm}^{-2}$  ( $10^{17} \text{ photons cm}^{-2} \text{ s}^{-1}$ ) (although the instantaneous power within the subnanosecond pulse is much higher, hence the higher than steady state initial charge

**Received:** June 11, 2011

**Accepted:** June 22, 2011

**Published:** June 22, 2011



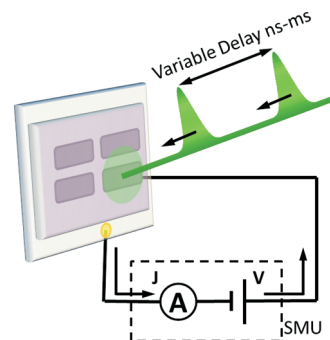
**Figure 1.** Quasi-steady-state current–voltage characteristics of an rr-P3HT/PCBM device under illumination by a (single) laser (pulse length: 100 fs; repetition rate: 1 kHz; wavelength: 532 nm) at fluences of 23 (solid line), 84 (dashed line), 229 (dash–dotted line), 500 (dash–double dotted line), and 1189  $\text{nJ cm}^{-2}$  (dotted line).

densities). The dark current is not substantially affected by the illumination and therefore is much more significant relative to the photocurrent under pulsed excitation. The dark current's influence on the shape of the  $JV$  curve is therefore much more pronounced under pulsed illumination, explaining the strongly rising current as the reverse bias approaches  $-1$  V (making the leakage current appear much worse than that under solar illumination; see Supporting Information) and also causing the open-circuit voltage ( $<0.4$  V) to be considerably smaller than that under CW illumination (0.58 V). At fluences below  $250 \text{ nJ cm}^{-2}$ , the short-circuit current increases approximately linearly with increasing fluence, while the slope of the  $JV$  curve at this voltage is close to 0. When the fluence is increased beyond  $250 \text{ nJ cm}^{-2}$ , the short-circuit current starts to deviate from the linear fluence dependence, indicating that nongeminate recombination begins to play a role in the charge recombination even at short circuit. This is also accompanied by an increase of the slope of the  $JV$  curve at short circuit, indicating that in the fluence range typically used in transient absorption experiments ( $>5000 \text{ nJ cm}^{-2}$ ), field-dependent nongeminate recombination significantly alters the device characteristics. Therefore, in efficient photovoltaic systems wherein most absorbed photons create free charge carriers, bias-dependent transient absorption measurements do not provide straightforward access to the processes that occur in a cell operating under solar illumination.

In comparison to the optical-probe-based transient absorption, electrical detection offers higher sensitivity, allowing much less intense excitation pulses to be used and therefore nongeminate recombination to be studied at carrier densities more directly relevant to solar illumination conditions. However, the experimental constraints of the electrical detection limit the time resolutions of these methods.

Herein, we present a method that combines the high sensitivity of the electrical measurements with the readily attainable high time resolution of the optical measurements. The experimental setup is sketched in Scheme 1. A standard test solar cell with a pixel area of  $0.14 \text{ cm}^2$  was mounted in a vacuum chamber and kept under dynamic vacuum at pressures  $<10^{-5}$  mbar and connected to a Keithley 2400 SMU set to source voltage and measure current. The sample was illuminated by two almost collinear, 532 nm, synchronized, 1 kHz repetition rate pulsed lasers, both defocused to illuminate the entire pixel and adjusted so that they individually (i.e., in the absence of the other pulse) generated the same quasi-steady-state

**Scheme 1.** Schematic of the Experimental Setup Used for Measuring Current–Voltage Characteristics of Photovoltaic Devices under Illumination by Two Pulsed Lasers at Various Time Delays between the Pulses



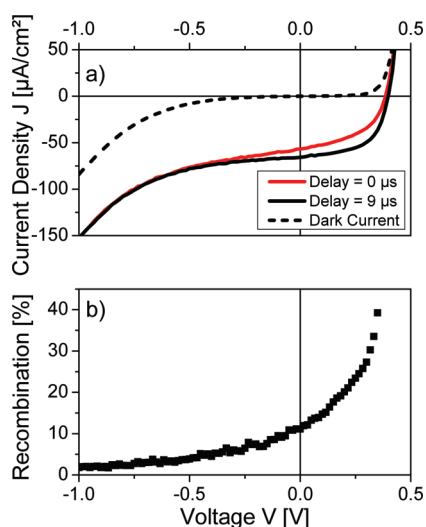
short-circuit photocurrent. The time delay between the two laser pulses can be varied by an electronic delay generator. For each time delay, a  $JV$  curve was taken by the SMU with sufficient settling time to allow the system to reach quasi-steady-state conditions for each applied voltage before the current was read. The delay between the optical pulses was adjusted, and the measurement processes were repeated to build a data set of the measured  $JV$  curves as a function of delay time between the two excitation pulses.

Depending on the applied voltage and time delay (and as mentioned above also on the intensity of the pulses; see Figure 1), a fraction of the charges generated by the first excitation pulse will have recombined or been extracted before the second pulse arrives. If the fraction of charges remaining from the first excitation pulse is low when the second pulse arrives, then the interaction between the pulses will be small, and the quasi-steady-state photocurrent measured will approach twice that of a single pulse. On the other hand, when a significant fraction of the charges generated by the first pulse are still in the device when the second pulse arrives, there is an opportunity for the carrier densities to interact, and if nongeminate recombination is indeed important, then it will increase the total fraction of recombination and lead the quasi-steady-state photocurrent measured to be less than twice that of a single pulse. By measuring complete  $JV$  characteristics for each delay time, we investigate how the applied bias affects nongeminate recombination and the dwell time of charge carriers in a device.

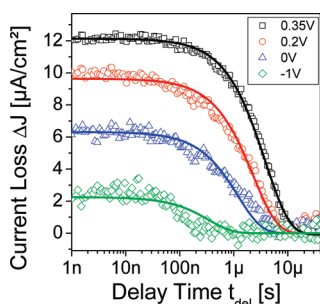
In Figure 2a, we present  $JV$  characteristics of an rr-P3HT/PCBM solar cell (power conversion efficiency of 2.9%; see Supporting Information) in the dark and under illumination by two laser pulses at delay times of 0 and  $9 \mu\text{s}$  between the laser pulses. Both excitation pulses had fluences of  $150 \text{ nJ cm}^{-2}$ . This fluence generates a charge carrier density of approximately  $4 \times 10^{16} \text{ cm}^{-3}$  (Supporting Information), which is comparable to the charge carrier density in a device under CW illumination at open-circuit conditions and roughly 1 order of magnitude higher than that at short circuit.<sup>9</sup> This value was chosen because, as has already been discussed in literature, in annealed rr-P3HT/PCBM devices, charge carrier densities below  $1 \times 10^{16} \text{ cm}^{-3}$  lead to negligibly small nongeminate recombination losses and are not suitable for studying nongeminate recombination (Supporting Information).<sup>18</sup>

At long delay times ( $>9 \mu\text{s}$ ), the extracted photocurrent is twice the value of the photocurrent obtained by illumination with





**Figure 2.** (a) Current–voltage characteristics in the dark (dashed black line) and under illumination by two laser pulses with a delay of 0 (red line) and 9  $\mu\text{s}$  (black line) with respect to each other. (b) Bias dependence of the additional nongeminate recombination caused by the overlap of the charge carrier populations at 0  $\mu\text{s}$  delay with respect to a delay of 9  $\mu\text{s}$ . The nongeminate recombination is clearly bias-dependent and becomes very significant at low internal fields. The pulse energy used was  $\sim 150 \text{ nJ cm}^{-2}$  at a repetition rate of 1 kHz for both lasers.



**Figure 3.** Current loss  $\Delta J$  due to nongeminate recombination of the overlapping charge carrier populations created by the two pump pulses as a function of delay time at applied voltages of +0.35 (black squares), 0.2 (red circles), 0 (blue triangles), and  $-1 \text{ V}$  (green diamonds). The lines are fits to the solution of our model for charge extraction and recombination.

one laser pulse of a fluence of  $150 \text{ nJ cm}^{-2}$  (compare Figure 1) over the entire voltage range displayed. This suggests that the charge carrier populations created by each pulse do not interact with each other and that there is no additional nongeminate recombination occurring. As the delay time decreases, the overall current that can be extracted from the device is reduced, indicating that increased nongeminate recombination begins to play a role, especially in the regime between short-circuit and open-circuit conditions. We quickly note that this reduction cannot be explained by increased exciton charge annihilation because in earlier work, we have shown that such annihilation is negligible for pump fluences below  $5 \mu\text{J cm}^{-2}$ , which is much greater than the sum of the pump fluences used here.<sup>13</sup>

The ratio of the  $JV$  curves at 9  $\mu\text{s}$  delay (when no additional nongeminate recombination occurs) and 0  $\mu\text{s}$  delay (when the

**Table 1.** Parameters Extracted from Fitting Current Loss Data Presented in Figure 3<sup>a</sup>

parameter	value
$N_0$	$(3.7 \pm 0.1) \times 10^{16} \text{ cm}^{-3}$
$\gamma$	$(4.0 \pm 0.5) \times 10^{-12} \text{ cm}^3 \text{ s}^{-1}$
$k_{\text{extr}}(0.35 \text{ V applied, } \sim -0.23 \text{ V internal})$	$(2.5 \pm 0.1) \times 10^5 \text{ s}^{-1}$
$k_{\text{extr}}(0.20 \text{ V applied, } \sim -0.38 \text{ V internal})$	$(4.4 \pm 0.1) \times 10^5 \text{ s}^{-1}$
$k_{\text{extr}}(0.00 \text{ V applied, } \sim -0.58 \text{ V internal})$	$(9.2 \pm 0.2) \times 10^5 \text{ s}^{-1}$
$k_{\text{extr}}(-0.5 \text{ V applied, } \sim -1.08 \text{ V internal})$	$(2.2 \pm 0.1) \times 10^6 \text{ s}^{-1}$
$k_{\text{extr}}(-1.0 \text{ V applied, } \sim -1.58 \text{ V internal})$	$(3.3 \pm 0.1) \times 10^6 \text{ s}^{-1}$

<sup>a</sup>  $N_0$  and  $\gamma$  are shared between all fits, while  $k_{\text{extr}}$  varies with the applied voltage.

most additional nongeminate recombination occurs) allows us to directly measure the amount of additional nongeminate recombination at 0  $\mu\text{s}$  and its dependence on the fluence. As shown in Figure 2b, the resulting nongeminate recombination clearly depends on the applied voltage and strongly increases toward the open-circuit voltage. This suggests that lower internal fields lead to lower extraction rates, shifting the competition between extraction and recombination in favor of recombination.

In order to gain information about the carrier extraction time, we plot in Figure 3 the evolution of the loss in extracted current for a given voltage as a function of the delay time between the laser pulses. This is shown for four different values of external bias, (i) close to the open-circuit voltage (0.35 V), (ii) in between open and short circuit (0.2 V), (iii) at short circuit (0 V), and (iv) at negative bias ( $-1 \text{ V}$ ). It is immediately apparent that not only the amount of recombination but also the time scale on which it occurs are strongly influenced by the external bias. As mentioned earlier, this current loss is caused by additional nongeminate recombination caused by the interaction of charges created by the first laser pulse with charges created by the second laser pulse. Thus, it is a measure for the number of charges remaining in the sample from the excitation by the first laser pulse at the time when the second pulse creates an additional, new charge population. Close to the open-circuit voltage, when the internal field in the device is weak, extraction is slow, and we see that the charges from the first pulse stay in the sample for up to almost 10  $\mu\text{s}$ . At the  $-1 \text{ V}$  bias, charge carriers are quickly swept out of the device within a few hundred nanoseconds.

For a more quantitative analysis and to elucidate the implications of our results on steady-state device performance, we developed a simple numerical model to estimate the extraction rate (and thereby the effective mobility) by fitting the data presented in Figure 3. The model is based on the assumption that charge carriers can either be extracted with a bias-dependent extraction rate constant  $k_{\text{extr}}(V)$  or recombine with a nongeminate (bimolecular) rate constant  $\gamma$ , in accordance with a reduced Langevin-type model. This leads to the differential equation for the photogenerated electron density ( $n$ ) of

$$\frac{dn}{dt} = -k_{\text{extr}}(V)n - \gamma n^2$$

which has the analytic solution

$$n(t) = \frac{k_{\text{extr}}(V)N_0}{-\gamma N_0 + e^{k_{\text{extr}}t}(k_{\text{extr}} + \gamma N_0)}$$

where  $N_0$  is the initial photoinduced electron density. The charge density extracted from the first and second laser pulses when they are separated by a time  $\tau$  can be found by

$$n_1^{\text{extr}}(\tau) = \int_0^\tau k_{\text{extr}}(V) \frac{k_{\text{extr}}(V)N_0}{-\gamma N_0 + e^{k_{\text{extr}}(V)t}(k_{\text{extr}}(V) + \gamma N_0)} dt$$

and

$$n_2^{\text{extr}}(\tau) = \int_0^\infty k_{\text{extr}}(V) \frac{k_{\text{extr}}(V)(N_0 + n_1(\tau))}{-\gamma(N_0 + n_1(\tau)) + e^{k_{\text{extr}}(V)t}(k_{\text{extr}}(V) + \gamma(N_0 + n_1(\tau)))} dt$$

These integrals have the analytic solutions

$$n_1^{\text{extr}}(\tau) = -\frac{k_{\text{extr}}(V)(k_{\text{extr}}(V)\tau + \ln[k_{\text{extr}}(V)] - \ln[-\gamma N_0 + e^{k_{\text{extr}}(V)\tau}(k_{\text{extr}}(V) + \gamma N_0)])}{\gamma}$$

and

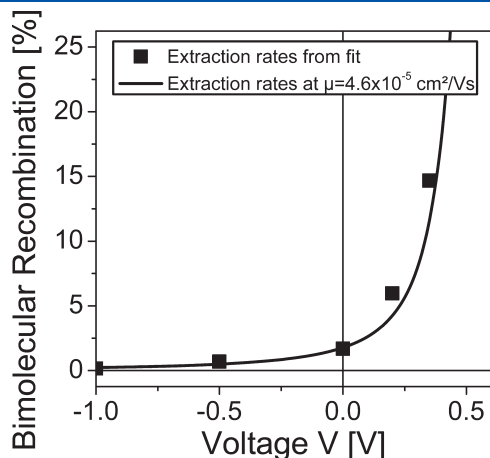
$$n_2^{\text{extr}}(\tau) = -\frac{k_{\text{extr}}(V) \ln \left[ \frac{k_{\text{extr}}(V)}{k_{\text{extr}}(V) + \gamma(N_0 + n_1(\tau))} \right]}{\gamma}$$

The total current for a given delay time between the excitation pulses can then be calculated as  $J(\tau) = e \cdot d \cdot \text{RR}(n_1(\tau) + n_2(\tau))$ , where  $d$  is the device thickness (80 nm), RR is the laser repetition rate (1 kHz), and  $e$  is the electronic charge. Using Origin 8.5G (OriginLab Corporation), we use this analytic expression to globally fit the data presented in Figure 3, with  $N_0$  and  $\gamma$  as shared fitting parameters while  $k_{\text{extr}}(V)$  is allowed to vary for the different voltages. The results of the fit are shown as solid lines in Figure 3, and the output parameters are presented in Table 1.

We can compare the nongeminate (bimolecular) recombination constant extracted from our fitting,  $\gamma = (4.0 \pm 0.5) \times 10^{-12} \text{ cm}^3 \text{ s}^{-1}$ , with that predicted by the Langevin equation,  $\gamma_1 = q(\mu_e + \mu_h)/\epsilon\epsilon_0$ . If we use  $\mu_e + \mu_h = 6 \times 10^{-5} \text{ cm}^2 \text{ V}^{-1} \text{ s}^{-1}$ , which we recently determined in a time-of-flight study,<sup>19</sup>  $\gamma_1 = 4 \times 10^{-11} \text{ cm}^3 \text{ s}^{-1}$ , while if we use  $\mu_e + \mu_h = 3.9 \times 10^{-3} \text{ cm}^2 \text{ V}^{-1} \text{ s}^{-1}$ , found from measurements of space charge limited currents in electron- and hole-only devices,<sup>20</sup>  $\gamma_1 = 2 \times 10^{-9} \text{ cm}^3 \text{ s}^{-1}$ . Consistent with previous reports,<sup>18,21–23</sup> our results demonstrate that the actual nongeminate recombination rate is between 1 and 3 orders of magnitude slower than that predicted by the Langevin

equation; however, our extracted value for  $\gamma$  is also roughly an order of magnitude larger than the value obtained from transient absorption measurements made at or extrapolated to similar charge densities.<sup>13,14</sup> We also determined  $\gamma$  from transient photovoltage experiments to be  $2 \times 10^{-12} \text{ cm}^3 \text{ s}^{-1}$  at a charge density of  $3.5 \times 10^{17} \text{ cm}^{-3}$ , which is also roughly consistent with these findings.

The effective mobility of the charge carriers can be estimated from our extracted  $k_{\text{extr}}(V)$  values as  $\mu = k_{\text{extr}}(V)d^2/2V$ , where  $V$  is the internal voltage. Averaging the value of the mobilities calculated for each  $k_{\text{extr}}(V)$  yields an average effective carrier mobility of  $4.6 \times 10^{-5} \text{ cm}^2 \text{ V}^{-1} \text{ s}^{-1}$ , in good agreement with those previously measured using the TOF technique.<sup>19</sup> Knowledge of both the extraction rate and nongeminate recombination rate allows us to estimate the role of nongeminate recombination at a given field under steady-state solar illumination. At steady state under AM1.5G illumination, the rate equation for the electron density is given by  $dn/dt = 0 = G - k_{\text{extr}}(V)n - \gamma n^2$ , where  $G$  is the generation rate, and assuming an average external quantum efficiency of 50% in the spectral range between 350 and 650 nm, it is  $7 \times 10^{21} \text{ cm}^{-3} \text{ s}^{-1}$ . Numerically solving this equation for the parameters presented in Table 1 leads to the solid squares shown in Figure 4. These results are in very good agreement with the charge carrier densities and recombination currents determined by Shuttle et al.<sup>9</sup> We see that the nongeminate recombination loss is also highly field dependent in the steady state, increasing significantly as the internal field in the device decreases. Consistent with recent measurements,<sup>18</sup> we find that at short-circuit conditions under solar illumination, the current loss due to nongeminate recombination is small, only approximately 2%, explaining the often-reported almost linear light intensity dependence of short-circuit current. However, as the internal field in the device decreases toward open-circuit conditions and the dwell time of the carriers in the device increases, nongeminate recombination becomes non-negligible and plays an important role in the reduction of the device fill factor. The solid line in Figure 4 illustrates the case when the average effective mobility is used to calculate  $k_{\text{extr}}(V)$ , allowing the recombination rate to be interpolated for all fields. This line fits reasonably well to the data points, providing a sufficient estimate of the fraction of nongeminate



**Figure 4.** Nongeminate recombination as a function of external bias under steady-state conditions. Black squares are calculated from the parameters presented in Table 1. The solid line is calculated using an effective charge carrier mobility of  $4.6 \times 10^{-5} \text{ cm}^2 \text{ V}^{-1} \text{ s}^{-1}$  to determine the extraction rates.

recombination; however, the neglect of the density dependence of the mobility likely causes some discrepancy.<sup>24</sup>

In conclusion, we have developed a method to directly observe the bias dependence of nongeminate recombination in organic solar cells. Our measurements reveal that nongeminate recombination in the reference system rr-P3HT/PCBM is strongly bias dependent, and this dependence is caused by the reduction of charge extraction rates at lower internal fields. Extending our results to steady-state solar illumination conditions confirms that the bias dependence of the nongeminate recombination has an impact on the device fill factor and thus on the power conversion efficiency of rr-P3HT/PCBM devices. In this context, the observation of a suppressed recombination rate constant with comparison to a Langevin rate constant is considered critical for high device performance. Altogether, this suggests that nongeminate carrier recombination, especially when low mobilities and/or low internal fields extend the carrier dwell time, is an important loss process in organic photovoltaic devices. Consequently, new material systems should be optimized to have a reduced recombination rate combined with a short charge carrier dwell time in the device in order to minimize recombination losses.

## EXPERIMENTAL SECTION

P3HT (Sepiolid P200,  $M_w = 25\,000\text{ g mol}^{-1}$ , PDI = 1.6, regioregularity > 98%) was supplied by BASF SE. PCBM (~99%) was purchased from Sigma Aldrich. All materials were used as received. P3HT and PCBM were dissolved separately in chlorobenzene at 70 °C with concentrations of 18 mg mL<sup>-1</sup>, and the solutions were mixed in a 3:2 ratio and then spin-cast onto PEDOT/PSS (Clevios P VP AI 4083, H.C. Starck) coated ITO substrates in a nitrogen-filled glovebox with subsequent evaporation of a 100 nm thick layer of aluminum followed by annealing for 20 min at 120 °C. The power conversion efficiency of the devices measured was 2.9% with a peak short-circuit external quantum efficiency of 65% between 500 and 530 nm.

For measuring current–voltage characteristics under illumination by two pulsed lasers, a Keithley 2400 source measure unit was used to source voltage and measure current. For the first laser, a commercial titanium/sapphire laser (Coherent LIBRA HE) was used to pump a home-built narrowband noncollinear optical parametric amplifier to generate pulses with a center wavelength of 530 nm, a typical pulse length of <1 ps, and a repetition rate of 1 kHz. The second laser used was a frequency-doubled (532 nm) actively Q-switched Nd:YVO<sub>4</sub> laser (AOT Ltd. MOPA) with a pulse length of ~600 ps and a repetition rate of 1 kHz. The variable delay time between both lasers was controlled by an electronic delay generator (Stanford Research Systems DG535). All measurements were performed at room temperature under dynamic vacuum at pressures < 10<sup>-5</sup> mbar.

## ASSOCIATED CONTENT

**S Supporting Information.** Current–voltage characteristics of the solar cell under simulated AM1.5G illumination. Fluence dependence of the extracted charge under pulsed laser illumination. This material is available free of charge via the Internet at <http://pubs.acs.org>.

## AUTHOR INFORMATION

### Corresponding Authors

\*E-mail: [ian.howard@mpip-mainz.mpg.de](mailto:ian.howard@mpip-mainz.mpg.de) (I.A.H.); [laquai@mpip-mainz.mpg.de](mailto:laquai@mpip-mainz.mpg.de) (F.L.).

## ACKNOWLEDGMENT

We thank M. Kastler (BASF SE) for provision of Sepiolid P200, A. Becker for technical support, and Lukas Kaltschnee for TPV measurements. I.A.H. thanks the Alexander von Humboldt Foundation for a postdoctoral fellowship. F.L. thanks the Max Planck Society for funding a Max Planck Research Group. R.M. thanks the Max Planck Graduate Center (MPGC) for financial support.

## REFERENCES

- (1) Liang, Y. Y.; Xu, Z.; Xia, J. B.; Tsai, S. T.; Wu, Y.; Li, G.; Ray, C.; Yu, L. P. For the Bright Future-Bulk Heterojunction Polymer Solar Cells with Power Conversion Efficiency of 7.4%. *Adv. Mater.* **2010**, *22*, E135.
- (2) Chu, T.-Y.; Lu, J.; Beaupre, S.; Zhang, Y.; Pouliot, J.-R. M.; Wakim, S.; Zhou, J.; Leclerc, M.; Li, Z.; Ding, J.; et al. Bulk Heterojunction Solar Cells Using Thieno[3,4-*c*]pyrrole-4,6-dione and Dithieno[3,2-*b*:2',3'-*d*]silole Copolymer with a Power Conversion Efficiency of 7.3%. *J. Am. Chem. Soc.* **2011**, *133*, 4250.
- (3) Price, S. C.; Stuart, A. C.; Yang, L.; Zhou, H.; You, W. Fluorine Substituted Conjugated Polymer of Medium Band Gap Yields 7% Efficiency in Polymer–Fullerene Solar Cells. *J. Am. Chem. Soc.* **2011**, *133*, 4625.
- (4) Zhou, H. X.; Yang, L. Q.; Stuart, A. C.; Price, S. C.; Liu, S. B.; You, W. Development of Fluorinated Benzothiadiazole as a Structural Unit for a Polymer Solar Cell of 7% Efficiency. *Angew. Chem., Int. Ed.* **2011**, *50*, 2995.
- (5) Marsh, R. A.; Hodgkiss, J. M.; Friend, R. H. Direct Measurement of Electric Field-Assisted Charge Separation in Polymer:Fullerene Photovoltaic Diodes. *Adv. Mater.* **2010**, *22*, 3672.
- (6) Deibel, C. Charge Carrier Dissociation and Recombination in Polymer Solar Cells. *Phys. Status Solidi A* **2009**, *206*, 2731.
- (7) Kniepert, J.; Schubert, M.; Blakesley, J. C.; Neher, D. Photo-generation and Recombination in P3HT/PCBM Solar Cells Probed by Time-Delayed Collection Field Experiments. *J. Phys. Chem. Lett.* **2011**, *2*, 700.
- (8) Jamieson, F. C.; Agostinelli, T.; Azimi, H.; Nelson, J.; Durrant, J. R. Field-Independent Charge Photogeneration in PCPDTBT/PC70BM Solar Cells. *J. Phys. Chem. Lett.* **2010**, *1*, 3306.
- (9) Shuttle, C. G.; Hamilton, R.; O'Regan, B. C.; Nelson, J.; Durrant, J. R. Charge-Density-Based Analysis of the Current–Voltage Response of Polythiophene/Fullerene Photovoltaic Devices. *Proc. Natl. Acad. Sci. U.S.A.* **2010**, *107*, 16448.
- (10) Mauer, R.; Howard, I. A.; Laquai, F. Effect of Nongeminate Recombination on Fill Factor in Polythiophene/Methanofullerene Organic Solar Cells. *J. Phys. Chem. Lett.* **2010**, *1*, 3500.
- (11) Cowan, S. R.; Roy, A.; Heeger, A. J. Recombination in Polymer–Fullerene Bulk Heterojunction Solar Cells. *Phys. Rev. B* **2010**, *82*, 245207.
- (12) Li, Z.; Gao, F.; Greenham, N. C.; McNeill, C. R. Comparison of the Operation of Polymer/Fullerene, Polymer/Polymer, and Polymer/Nanocrystal Solar Cells: A Transient Photocurrent and Photovoltage Study. *Adv. Funct. Mater.* **2011**, *21*, 1419.
- (13) Howard, I. A.; Mauer, R.; Meister, M.; Laquai, F. Effect of Morphology on Ultrafast Free Carrier Generation in Polythiophene:Fullerene Organic Solar Cells. *J. Am. Chem. Soc.* **2010**, *132*, 14866.
- (14) Clarke, T. M.; Jamieson, F. C.; Durrant, J. R. Transient Absorption Studies of Bimolecular Recombination Dynamics in Polythiophene/Fullerene Blend Films. *J. Phys. Chem. C.* **2009**, *113*, 20934.

(15) Guo, J.; Ohkita, H.; Bente, H.; Ito, S. Charge Generation and Recombination Dynamics in Poly(3-hexylthiophene)/Fullerene Blend Films with Different Regioregularities and Morphologies. *J. Am. Chem. Soc.* **2010**, *132*, 6154.

(16) Etzold, F.; Howard, I. A.; Mauer, R.; Meister, M.; Kim, T.-D.; Lee, K.-S.; Baek, N. S.; Laquai, F. Ultrafast Exciton Dissociation Followed by Nongeminate Charge Recombination in PCDTBT:PCBM Photovoltaic Blends. *J. Am. Chem. Soc.* **2011**, *133*, 9469.

(17) McNeill, C. R.; Hwang, I.; Greenham, N. C. Photocurrent Transients in All-Polymer Solar Cells: Trapping and Detrapping Effects. *J. Appl. Phys.* **2009**, *106*, 024507.

(18) Koster, L. J. A.; Kemerink, M.; Wienk, M. M.; Maturová, K.; Janssen, R. A. J. Quantifying Bimolecular Recombination Losses in Organic Bulk Heterojunction Solar Cells. *Adv. Mater.* **2011**, 1670.

(19) Mauer, R.; Kastler, M.; Laquai, F. The Impact of Polymer Regioregularity on Charge Transport and Efficiency of P3HT:PCBM Photovoltaic Devices. *Adv. Funct. Mater.* **2010**, *20*, 2085.

(20) Mihailetschi, V. D.; Xie, H. X.; de Boer, B.; Koster, L. J. A.; Blom, P. W. M. Charge Transport and Photocurrent Generation in Poly(3-hexylthiophene): Methanofullerene Bulk-Heterojunction Solar Cells. *Adv. Funct. Mater.* **2006**, *16*, 699.

(21) Deibel, C.; Baumann, A.; Dyakonov, V. Polaron Recombination in Pristine and Annealed Bulk Heterojunction Solar Cells. *Appl. Phys. Lett.* **2008**, *93*, 163303.

(22) Deibel, C.; Wagenpfahl, A.; Dyakonov, V. Origin of Reduced Polaron Recombination in Organic Semiconductor Devices. *Phys. Rev. B* **2009**, *80*, 075203.

(23) Juska, G.; Arlauskas, K.; Stuchlik, J.; Österbacka, R. Non-Langevin Bimolecular Recombination in Low-Mobility Materials. *J. Non-Cryst. Solids* **2006**, *352*, 1167.

(24) Shuttle, C. G.; Hamilton, R.; Nelson, J.; O'Regan, B. C.; Durrant, J. R. Measurement of Charge-Density Dependence of Carrier Mobility in an Organic Semiconductor Blend. *Adv. Funct. Mater.* **2010**, *20*, 698.





# 5

## General Discussion

For a complete picture of the device physics of organic solar cells a basic understanding of the origin and magnitude of the involved rate constants is a necessary prerequisite. At steady-state conditions all photogenerated free charge carriers are either extracted or recombine non-geminately. In terms of a rate equation this reads as follows. The free charge generation rate  $G$  equals the sum of charge extraction rate  $E$  and non-geminate recombination rate  $R$  (see also section 3.4):

$$G = E + R = k_{extr} n + \gamma n^2. \quad (5.1)$$

This equation can be solved to give the photogenerated charge carrier density in a solar cell as a function of the charge extraction rate constant  $k_{extr}$ , the Langevin recombination rate constant  $\gamma$  and the charge generation rate:

$$n = \frac{k_{extr}}{2\gamma} \left[ \sqrt{1 + 4 \frac{\gamma G}{k_{extr}^2}} - 1 \right]. \quad (5.2)$$

The extractable photocurrent can be calculated from the extraction rate and the steady-state charge carrier density in the device:

$$J_{photo} = \frac{1}{A} \frac{dQ_{extr}}{dt} = -ed E = -ed k_{extr} n = -ed \frac{k_{extr}^2}{2\gamma} \left[ \sqrt{1 + 4G \frac{\gamma}{k_{extr}^2}} - 1 \right]. \quad (5.3)$$

In this context  $A$  is the area of the sample,  $d$  its thickness,  $Q_{extr}$  is the electric charge extracted from the sample and  $e$  the elementary charge. In general,  $G$ ,  $\gamma$  and  $k_{extr}$  can (besides the material properties) depend on the applied electric field, the temperature and the charge carrier density, which will be discussed in the course of this chapter. It should be noted that the analytic description of the photocurrent given here assumes that the involved rate constants do not depend on the charge carrier density. While this assumption may lead to quantitative deviations from experimental results, it still allows a qualitatively correct analysis of the importance of the respective parameters. A more quantitative analysis in the case of a density dependence of the rate constants requires that the steady-state charge carrier density is calculated numerically from the equation above. From the parameterization of the photocurrent presented here, it becomes apparent that the competition between non-geminate recombination and extraction is important for the amount of photocurrent that can be collected from a solar cell, because these two processes enter the expression for the photocurrent exclusively via the ratio of the respective rate constants.

Altogether it can be concluded that with a detailed understanding of the extraction and bimolecular recombination rate constants as well as the free charge generation rate a complete description of the photocurrent of a solar cell is possible. As has been shown in the preceding discussion of the experimental results, time-resolved experiments can give insight into these rate constants and their dependence on both material properties as well as external stimuli like an electric field or the temperature. In this chapter the different experimental results will be discussed in this general framework in order to clarify the connection between the molecular properties and solar cell performance of the studied materials.



## 5.1 Charge Generation

The charge generation rate contains all phenomena that lead to the creation of free charge carriers like e.g. the absorption of light, singlet exciton formation, diffusion and dissociation as well as charge-transfer exciton formation, recombination and dissociation. It is first of all given by the flux of photons from the solar spectrum in the spectral region that can be absorbed in the active layer. The absorption onset of annealed RR-P3HT:PCBM solar cells is  $\sim 620$  nm. In the range between 280 nm and 620 nm the AM1.5G spectrum contains a photon flux of  $9.97 \times 10^{16} \text{ cm}^{-2} \text{ s}^{-1}$ , which gives an upper estimate for the charge generation rate of  $G_{\text{max}} = 9.97 \times 10^{21} \text{ cm}^{-3} \text{ s}^{-1}$  in an active layer of 100 nm thickness, assuming that all of these photons are absorbed in the active layer. Importantly, a shift of the absorption onset to 850 nm (decrease of the band gap by  $\sim 1/4$ ) would double the absorbable photon flux. Of course not every incident photon is absorbed in the active layer, which causes a reduction of the charge generation rate. Optical simulations using a transfer matrix formalism can be applied to estimate the impact of this loss mechanism. Such simulations demonstrate that reflection from a device and parasitic absorption in the electrodes can lead to a reduction of the charge generation rate by 10-50%, depending on the exact thickness and optical constants of every layer in the device. Absorption measurements on P3HT:PCBM solar cells, with optimized layer thicknesses to give 4% power conversion efficiency, have shown that this loss mechanism accounts for a reduction of the charge generation rate by  $\sim 20\%$  which leaves  $G_{\text{abs}} = 7.98 \times 10^{21} \text{ cm}^{-3} \text{ s}^{-1}$  [105].

The next step in charge generation after the absorption of photons is the diffusion of the resultant excitons to a nearby interface, which happens in competition with the recombination of excitons. The results of the transient absorption experiments suggest that in annealed blends of efficient solar cells the phase segregation between P3HT and PCBM is so large that the diffusion of excitons to the interface takes up to 10 ps. This is relatively short compared to the exciton life time of  $(576 \pm 2)$  ps as determined by time resolved photoluminescence spectroscopy, so that only less than 2% of excitons

recombine before being dissociated. This results in a total exciton dissociation rate of  $G_{\text{exc}} = 7.82 \times 10^{21} \text{ cm}^{-3} \text{ s}^{-1}$ .

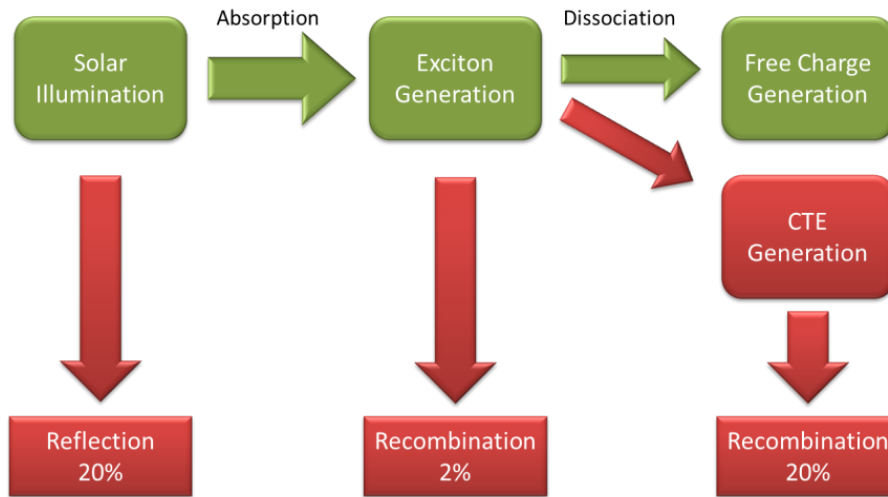
As has been discussed extensively in the theoretical framework and the experimental results the outcome of the exciton quenching can either be directly generated free charge carriers or charge-transfer excitons. The transient absorption (TA) experiments suggest that in annealed blends of RR-P3HT and PCBM even in the absence of an electric field more than 80% of the excitons dissociate into free charge carriers and only less than 20% form charge-transfer excitons. This is in stark contrast to blends of regiorandom (RRa) P3HT and PCBM in which this splitting ratio is 20% free charge carriers to 80% charge-transfer excitons. As the energetic driving force for separation is very similar in these two systems, the reason for this large difference must be associated with morphological constraints. In RRa-P3HT:PCBM no diffusion limited quenching of excitons could be observed, which means that all excitons generated in the RRa-P3HT phase are dissociated within the time resolution of the TA setup (i.e. less than 100 fs). This implies a much smaller degree of phase segregation and a morphology that resembles a fine distribution of PCBM molecules in the RRa-P3HT matrix. As has been discussed in the introduction of the role of morphology on the formation of free charge carriers such a morphology is not favorable for the generation of free charge carriers, as a certain degree of phase segregation is necessary for the charge carriers to be able to separate themselves from one another far enough to be considered free. In agreement with these considerations in unannealed RR-P3HT:PCBM blends, that possess an intermediate degree of phase segregation in between RRa-P3HT:PCBM and annealed RR-P3HT:PCBM, the splitting ratio was found to be 68% free charge carriers and 32% charge-transfer excitons. Besides the morphology the charge carrier mobility also differs over a broad range between these three types of blends. However, the mobility does not seem to have any effect on the generation of free charge carriers. Reducing the temperature to liquid nitrogen temperature (77 K) and thus the charge carrier mobility by approximately two orders of magnitude (without changing the

morphology) does not change the splitting ratios of free charge carriers to charge-transfer excitons for both RR-P3HT:PCBM and RRa-P3HT:PCBM.

Additionally, according to the Onsager-Braun model the charge-transfer excitons have the potential to be separable by application of an electric field or increased temperature. However, the temperature independence of the charge carrier generation already is in contrast to the Onsager-Braun model. Furthermore, simulations of the current voltage characteristics at high and low temperatures as well as the analysis of the time delayed double pump experiments support that charge-transfer excitons cannot be dissociated by electric field strengths relevant for device performance. Furthermore, recent work from other groups affirms these findings [62,105,106]. For example, Burkhard et al. determined an internal quantum efficiency in P3HT:PCBM solar cells of 80% (at short circuit conditions), which is in excellent agreement with the 20% loss by geminately recombining charge-transfer excitons observed here. Furthermore, the external quantum efficiency of optimized P3HT:PCBM solar cells is frequently reported to be ~65%, which is very well compatible with a loss of 20% due to absorption (vide supra) and another 20% due to geminate recombination totaling a loss factor of 36%. The final estimation of the charge generation rate including all of the above considerations is  $G = 6.26 \times 10^{21} \text{ cm}^{-3} \text{ s}^{-1}$ , irrespective of applied electric field. Assuming that all of the generated free charge carriers can be extracted without recombining non-geminately, i.e.  $J = -edG$ , yields a photocurrent of  $10.0 \text{ mA/cm}^2$  which is a good approximation of the short circuit current in P3HT:PCBM solar cells with ~4% power conversion efficiency.<sup>4</sup>

---

<sup>4</sup> It should however be noted, that variations in the thicknesses of the layers inside a solar cell can easily change the short circuit current by as much as  $3 \text{ mA/cm}^2$ , because of changes in the photon absorption profile.



**Figure 32.** Summary of the processes involved in the generation of free charge carriers (CTE= Charge-transfer exciton).

## 5.2 Charge Recombination

As geminate recombination is already covered by the charge generation rate, in this part only the non-geminate recombination of free charge carriers will be discussed. The most basic requirement for two spatially separated charge carriers to recombine is that they meet in the same place. This directly leads to a Langevin-type non-geminate recombination rate as has been discussed in the introduction more extensively. In this work transient absorption spectroscopy was used to directly observe the kinetics of non-geminate recombination. It was found to follow a modified Langevin rate

$$\frac{dn}{dt} = -\gamma(n) n^2 = -\xi \frac{e(\mu_e + \mu_h)}{\varepsilon_0 \varepsilon_r} n^{\lambda+1}. \quad (5.4)$$

Here, the recombination rate constant  $\gamma$  differs from the traditional Langevin rate constant in two ways. The first one is that the rate constant is not independent of the charge carrier density. The overall reaction order in annealed RR-P3HT:PCBM blends is increased by 0.45 to  $\lambda+1 = 2.45$ . This can have two possible explanations. On the one hand Juska et al. [95] have shown that if the charge transport is essentially limited to a two-dimensional plane, the reaction order of the recombination is increased to 2.5. The tendency of regioregular P3HT to form well-ordered lamellar structures could indeed

justify the assumption of two-dimensional hole transport. However, similar studies of non-geminate recombination have shown that the reaction order is strongly influenced by the processing conditions of the sample [94] and also varies for different (more amorphous and therefore more isotropic) donor polymers used [107]. Furthermore, the overall reaction order increases with decreasing temperature, as was shown with the temperature dependent TA measurements. This is unlikely to be explained by a two-dimensional limitation of charge transport alone. The second explanation for the increased reaction order could be a charge carrier density dependence of the charge carrier mobility. In fact, Shuttle et al. recently measured the charge carrier density dependence of both the recombination rate constant and the charge carrier mobility in P3HT:PCBM solar cells and observed identical density dependencies for both parameters, strongly suggesting that the charge carrier mobility is responsible for the additional density dependence of the recombination rate [75]. Also at lower temperatures a stronger dependence of the mobility on the charge carrier density can be expected [73] leading to a higher reaction order in agreement with the temperature dependent TA measurements.

The second deviation from the expected Langevin recombination rate constant is the reduction prefactor  $\xi$ . Using the charge carrier mobilities determined from the TOF measurements of  $5 \times 10^{-5} \text{ cm}^2/\text{Vs}$  for both electrons and holes and a relative permittivity of 3.5 yields a Langevin recombination rate constant of  $\gamma_{\text{Langevin}} = 5.2 \times 10^{-11} \text{ cm}^3 \text{ s}^{-1}$ . The experimentally determined effective rate constant corresponding to a second order recombination process is  $3 \times 10^{-13} \text{ cm}^3 \text{ s}^{-1}$  for annealed RR-P3HT:PCBM and  $1.7 \times 10^{-13} \text{ cm}^3 \text{ s}^{-1}$  for unannealed RR-P3HT:PCBM, both at a charge carrier density of  $10^{16} \text{ cm}^{-3}$ , which is a factor  $\xi = 5.8 \times 10^{-3}$  and  $3.4 \times 10^{-2}$  smaller than the calculated value of  $\gamma_{\text{Langevin}}$ , respectively. These values are compatible with other recent experimental results [91-93]. This reduction of the recombination rate constant is inherent to bulk heterojunction films. The theory of Langevin recombination was developed for recombination of charge carriers in a homogeneous, three

dimensionally isotropic medium. In a bulk heterojunction, however, the charge carriers are confined to either the donor or the acceptor phase and can only recombine if they meet at the interface. This strongly reduces the probability for recombination events which leads to a reduction of the rate constant. The reduction factor is therefore closely related to the morphology and the actual area of the interface that can offer sites for recombination events. The observation that annealing leads to a reduction of the effective recombination rate constant by an entire order of magnitude suggests that annealing leads to a higher degree of phase segregation and thus to a smaller interfacial area.

The influence of external stimuli on the recombination rate constant mainly follows that of the charge transport properties. Field dependent TOF measurements demonstrated a negligible field dependence of the charge carrier mobility, so that the recombination rate constant can be assumed to be independent of an applied electric field. It should be noted however, that this does not mean that the non-geminate recombination rate itself is independent of an applied electric field in solar cell devices, because as will be discussed later, the steady-state charge carrier density in a solar cell strongly depends on the applied voltage. As in turn the recombination rate depends on the charge carrier density, it will change with the electric field along with the charge carrier density in the device. The temperature dependence of the charge carrier mobility that was also determined by TOF is very well compatible with the reduction of the recombination rate constant by two orders of magnitude when going from room to liquid nitrogen temperature determined with TA measurements as already mentioned above.

### 5.3 Charge Extraction

The charge extraction rate constant is dominated by the charge transport properties of the photovoltaic blend and the device thickness. A directional movement of charge carriers can either take place in the form of drift in an electric field or diffusion due to gradients of the concentration of the charge carriers. Generally, both effects are important for the description of the photocurrent of organic solar cells and a complete description of the field-dependence of the photocurrent requires the use of a numerical drift-diffusion model, as for example implemented in the software Setfos. Neglecting the diffusional contribution to charge transport allows the formulation of an analytic description of the field dependence of the photocurrent at the cost of losing precision at low electric field strengths (i.e. close to the open circuit voltage) where diffusion is most important [108].<sup>5</sup> In the following discussion this simplification will be used, because apart from the case of low electric fields the analytical model gives some very useful insights into the fundamental principles of the field-dependence of the photocurrent of solar cell devices and is much more intuitive and tractable to discuss than the full drift-diffusion description.

Assuming that charge extraction is exclusively driven by the drift of charge carriers in the applied electric field and again neglecting the field-dependence of the charge carrier mobility (vide supra), the charge extraction rate constant can be expressed as follows:

$$k_{extr}(F, T) = \frac{2}{d} \mu(T) F. \quad (5.5)$$

Here the factor 2 accounts for the fact that charge carriers on average have to travel a distance equal to half of the thickness  $d$  of the active layer before being extracted at an electrode (thus assuming a homogeneous charge generation

---

<sup>5</sup> On one hand the drift component, that is proportional to the electric field, vanishes at low electric fields. On the other hand, close to the open circuit voltage charge injection from the electrodes sets in leading to increased concentrations of electrons (holes) near the aluminum (ITO/PEDOT:PSS) electrode and thus to concentration gradients that can cause a diffusion component. The photogeneration of charge carriers is assumed to be distributed homogeneously throughout the volume of the bulk heterojunction.

profile throughout the active layer). The value expected for  $k_{\text{extr}}$  in annealed RR-P3HT:PCBM can be estimated from the TOF charge carrier mobility  $\mu = 5 \times 10^{-5} \text{ cm}^2/\text{Vs}$  and the internal field of an organic solar cell close to short circuit conditions  $F = U/d = 0.6 \text{ V}/100 \text{ nm} = 6 \times 10^4 \text{ V/cm}$  as  $k_{\text{extr}} = 6 \times 10^5 \text{ s}^{-1}$ , which is compatible with the results of the double pump experiments, that give a value of  $k_{\text{extr}} = 9 \times 10^5 \text{ s}^{-1}$  at a similar field strength.

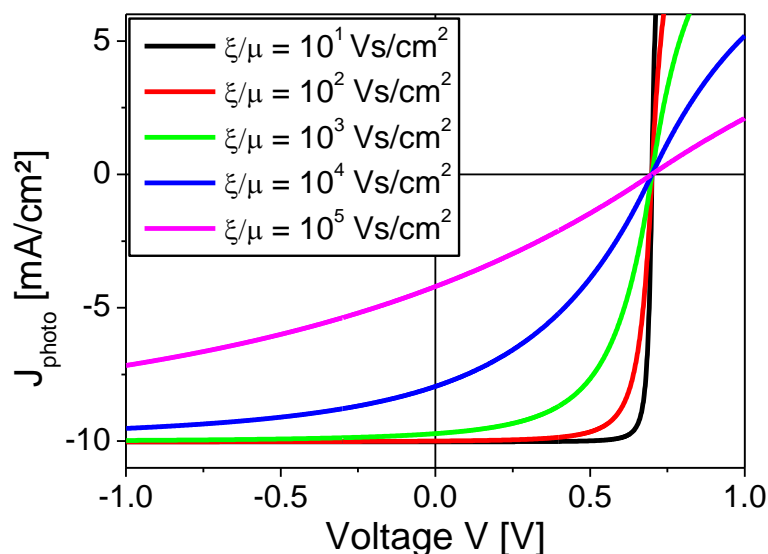
In total, all experiments performed for this work lead to the conclusion that the extraction rate constant is the only significantly field-dependent parameter in the description of the photocurrent of annealed RR-P3HT:PCBM solar cells. Using the expressions for the extraction rate constant  $k_{\text{extr}}$  (5.5) and  $\gamma = \xi (\mu_e + \mu_h) e / (\varepsilon_0 \varepsilon_r) \cong 2 \xi \mu e / (\varepsilon_0 \varepsilon_r)$  in formula (5.3) for calculating the photocurrent  $J_{\text{photo}}$  yields the following field dependence of the photocurrent:

$$J_{\text{photo}}(F) = -\frac{\varepsilon_0 \varepsilon_r}{d} \frac{\mu}{\xi} F^2 \left[ \sqrt{1 + \frac{2ed^2}{\varepsilon_0 \varepsilon_r} \frac{\xi}{\mu} \frac{G}{F^2}} - 1 \right]. \quad (5.6)$$

Apparently, increasing the charge carrier mobility has the same effect on the photocurrent as decreasing the prefactor of the non-geminate recombination rate constant  $\xi$ . From the point of view of device performance increasing the charge carrier mobility and simultaneously decreasing the interfacial area of the blend (that is mainly responsible for the prefactor  $\xi$ ) seems to be beneficial in this context. However, decreasing the interfacial area not only decreases the non-geminate recombination rate but also the amount of exciton quenching, so that there exists an optimum morphology that provides a balance between efficient charge generation and low non-geminate recombination losses.

In **Figure 33** the calculated voltage dependence of the photocurrent of a solar cell with a charge generation rate of  $G = 6.26 \times 10^{21} \text{ cm}^{-3} \text{ s}^{-1}$  (vide supra) is shown for different ratios of the reduction prefactor and the charge carrier mobility. The electric field  $F = (V_{\text{appl}} - V_{\text{BI}})/d$  used for this calculation is given by the difference between the built-in voltage  $V_{\text{BI}}$  (0.7 V) [64], the externally applied voltage  $V_{\text{appl}}$  and the active layer thickness  $d$ :  $F = (V_{\text{appl}} - V_{\text{BI}})/d$ .





**Figure 33.** Voltage dependence of the photocurrent of a solar cell for various ratios of the reduction prefactor  $\xi/\mu$  and the charge carrier mobility  $\mu$  assuming a charge generation rate of  $G = 6.26 \times 10^{21} \text{ cm}^{-3} \text{ s}^{-1}$  (vide supra). The electric field is calculated from the applied and built-in voltage as  $F = (V_{\text{appl}} - V_{\text{BI}})/d$  with  $V_{\text{BI}} = 0.7 \text{ V}$  [64].

At a high reverse bias (e.g. -1 V) essentially all charge carriers are extracted (except for the highest  $\xi/\mu$  ratio). When reducing the electric field by changing the voltage from a high reverse bias towards the built-in voltage not all charge carriers can be extracted and some recombine non-geminately. The number of charge carriers lost to recombination at any given voltage depends on the  $\xi/\mu$  ratio.

In P3HT:PCBM this ratio depends on the morphology on different length scales. On the one hand the regioregularity determines the packing of the polymer chains within the P3HT domains [76]. This results in a drastic variation of the charge carrier mobility for small changes in the regioregularity. The hole mobilities in the materials with regioregularities of >98% and 94% already differ by an entire order of magnitude (with the higher mobility for the higher regioregularity). In samples of unannealed RR-P3HT:PCBM (prepared from chloroform solutions) the packing of the P3HT chains is also unfavorable for charge transport and the hole-mobility is correspondingly much lower than in

annealed samples.[6] In short, the packing of the P3HT chains, be it due to the precise molecular structure of the polymer chains or the sample preparation conditions, influences the charge transport and thus the  $\xi/\mu$  ratio. Besides this, the degree of phase segregation plays an important role. The miscibility of PCBM with amorphous P3HT tends to be higher than with well-ordered P3HT, probably because of a size exclusion in the tightly packed lamellar structure of well-ordered P3HT that does not leave enough space for PCBM intercalation [31,109,110]. This generally means that blends of well-ordered RR-P3HT with PCBM show a higher degree of phase segregation and only some intermixing in a more amorphous region close to the interface. The degree of phase segregation and the extent of intermixing are thus also depending on the regioregularity of the P3HT. At the extremes the annealed >98% RR-P3HT:PCBM shows a high degree of phase segregation with only little intermixing and RRa-P3HT:PCBM lacks phase segregation almost completely and rather consists of finely dispersed PCBM in a P3HT matrix as was determined by the transient absorption experiments. Consequently, the interfacial area differs widely between these morphologies and so does the recombination reduction factor  $\xi$ .

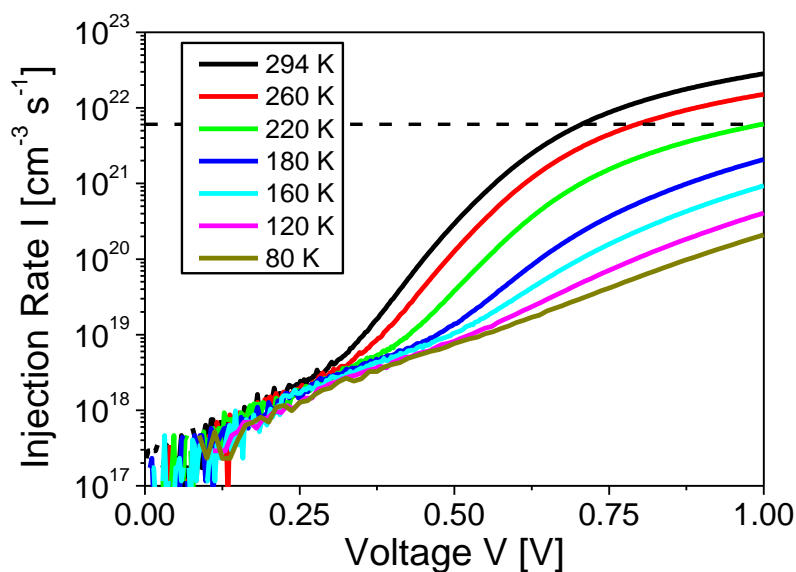
In annealed RR-P3HT:PCBM the ratio of recombination reduction factor to mobility is  $\sim 10^2$  Vs/cm<sup>2</sup>, which corresponds to the red line in **Figure 33**. When cooling annealed RR-P3HT:PCBM to liquid nitrogen temperature and thus reducing the charge carrier mobility by  $\sim 2$  orders of magnitude, the  $\xi/\mu$  ratio is increased to  $10^4$  Vs/cm<sup>2</sup> (blue line). This is very well compatible with the temperature dependent reduction of the device performance of annealed RR-P3HT:PCBM solar cells observed at low temperatures [64]. In unannealed RR-P3HT:PCBM (prepared from chloroform) this ratio is even higher. Here, in spite of the hole mobility being much lower than in the annealed case [6] the effective recombination rate constant is almost an order of magnitude higher, which demonstrates that the recombination reduction factor must also be much bigger than in annealed RR-P3HT:PCBM. Using the values of the charge carrier mobility determined by Mihailetschi et al. [6] for unannealed RR-

P3HT:PCBM  $\xi/\mu$  can be estimated to be  $\sim 10^5$  Vs/cm<sup>2</sup> (magenta line), partially explaining the poor performance of unannealed devices.

## 5.4 Charge Injection

Besides charge generation, recombination and extraction, the injection of charge carriers into the device from the electrodes is important for device performance. Unfortunately, charge injection is not readily accessible by optical spectroscopic methods and was thus not studied in detail in the course of this work. However, some observations were made and will be discussed here.

In a first approximation, the injection current in a solar cell corresponds to the current flowing through the device in the absence of illumination, i.e. the dark current. At voltages below the built-in voltage the polarity of the electric field in the device is directed so that a drift current can only flow, if electrons are injected from the ITO/PEDOT:PSS electrode into the LUMO of PCBM and holes from the aluminum electrode into the HOMO of P3HT. Due to the huge offset between these energy levels of  $>0.5$  eV this injection is not possible at moderate electric fields. Only under very high reverse bias is the energy of the electric field sufficient to drive injection across this barrier in analogy to the breakdown of an inorganic diode. The fact that a dark current flow is observed in the voltage regime relevant for solar cell operation thus suggests that in this range the dark current is exclusively caused by diffusion and that the charge injection mechanism is thermionic injection [81]. This proposes that the injection current depends on the temperature of the device, an assertion which is in good agreement with the experimental results described above (see **Figure 34**). Importantly, this implies that the dark current is not exactly equal to the injection current in a solar cell under illumination, as relaxation processes of the involved excited states and parasitic absorption of photons in the electrodes increase the temperature of the device under illumination and thus change the rate of injection in the illuminated device as compared to the injection in the dark. Furthermore, the presence of photogenerated charge carriers alters the concentration gradient of charge carriers in the active layer which also leads to deviations between the dark current and the injection current under illumination.



**Figure 34.** Injection rate  $I$  in the dark at various temperatures between room temperature and liquid nitrogen temperature in an annealed RR-P3HT:PCBM solar cell. The rate was calculated from  $I = J_{dark}/ed$ . The black dashed line at  $6 \times 10^{21} \text{ cm}^{-3} \text{ s}^{-1}$  indicates the charge generation rate under AM1.5G illumination for comparison.

Looking from the perspective of the photocurrent, the injection of charge carriers alters the steady-state charge carrier density in the device and can thus lead to a change in the amount of non-geminately recombining charge carriers. However, as the density of injected charge carriers is highest at the respective electrodes and falls off into the active layer (correspondingly to the charge density gradient), the spatial distribution of the injected and photogenerated charge carrier densities are different. Furthermore, non-geminate recombination requires a spatial overlap of the electron and hole densities. Because of this constraint it is not straight-forward to quantitatively describe the interaction between injected and photogenerated charge carriers. It is however clear, that the open circuit voltage of a solar cell under illumination is determined by the voltage at which the injection current compensates the photocurrent. At room temperature the injection rate close to the open circuit voltage is of the same order of magnitude as the charge generation rate under AM1.5G illumination, i.e.  $10^{21}$ - $10^{22} \text{ cm}^{-3} \text{ s}^{-1}$  (see dashed

line in **Figure 34**). At lower temperatures the decreased injection rate leads to a shift of the open circuit voltage towards the built-in voltage.

# 6

## Conclusions and Outlook

### 6.1 Conclusions

For this thesis the relationship between molecular structure, relevant physical mechanisms and solar cell performance was studied in the material system P3HT:PCBM. First of all, a close correlation between the molecular structure, i.e. the regioregularity, and the morphology of P3HT in thin solid films was observed [76]. P3HT with high regioregularity tends to form well-ordered lamellar structures, whereas in regiorandom P3HT, overlapping side-chains lead to torsions in the backbone of the polymer that prevent planarization and close packing density due to steric repulsion [109]. This variation in the packing behavior goes along with a red-shift and more pronounced vibronic features of the absorption spectrum at higher regioregularities, which is beneficial for the overlap with the solar emission spectrum.

Furthermore, the packing behavior was found to have a strong influence on the charge transport properties. At the highest regioregularity studied in this

work, i.e. >98%, the hole-mobility can be as high as  $3 \times 10^{-4} \text{ cm}^2/\text{Vs}$ , a slight reduction of the regioregularity to 94% decreases the charge carrier mobility by almost an order of magnitude to  $6 \times 10^{-5} \text{ cm}^2/\text{Vs}$ , and finally in regiorandom P3HT transport is very slow and dispersive, so that a meaningful mobility cannot be determined by TOF experiments. These values refer to the hole-mobility of pristine P3HT at room temperature. In blends of annealed (<98%) RR-P3HT and PCBM electron- and hole-mobilities are virtually identical with a value of  $5 \times 10^{-5} \text{ cm}^2/\text{Vs}$  at room temperature. The properties of such blends critically depend on the miscibility of the two constituent materials. As could be inferred from the exciton quenching kinetics measured by transient absorption spectroscopy, the miscibility of P3HT and PCBM is much higher in amorphous P3HT than in well-ordered P3HT, most probably due to a reduced intercalation of PCBM molecules into the lamellar structure of RR-P3HT. This was recently confirmed with the help of X-ray diffraction experiments by Collins et. al. [110]. Generally speaking, RR-P3HT:PCBM blends consist of a pure well-ordered RR-P3HT phase, a pure PCBM phase and an amorphous mixed phase [111] with the exact ratio between these three phases depending on the packing behavior of the P3HT.

Additional results from transient absorption spectroscopy suggested, that the dissociation of excitons leads to the population of two distinct pools of charge carriers: spatially separated (free) charge carriers and geminately bound charge-transfer excitons. Interestingly, estimations of the internal quantum efficiency, temperature dependent transient absorption spectroscopy and the time delayed double pulse experiments suggested, that the latter are exclusively subject to recombination, and cannot be dissociated by the application of an electric field (in the range relevant for solar cell device performance) or with thermal activation. This is in stark contrast to the Onsager-Braun model that is frequently used to describe charge generation in numerical models of organic solar cells. In annealed RR-P3HT:PCBM about 80% to 85% of dissociated excitons lead to the formation of free charge carriers, whereas in RRa-P3HT:PCBM only 20-25% of the excitons are

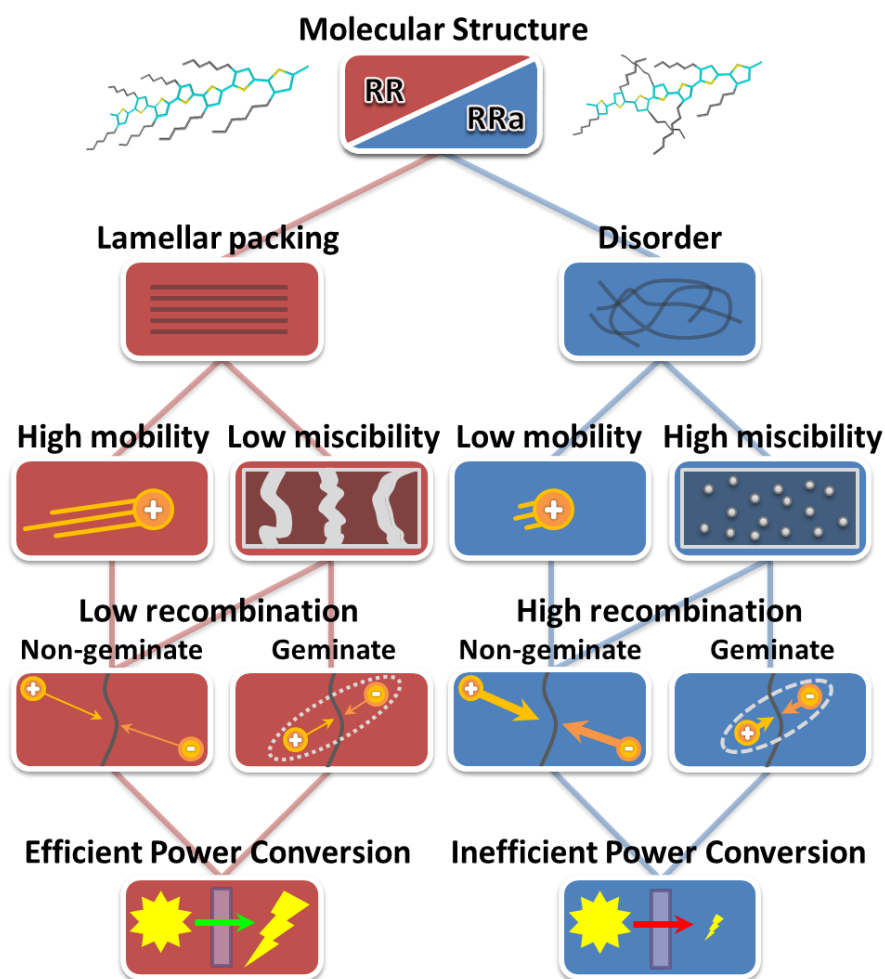


converted into free charge carriers. This correlates very well with the quantum efficiency of solar cells built from these materials.

The results of the newly developed time delayed double pulse experiment quantified that photogenerated charge carriers on average stay in the active layer of an organic solar cell for hundreds of nanoseconds to tens of microseconds before extraction or recombination, in an applied bias range between -1 V and open circuit voltage. This confirms that the charge carrier mobilities determined by TOF can indeed be relevant for describing the device performance of organic solar cells, despite being measured in much thicker samples. Importantly, the information about the charge carrier extraction kinetics can, in combination with the previous experimental results, be used to estimate non-geminate recombination losses in organic solar cells as a function of the applied bias. For annealed RR-P3HT:PCBM this estimation predicts that at the maximum power point, i.e. the operation voltage of a solar cell, ~20% of the photogenerated free charge carriers recombine non-geminately, in spite of the relatively high charge carrier mobilities [102]. Relating this to the figures of merit used to describe solar cell performance, this means that non-geminate recombination reduces the fill factor by about 20% compared to the maximum possible fill factor imposed by the voltage dependence of the dark current. This is confirmed by device characterizations that suggest a maximum possible fill factor of about 75% from the dark current and an actual fill factor under solar illumination of 60%. Hence, in annealed RR-P3HT:PCBM, geminate and non-geminate recombination present equally important loss channels.

In summary, in annealed RR-P3HT:PCBM blends, free charge carriers can be created rather efficiently with relatively small losses due to geminate or non-geminate recombination. Consequently, the main reason for this material system to have a power conversion efficiency of only ~4% is that the extracted charge carriers can only maintain a small fraction of the incident photon energy. Energy losses occur because of the limited overlap of the absorption with the solar emission spectrum, relaxation of the excitons to the lowest excited singlet exciton state, the free energy offset during charge transfer and

relaxation of electrons and holes to the LUMO and HOMO levels during charge extraction, respectively. The development of new material systems should therefore aim at combining the good properties of P3HT concerning especially the high charge carrier mobility, favorable phase segregation with PCBM as well as field-independent charge generation, with decreasing the loss of energy by optimizing the band gap of the absorbing material, minimizing the energetic offset during charge generation and thus maximizing the photon-energy scavenging by each charge carrier. Recently, some promising developments in this direction have been reported [13]. The donor polymer PTB7 combines a high internal quantum efficiency (>85%), a hole-mobility similar to P3HT ( $5.8 \times 10^{-4} \text{ cm}^2/\text{Vs}$  measured by SCLC) and an absorption onset at 750 nm to give a power conversion efficiency of 7.4%. Concerning acceptors, a new soluble fullerene derivative has been introduced, that has a LUMO level 0.17 eV higher than that of PCBM. In combination with P3HT, this indene-C60 bisadduct (ICBA) showed a power conversion efficiency of 6.5% due to an increase in the open circuit voltage to 0.84 V (compared to 0.59 V for P3HT:PCBM) [112]. Altogether, the critical efficiency limit for commercialization of organic solar cells seems to be within reach.



**Figure 35.** Graphical summary of the relation between the main experimental results of this thesis. Regioregular (RR) P3HT packs in a lamellar structure, which leads to a high hole-mobility and a low miscibility with PCBM. The low miscibility in turn leads to low geminate and non-geminate recombination losses. The high charge carrier mobility results in a fast charge carrier extraction and thus further reduces non-geminate recombination in solar cells. It does not however influence the amount of geminate recombination. Altogether, this combines to give efficient power conversion in solar cell devices. The regiorandom (RRa) P3HT does not show signs of ordering and forms amorphous films. The lack of order leads to a low hole-mobility and a high miscibility with PCBM. The latter gives rise to high geminate and non-geminate recombination losses. The low hole-mobility adds to these losses, as charge extraction is not sufficiently fast. In combination, this results in a poor power conversion efficiency.

## **6.2 Outlook**

In spite of the aforementioned progress in the field of organic solar cells, there are still some unresolved questions that should be addressed in future research. In this section a few recommendations for further investigations will be presented.

### **6.2.1 New donor materials**

As has been demonstrated in the course of this work, in P3HT all properties beneficial for device performance directly derive from the ability of P3HT to self-assemble into a well-ordered lamellar structure. New high performance materials like PTB7 lack this ability and show only a low degree of ordering in bulk heterojunctions [113]. A detailed study of the charge generation and recombination processes, similar to the one presented for P3HT in this thesis, could shed some light onto why good order is not a necessity for good device performance in such systems. Better insights in this regard could lead to valuable suggestions for the development of the next generation of donor materials.

### **6.2.2 New acceptor materials**

Apart from being expensive, PCBM is not an ideal acceptor material because of its low absorption coefficient and relatively large offset of the energy levels with most donor materials. A first step towards improved acceptor materials has been made with the development of ICBA that on the one hand has slightly more favorable energy levels, but on the other hand still does not significantly contribute to the absorption of light, as any fullerene based acceptor. A promising class of materials that combines high absorption coefficients with good charge carrier mobilities and tunable energy levels are perylene dyes [15]. However, the morphology of blends of such dyes (e.g. perylene diimides) with donor polymers differs very much from that of fullerene based acceptors. A systematic study of the influence of functionalizing side-groups on charge generation and recombination might present possibilities to develop replacements for fullerene based acceptors.

### 6.2.3 Charge Generation

Most of the charge generation process in organic solar cells happens within 100 fs after exciton creation.<sup>6</sup> This very short time range is not accessible with the spectroscopic setup used for this thesis. Improving the time resolution of the transient absorption spectroscopy setup by introducing additional pulse compression optics could solve this problem. A detailed investigation of the processes happening on this very short time-scale could reveal new interesting physical aspects of the charge generation process. Furthermore, polarization resolved transient absorption spectroscopy experiments could be performed to study the motion of singlet excitons in the donor phase and of charge-transfer excitons along the interface [114]. Such measurements might, for example, contribute to uncover the origin of the lack of temperature dependence of the geminate recombination of charge-transfer excitons in P3HT:PCBM or other material systems.

### 6.2.4 Charge Transport

The results of this thesis have highlighted that fast charge transport is of utmost importance for good device performance of organic solar cells. Furthermore, the density dependence of the charge carrier mobility has an additional influence on charge extraction and non-geminate recombination, as could be concluded from the transient absorption experiments and also confirmed by others [75]. Determining the temperature dependence of the density dependence of the charge carrier mobility of P3HT:PCBM would be useful for a quantitative description of the temperature dependence of the non-geminate recombination rate constant. This could be achieved with charge extraction experiments [75] at various temperatures. As the density dependence of the mobility generally is an important property for device performance it should be routinely studied for any new material system.

---

<sup>6</sup> Except for exciton diffusion.



---

# References

- [1] Kim, H., Personal Correspondence.
- [2] Reyes-Reyes, M.; Kim, K.; Carroll, D. L. *Applied Physics Letters* **2005**, *87*, 083506.
- [3] Campoy-Quiles, M.; Ferenczi, T.; Agostinelli, T.; Etchegoin, P. G.; Kim, Y.; Anthopoulos, T. D.; Stavrinou, P. N.; Bradley, D. D. C.; Nelson, J. *Nat Mater* **2008**, *7*, 158.
- [4] Peet, J.; Kim, J. Y.; Coates, N. E.; Ma, W. L.; Moses, D.; Heeger, A. J.; Bazan, G. C. *Nat Mater* **2007**, *6*, 497.
- [5] Chen, H.-Y.; Hou, J.; Zhang, S.; Liang, Y.; Yang, G.; Yang, Y.; Yu, L.; Wu, Y.; Li, G. *Nat Photon* **2009**, *3*, 649.
- [6] Mihailetschi, V. D.; Xie, H. X.; de Boer, B.; Koster, L. J. A.; Blom, P. W. M. *Advanced Functional Materials* **2006**, *16*, 699.
- [7] Deibel, C.; Strobel, T.; Dyakonov, V. *Physical Review Letters* **2009**, *103*, 036402.
- [8] Veldman, D.; Ipek, O.; Meskers, S. C. J.; Sweelssen, J.; Koetse, M. M.; Veenstra, S. C.; Kroon, J. M.; Bavel, S. S. v.; Loos, J.; Janssen, R. A. J. *Journal of the American Chemical Society* **2008**, *130*, 7721.
- [9] Shaheen, S. E.; Brabec, C. J.; Sariciftci, N. S.; Padinger, F.; Fromherz, T.; Hummelen, J. C. *Applied Physics Letters* **2001**, *78*, 841.
- [10] Padinger, F.; Rittberger, R. S.; Sariciftci, N. S. *Advanced Functional Materials* **2003**, *13*, 85.
- [11] Li, G.; Shrotriya, V.; Huang, J.; Yao, Y.; Moriarty, T.; Emery, K.; Yang, Y. *Nat Mater* **2005**, *4*, 864.
- [12] Park, S. H.; Roy, A.; Beaupre, S.; Cho, S.; Coates, N.; Moon, J. S.; Moses, D.; Leclerc, M.; Lee, K.; Heeger, A. J. *Nat Photon* **2009**, *3*, 297.
- [13] Liang, Y.; Xu, Z.; Xia, J.; Tsai, S.-T.; Wu, Y.; Li, G.; Ray, C.; Yu, L. *Advanced Materials* **2010**, *22*, E135.

- [14] Wang, D. H.; Park, K. H.; Seo, J. H.; Seiffter, J.; Jeon, J. H.; Kim, J. K.; Park, J. H.; Park, O. O.; Heeger, A. J. *Advanced Energy Materials* **2011**, *1*, 766.
- [15] Kamm, V.; Battagliarin, G.; Howard, I. A.; Pisula, W.; Mavrinskiy, A.; Li, C.; Müllen, K.; Laquai, F. *Advanced Energy Materials* **2011**, *1*, 297.
- [16] Dang, M. T.; Hirsch, L.; Wantz, G. *Advanced Materials* **2011**, *23*, 3597.
- [17] Thomson-Reuters, www.webofknowledge.com, 2011
- [18] Pope, M.; Swenberg, C. E. *Electronic Processes in Organic Crystals and Polymers*; Oxford University Press: New York, 1999.
- [19] Heeger, A. J. *Angewandte Chemie International Edition* **2001**, *40*, 2591.
- [20] Peierls, R. E. *Quantum theory of solids*; Clarendon Press: Oxford, 1955.
- [21] Lochner, K.; Bässler, H.; Tieke, B.; Wegner, G. *physica status solidi (b)* **1978**, *88*, 653.
- [22] Valeur, B. *Molecular Fluorescence: Principles and applications*; Wiley-VCH: Weinheim, 2002.
- [23] Marcus, R. A. *Journal of Chemical Physics* **1956**, *24*, 966.
- [24] Jortner, J. *Journal of Chemical Physics* **1976**, *64*, 4860.
- [25] May, V.; Kühn, O. *Charge and Energy Transfer Dynamics in Molecular Systems*; 1 ed.; Wiley-VCH Verlag GmbH & Co.KGAA.: Weinheim, 2004.
- [26] Shaw, P. E.; Ruseckas, A.; Samuel, I. D. W. *Advanced Materials* **2008**, *20*, 3516.
- [27] Cowan, S. R.; Banerji, N.; Leong, W. L.; Heeger, A. J. *To be published in Advanced Materials* **2012**.
- [28] Onsager, L. *Phys. Rev.* **1938**, *54*, 554.
- [29] Braun, C. L. *Journal of Chemical Physics* **1984**, *80*, 4157.
- [30] Tachiya, M. *J. Chem. Phys.* **1988**, *89*, 6929.
- [31] Howard, I. A.; Mauer, R.; Meister, M.; Laquai, F. *Journal of the American Chemical Society* **2010**, *132*, 14866.
- [32] Hallermann, M.; Haneder, S.; Como, E. D. *Charge-transfer states in conjugated polymer/fullerene blends: Below-gap weakly bound excitons for polymer photovoltaics*; AIP, 2008; Vol. 93.
- [33] Offermans, T.; van Hal, P. A.; Meskers, S. C. J.; Koetse, M. M.; Janssen, R. A. J. *Physical Review B* **2005**, *72*, 045213.



- 
- [34] Rand, B. P.; Burk, D. P.; Forrest, S. R. *Physical Review B* **2007**, *75*, 115327.
- [35] Veldman, D.; Meskers, S. C. J.; Janssen, R. A. J. *Advanced Functional Materials* **2009**, *19*, 1939.
- [36] Blom, P. W. M.; Mihailetschi, V. D.; Koster, L. J. A.; Markov, D. E. *Advanced Materials* **2007**, *19*, 1551.
- [37] Kern, J.; Schwab, S.; Deibel, C.; Dyakonov, V. *physica status solidi (RRL) – Rapid Research Letters* **2011**, n/a.
- [38] Vandewal, K.; Gadisa, A.; Oosterbaan, W. D.; Bertho, S.; Banishoeib, F.; Van Severen, I.; Lutsen, L.; Cleij, T. J.; Vanderzande, D.; Manca, J. V. *Advanced Functional Materials* **2008**, *18*, 2064.
- [39] Clarke, T. M.; Durrant, J. R. *Chemical Reviews* **2010**, *110*, 6736.
- [40] Deibel, C.; Dyakonov, V. *Reports on Progress in Physics* **2010**, *73*, 096401.
- [41] Ohkita, H.; Cook, S.; Astuti, Y.; Duffy, W.; Tierney, S.; Zhang, W.; Heeney, M.; McCulloch, I.; Nelson, J.; Bradley, D. D. C.; Durrant, J. R. *Journal of the American Chemical Society* **2008**, *130*, 3030.
- [42] Brabec, C. J.; Zerza, G.; Cerullo, G.; De Silvestri, S.; Luzzati, S.; Hummelen, J. C.; Sariciftci, S. *Chemical Physics Letters* **2001**, *340*, 232.
- [43] Hwang, I.-W.; Moses, D.; Heeger, A. J. *The Journal of Physical Chemistry C* **2008**, *112*, 4350.
- [44] Kraabel, B.; Lee, C. H.; McBranch, D.; Moses, D.; Sariciftci, N. S.; Heeger, A. J. *Chemical Physics Letters* **1993**, *213*, 389.
- [45] Zhang, F.; Jespersen, K. G.; Björström, C.; Svensson, M.; Andersson, M. R.; Sundström, V.; Magnusson, K.; Moons, E.; Yartsev, A.; Inganäs, O. *Advanced Functional Materials* **2006**, *16*, 667.
- [46] Bakulin, A. A.; Hummelen, J. C.; Pshenichnikov, M. S.; van Loosdrecht, P. H. M. *Advanced Functional Materials* **2010**, *20*, 1653.
- [47] Guo, J.; Ohkita, H.; Benten, H.; Ito, S. *Journal of the American Chemical Society* **2010**, *132*, 6154.
- [48] Müller, J. G.; Lupton, J. M.; Feldmann, J.; Lemmer, U.; Scharber, M. C.; Sariciftci, N. S.; Brabec, C. J.; Scherf, U. *Physical Review B* **2005**, *72*, 195208.
-

- [49] Tvingstedt, K.; Vandewal, K.; Gadisa, A.; Zhang, F.; Manca, J.; Inganäs, O. *Journal of the American Chemical Society* **2009**, *131*, 11819.
- [50] Tvingstedt, K.; Vandewal, K.; Zhang, F.; Inganas, O. *Journal of Physical Chemistry C* **2010**, *114*, 21824.
- [51] Morteani, A. C.; Sreearunothai, P.; Herz, L. M.; Friend, R. H.; Silva, C. *Physical Review Letters* **2004**, *92*, 247402.
- [52] Clarke, T.; Ballantyne, A.; Jamieson, F.; Brabec, C.; Nelson, J.; Durrant, J. *Chemical Communications* **2009**, 89.
- [53] Savenije, T. J.; Kroeze, J. E.; Yang, X.; Loos, J. *Advanced Functional Materials* **2005**, *15*, 1260.
- [54] Quist, P. A. C.; Martens, T.; Manca, J. V.; Savenije, T. J.; Siebbeles, L. D. A. *Solar Energy Materials and Solar Cells* **2006**, *90*, 362.
- [55] Groves, C.; Marsh, R. A.; Greenham, N. C. *Monte Carlo modeling of geminate recombination in polymer-polymer photovoltaic devices*; AIP, 2008; Vol. 129.
- [56] Holcombe, T. W.; Norton, J. E.; Rivnay, J.; Woo, C. H.; Goris, L.; Piliago, C.; Griffini, G.; Sellinger, A.; Bredas, J. L.; Salleo, A.; Frechet, J. M. J. *Journal of the American Chemical Society* **2011**, *133*, 12106.
- [57] Deibel, C. *Physica Status Solidi a-Applications and Materials Science* **2009**, *206*, 2731.
- [58] Liu, T.; Cheung, D. L.; Troisi, A. *Physical Chemistry Chemical Physics* **2011**, *13*, 21461.
- [59] Arkhipov, V. I.; Heremans, P.; Bäessler, H. *Why is exciton dissociation so efficient at the interface between a conjugated polymer and an electron acceptor?*; AIP, 2003; Vol. 82.
- [60] Verlaak, S.; Heremans, P. *Physical Review B* **2007**, *75*, 115127.
- [61] Sreearunothai, P.; Morteani, A. C.; Avilov, I.; Cornil, J.; Beljonne, D.; Friend, R. H.; Phillips, R. T.; Silva, C.; Herz, L. M. *Physical Review Letters* **2006**, *96*, 117403.
- [62] Kniepert, J.; Schubert, M.; Blakesley, J. C.; Neher, D. *The Journal of Physical Chemistry Letters* **2011**, *2*, 700.

- 
- [63] Marsh, R. A.; Hodgkiss, J. M.; Friend, R. H. *Advanced Materials* **2010**, *22*, 3672.
- [64] Mauer, R.; Howard, I. A.; Laquai, F. *J. Phys. Chem. Lett.* **2010**, *1*, 3500.
- [65] McMahon, D. P.; Cheung, D. L.; Troisi, A. *The Journal of Physical Chemistry Letters* **2011**, *2*, 2737.
- [66] Kanai, Y.; Grossman, J. C. *Nano Letters* **2007**, *7*, 1967.
- [67] Baranovski, S. *Charge Transport in Disordered Solids with Applications in Electronics*; John Wiley & Sons Ltd.: Weinheim, 2006.
- [68] Borsenberger, P. *J. Chem. Phys.* **1991**, *94*, 5447.
- [69] Miller, A.; Abrahams, E. *Phys. Rev.* **1960**, *120*, 745.
- [70] Arkhipov, V. I.; Emelianova, E. V.; Bäessler, H. *Philosophical Magazine Part B* **2001**, *81*, 985.
- [71] Bäessler, H.; Borsenberger, P. *Chemical Physics* **1993**, *177*, 763.
- [72] Heun, S.; Borsenberger, P. *Chemical Physics* **1995**, *200*, 245.
- [73] Pasveer, W. F.; Cottaar, J.; Tanase, C.; Coehoorn, R.; Bobbert, P. A.; Blom, P. W. M.; de Leeuw, D. M.; Michels, M. A. J. *Physical Review Letters* **2005**, *94*, 206601.
- [74] Blom, P. W. M.; de Jong, M. J. M.; van Munster, M. G. *Physical Review B* **1997**, *55*, R656.
- [75] Shuttle, C. G.; Hamilton, R.; Nelson, J.; O'Regan, B. C.; Durrant, J. R. *Advanced Functional Materials* **2010**, *20*, 698.
- [76] Mauer, R.; Kastler, M.; Laquai, F. *Advanced Functional Materials* **2010**, *20*, 2085.
- [77] Kepler, R. G. *Phys. Rev.* **1960**, *119*, 1226.
- [78] LeBlanc, O. *J. Chem. Phys.* **1960**, *33*, 626.
- [79] Kim, H.; Schulte, N.; Zhou, G.; Müllen, K.; Laquai, F. *Advanced Materials* **2011**, *23*, 894.
- [80] Laquai, F.; Wegner, G.; Bäessler, H. *Philos. Trans. R. Soc. A-Math. Phys. Eng. Sci.* **2007**, *365*, 1473.
- [81] Lampert, M. A.; Mark, P. *Current Injection In Solids*; Academic Press: New York, 1970.
- [82] Rose, A. *Phys. Rev.* **1955**, *97*, 1538.
-

- [83] Staudigel, J., Universität Erlangen-Nürnberg, 1999.
- [84] Juška, G.; Arlauskas, K.; Stuchlik, J.; Österbacka, R. *Journal of Non-Crystalline Solids* **2006**, *352*, 1167.
- [85] Deibel, C.; Baumann, A.; Dyakonov, V. *Applied Physics Letters* **2008**, *93*, 163303.
- [86] Schubert, M.; Steyrlleuthner, R.; Bange, S.; Sellinger, A.; Neher, D. *physica status solidi (a)* **2009**, *206*, 2743.
- [87] Brondijk, J. J.; Maddalena, F.; Asadi, K.; van Leijen, H. J.; Heeney, M.; Blom, P. W. M.; de Leeuw, D. M. *physica status solidi (b)* **2012**, *249*, 138.
- [88] Wishart, J. F.; Rao, B. S. M. *Recent Trends in Radiation Chemistry*; World Scientific Publishing Co. Pte. Ltd.: Singapore, 2010.
- [89] Grozema, F. C.; Siebbeles, L. D. A. *The Journal of Physical Chemistry Letters* **2011**.
- [90] Langevin, P. *Annales De Chimie Et De Physique* **1903**, *28*, 433.
- [91] Clarke, T. M.; Jamieson, F. C.; Durrant, J. R. *Journal of Physical Chemistry C* **2009**, *113*, 20934.
- [92] Koster, L. J. A.; Kemerink, M.; Wienk, M. M.; Maturová, K.; Janssen, R. A. J. *Advanced Materials* **2011**, 1670.
- [93] Deibel, C.; Wagenpfahl, A.; Dyakonov, V. *Physical Review B* **2009**, *80*, 075203.
- [94] Shuttle, C. G.; O'Regan, B.; Ballantyne, A. M.; Nelson, J.; Bradley, D. D. C.; de Mello, J.; Durrant, J. R. *Applied Physics Letters* **2008**, *92*, 093311.
- [95] Juška, G. *Appl. Phys. Lett.* **2009**, *95*, 013303.
- [96] Shockley, W.; Queisser, H. J. *Journal of Applied Physics* **1961**, *32*, 510.
- [97] NREL, <http://rredc.nrel.gov/solar/spectra/>, 2011
- [98] Scott, J. C.; Pautmeier, L. T.; Schein, L. B. *Physical Review B* **1992**, *46*, 8603.
- [99] Hirao, A.; Nishizawa, H. *Physical Review B* **1996**, *54*, 4755.
- [100] Laquai, F., Johannes Gutenberg-Universität Mainz, 2006.
- [101] Bäessler, H. *Physica Status Solidi B-Basic Research* **1993**, *175*, 15.
- [102] Mauer, R.; Howard, I. A.; Laquai, F. *The Journal of Physical Chemistry Letters* **2011**, *2*, 1736.

- 
- [103] Häusermann, R.; Knapp, E.; Moos, M.; Reinke, N. A.; Flatz, T.; Ruhstaller, B. *Journal of Applied Physics* **2009**, *106*, 104507.
- [104] Fluxim *Setfos User Manual*; Fluxim AG: Feusisberg, 2010.
- [105] Burkhard, G. F.; Hoke, E. T.; McGehee, M. D. *Advanced Materials* **2010**, *22*, 3293.
- [106] Shuttle, C. G.; Hamilton, R.; O'Regan, B. C.; Nelson, J.; Durrant, J. R. *Proceedings of the National Academy of Sciences* **2010**, *107*, 16448.
- [107] Etzold, F.; Howard, I. A.; Mauer, R.; Meister, M.; Kim, T.-D.; Lee, K.-S.; Baek, N. S.; Laquai, F. d. r. *Journal of the American Chemical Society* **2011**, *133*, 9469.
- [108] Soldera, M.; Taretto, K.; Kirchartz, T. *physica status solidi (a)* **2012**, *209*, 207.
- [109] Kim, Y.; Cook, S.; Tuladhar, S. M.; Choulis, S. A.; Nelson, J.; Durrant, J. R.; Bradley, D. D. C.; Giles, M.; McCulloch, I.; Ha, C.-S.; Ree, M. *Nat Mater* **2006**, *5*, 197.
- [110] Collins, B. A.; Tumbleston, J. R.; Ade, H. *The Journal of Physical Chemistry Letters* **2011**, 3135.
- [111] Yin, W.; Dadmun, M. *ACS Nano* **2011**, *5*, 4756.
- [112] Zhao, G.; He, Y.; Li, Y. *Advanced Materials* **2010**, *22*, 4355.
- [113] Hammond, M. R.; Kline, R. J.; Herzing, A. A.; Richter, L. J.; Germack, D. S.; Ro, H.-W.; Soles, C. L.; Fischer, D. A.; Xu, T.; Yu, L.; Toney, M. F.; DeLongchamp, D. M. *ACS Nano* **2011**, *5*, 8248.
- [114] Howard, I. A., University of Cambridge, 2009.



# List of abbreviations

A	Acceptor
BHJ	Bulk Heterojunction
CT	Charge Transfer
CTE	Charge Transfer Exciton
D	Donor
DI-SCLC	Dark-Injection Space-Charge Limited Currents
DOS	Density Of States
EQE	External Quantum Efficiency
FF	Fill Factor
GSB	Ground State Bleach
HOMO	Highest Occupied Molecular Orbital
IQE	Internal Quantum Efficiency
ITO	Indium Tin Oxide
$J_{sc}$	Short-Circuit Current
LUMO	Lowest Unoccupied Molecular Orbital
$M_w$	Weight average of the Molecular weight
MPP	Maximum Power Point
Nd:YAG	Neobdym doped Yttrium Aluminum Garnet
NIR	Near Infrared spectral region (~700-2000nm)
OD	Optical Density

## List of abbreviations

---

OFET	Organic Field Effect Transistor
OLED	Organic Light Emitting Diode
OPA	Optical Parametric Amplifier
OPO	Optical Parametric Oscillator
OPV	Organic Photovoltaics
OSC	Organic Solar Cell
P3HT	Poly(3-hexylthiophene)
PCBM	[6,6] Phenyl C61 Butyric Acid Methyl Ester
PCE	Power Conversion Efficiency
PDI	Polydispersity Index
PEDOT:PSS	Poly(ethylenedioxythiophene):polystyrenesulphonic acid
PIA	Photoinduced Absorption
PL	Photoluminescence
QE	Quantum Efficiency
RC constant	Resistance $\times$ Capacitance constant of an electrical circuit
RR	Regioregular
RRa	Regiorandom
SCLC	Space Charge Limited Current
SE	Stimulated Emission
SSC	Spatially Separated Charge Carriers
SMU	Source Measure Unit
TA	Transient Absorption spectroscopy



TOF	Time-Of-Flight (charge carrier mobility measurement)
UV	Ultraviolet
UV/VIS	Linear optical absorption spectroscopy in the Ultraviolet and Visible spectral region
$V_{oc}$	Open-Circuit Voltage
VIS	Visible spectral range (~400-700 nm)

All other abbreviations, especially physical units and constants, have their usual meaning unless stated otherwise in the text.



---

# List of scientific contributions

## Publications in peer reviewed journals

- **R. Mauer**, I.A. Howard, F. Laquai: "Effect of External Bias on Nongeminate Recombination in Polythiophene:Methanofullerene Organic Solar Cells", *J. Phys. Chem. Lett.* **2011**, 2 (14), 1736-1741.
- F. Etzold, I.A. Howard, **R. Mauer**, M. Meister, T.D. Kim, K.S. Lee, N.S. Baek, F. Laquai: "Ultrafast Exciton Dissociation Followed by Nongeminate Charge Recombination in PCDTBT:PCBM Photovoltaic Blends", *J. Am. Chem. Soc.* **2011**, 133 (24), 9469-9479.
- **R. Mauer**, I.A. Howard, F. Laquai: "Effect of Nongeminate Recombination on Fill Factor in Polythiophene:Methanofullerene Organic Solar Cells", *J. Phys. Chem. Lett.* **2010**, 1 (24), 3500-3505.
- Kreyes, M. Amirkhani, I. Lieberwirth, **R. Mauer**, F. Laquai, K. Landfester, U. Ziener: "The Longest Beta-Unsubstituted Oligothiophenes and Their Self-Assembly in Solution", *Chem. Mater.* **2010**, DOI: 10.1021/cm1027095.
- I.A. Howard, **R. Mauer**, M. Meister, F. Laquai: "Effect of Morphology on Ultrafast Free Carrier Generation in Polythiophene:Fullerene Organic Solar Cells", *J. Am. Chem. Soc.* **2010**, 132 (42), 14866-14876.
- **R. Mauer**, M. Kastler, F. Laquai: "The Impact of Polymer Regioregularity on Charge Transport and Efficiency of P3HT:PCBM Photovoltaic Devices", *Adv. Funct. Mater.* **2010**, 20, 2085-2092.

## Chapters in edited books

- **R. Mauer**, I. A. Howard, F. Laquai, Chapter "Energy and Charge Transfer" to be published in "Semiconducting Polymer Composites", Edited by Xiaoniu Yang, Wiley-VCH, Weinheim, Germany.

## Conference contributions

- **R. Mauer**, I. A. Howard, F. Laquai, Interdisciplinary Workshop on Fundamental Function of Organic Solar Cells, Munich, 19<sup>th</sup> July 2011: “Bias-Dependent Nongeminate Recombination in Organic Solar Cells”.
- **R. Mauer**, I. A. Howard, F. Laquai, Spring Meeting of the Deutsche Physikalische Gesellschaft, Dresden, 14<sup>th</sup>-18<sup>th</sup> March 2011: “Bias-Dependent Transient Absorption on Organic Solar Cells”.
- **R. Mauer**, I. A. Howard, F. Laquai, Spring Meeting of the Deutsche Physikalische Gesellschaft, Dresden, 14<sup>th</sup>-18<sup>th</sup> March 2011: “Effect of Nongeminate Recombination on Polythiophene: Methanofullerene Organic Solar Cells”.
- **R. Mauer**, I. A. Howard, F. Laquai, Pacificchem, 15<sup>th</sup>-20<sup>th</sup> December 2010, Honolulu, USA: “The Influence of Morphology on Charge Transport and Recombination in P3HT:PCBM solar cells”.
- **R. Mauer**, M. Kastler, F. Laquai, Spring Meeting of the Deutsche Physikalische Gesellschaft, 22<sup>nd</sup>-26<sup>th</sup> March 2010, Regensburg: “Charge Transport in rr-P3HT:PCBM Blends - The Impact of Ultrahigh Regioregularity on Hole Transport and Device Performance”.
- **R. Mauer**, M. Kastler, F. Laquai, International Workshop on Self-Organized Materials for Optoelectronics, 24<sup>th</sup>-25<sup>th</sup> August 2009, Mainz: “Charge Transport in P3HT and P3HT:PCBM Bulk Heterojunction Composites for Organic Solar Cells”.



